

## CONTENTS

	Page
Improvements in Electron-Optical Picosecond Chronography	1
Abstract	2
Introduction	3
Chapter 1.....Ultra Short Pulse Measurements	5
1.1 Introduction	5
1.2 Correlation Techniques	7
1.2.1 A Linear Correlation Technique	7
1.2.2 Non-Linear Correlation by Second Harmonic Generation	9
1.2.3 The Method of Two Photon Fluorescence	12
1.3 Ultra Fast Shutters	18
1.3.1 The Optical Kerr Effect	18
1.3.2 Saturable Absorber Shutters	21
1.4 Linear Measurement Techniques	22
1.4.1 Photodiode-Oscilloscope Combinations	22
1.4.2 Electron-Optical Chronography	23
1.5 Summary of Ultra Short Pulse Measurement Techniques	29
Figures 1 - 9	
Chapter 2 .... The Photochron I Streak Camera	31
2.1 Introduction	31
2.2 The Photochron I Image Tube	31
2.3 Image Tube Electronics	34
2.4 The Image Intensifier	38
2.5 The Evaluation of the Photocrhon I Performance	41
Figures 10 - 14	
Plates 1 & 2	
Chapter 3 .... The Photochron II Image Tube	47
3.1 Introduction	47
3.2 Electron-Optical Magnification	48
3.3 Signal Induced Noise	54
3.4 The S1 Image Tube Streak Camera	58
3.5 The S20 Image Tube Streak Camera	64
3.6 Conclusions	66

Figures 15 - 27	
Plates 3 - 6	
Summary	70
References	73
Acknowledgements	78
Publications	79

To my Parents

IMPROVEMENTS IN ELECTRON - OPTICAL  
PICOSECOND CHRONOGRAPHY

Thesis presented on application for the degree of

Master of Philosophy

in the

Faculty of Science

by

Patrick Roy Bird B.Sc. (Manchester)

Department of Physics  
Imperial College  
University of London

November 1974

## Abstract

General methods for the measurement of the duration of ultra short luminous phenomena are described, with the emphasis on those methods which are most suited to the measurement of intense pulses of picosecond duration produced by mode-locked lasers.

The relative merits of such methods are briefly discussed and in particular the development of the high speed streak camera is highlighted. It is shown how the present temporal resolution limit of such cameras, which is of the order of 2 to 3 picoseconds may be improved to the sub-picosecond range by simple modifications to the electrostatic focussing system employed in these devices.

It is shown how the contribution to the overall camera temporal resolution limit due to electron transit time spread between the camera image tube input photocathode and output phosphor may be reduced. It is also shown how the spatial resolution of the camera image tube may be improved to lower the overall temporal resolution limit and simultaneously to increase the camera sensitivity.

A method to reduce the signal induced noise occurring when the electron beam image in the image tube section of the camera is deflected or 'streaked' is suggested.

Finally the experimental evaluation of the performance of the image-tube streak camera when used with passively mode-locked lasers capable of the production of picosecond duration pulses is discussed.

## INTRODUCTION

In the early 1960's the laser was described as 'a solution in search of a problem'. Now the applications of lasers are well known and numerous and of particular interest to many are the ultra short duration intense pulses which may be provided by the mode-locked laser (1.1). These pulses are of durations of the order of several picoseconds or less and find applications in photochemistry, photobiology and various other fields. To fully utilise these pulses it is important to know accurately the pulse durations and this thesis is concerned with methods of measurement of such pulses in particular with the method of electron-optical chronography, embodied by the high speed streak camera.

Chapter 1 describes methods of measurement of ultra short laser pulses. A linear method based upon the Michelson Interferometer (1-4) is described, but this only yields a lower limit for the pulse duration. Other non-linear methods which yield estimates of the actual pulse duration, including the methods of Second Harmonic Generation (5-9), Two Photon Fluorescence (12-17), and the Optical Kerr effect (29-35) are described. Of these the method of Two Photon Fluorescence is most popular and can resolve events of the order of 0.2 psecs duration (23).

Linear methods based upon the photoelectric effect include the well known photodiode - oscilloscope combination. However the relatively slow response times of commercially available photodiodes of the order of 100 psecs (65, 66) limit the resolution of such systems. In order to achieve resolution less than many tens of picoseconds it is necessary to use the method of electron-optical chronography first proposed by Zavoiskii and Fanchenko in 1956 (45). In this method an electron beam image of the temporal intensity variations of the original light signal is swept across a phosphor screen at velocities approaching that of light. This converts the temporal intensity variation into a spatial intensity variation from which the duration of the original pulse may be deduced.

The main limitation to the resolution of this method is due to the electron transit time spread in the electronic image tube between photocathode and phosphor screen, (39, 45). Early image tube streak cameras had resolution limits of the order of 20-60 psecs (51-53). The inclusion of a fine mesh electrode close to the photocathode to which a high voltage was applied lowered the resolution limit to below 10psecs (49, 50) and now presently available streak cameras have resolution limits in the range 2-3 psecs (59, 62).

Chapter 2 describes the elements of a streak camera system capable of a resolution of the order of 2 psecs (61). A system basically consists of, input and relay optics, an image tube, an image intensifier, and a recording camera. The constituent parts and the limitations they impose on the ultimate performance of the system are described in detail. In particular the limits set by the image tube portion are discussed, and in chapter 3 it is shown how, by simple alterations to the electrostatic focussing mechanism in the image tube and by a simultaneous increase in electric field near the photocathode the resolution limit may be reduced to the subpicosecond region.

A streak camera system incorporating this redesigned image tube is used to measure the outputs from the mode-locked Neodymium: glass and Rhodamine 6G dye, lasers. The results of these investigations show that the new streak camera system has the capability of subpicosecond resolution.

## CHAPTER 1

### ULTRA SHORT PULSE MEASUREMENTS

#### 1.1 INTRODUCTION

The rapid development of the laser over the last fifteen years and in particular the development of the mode-locked laser, capable of producing intense pulses of light of picosecond duration has accelerated research in the field of time measurement. This chapter is concerned with methods of measurement of such ultra short pulses.

Laser action was first demonstrated by Maiman (68) using a flashlamp pumped ruby rod. The output of this laser was typically hundreds of microseconds in duration. McClung and Hellwarth showed how the duration of the output could be shortened and peak powers increased by use of a technique called Q-switching (69). In Q-switched operation laser emission is prevented by use of an intracavity loss element. This may in its simplest form be a shutter which can quickly be removed (1). For example in the case of a shutter, the laser medium population inversion builds up to a high level while the shutter is in place. When the shutter is removed, preferably at the instant of peak inversion, a short duration pulse of high peak power is emitted. Q-switching techniques can yield pulses of peak powers  $\sim 10^8$  watts with durations  $\sim 10 - 100$  n secs. However because of the time required to build up sufficient inversion, pulse durations are limited to  $\sim 10^{-8}$  secs using this technique.

In order to produce shorter pulses in the picosecond region, the mode-locked laser must be employed. A mode-locked laser system generally comprises an amplifier (the laser active medium) and a loss element. The active medium is placed between two reflectors one of which is only partially reflecting to serve as an output coupler. There are a large number of possible axial modes of

oscillation of such a system, depending upon the amplification bandwidth of the laser medium  $\Delta\nu$ , and the length of the laser cavity. The separation frequency of these modes is  $\Delta f = c/2L$  where  $L$  is the separation of the laser cavity reflectors, and  $c$  the velocity of light. If a loss modulation is introduced into the system at a frequency equal to the separation of the axial modes then a fixed phase relationship is generated between the oscillating modes and the laser is said to be mode-locked (70). The output of such a laser consists of a train of pulses of duration  $t_p$  separated by the round trip time between the laser reflectors  $t_r = 2L/c$  where  $t_p \ll t_r$ .

If the peak of the gain - bandwidth profile of the laser medium occurs at a frequency  $\nu_0$  then the laser will initially oscillate in this single mode. With the introduction of a loss modulation at frequency  $\Delta f$  sidebands at  $\nu_0 \pm \Delta f$  are generated. In the instance when  $\Delta f = c/2L$  as described above these sidebands are coincident with the longitudinal modes of the laser cavity and are phase-locked with them. As the number of cavity round trips increases, so does the number of sidebands generated. The maximum number of sidebands generated is  $m$  where  $\Delta\nu = 2m \Delta f$ . As the output spectrum of the laser broadens, then the temporal envelope of the laser pulse sharpens. If all the modes can be phase-locked then by Fourier analysis a pulse of duration  $t_p \approx 1/\Delta\nu$  is generated. The output of the laser will now consist of pulses of duration  $t_p \approx 1/\Delta\nu$ , separated by the round trip time of the cavity  $t_r = 2L/c = 1/\Delta f$ .

This simple theoretical treatment implies that in the case of the Neodymium: glass laser for which  $\Delta\lambda = 10\text{nm}$  at a central wavelength of 1060 nm, that pulses of duration 0.3 psec could be obtained. The observed pulse durations are however of the order of ten times this value, which would indicate that not all the longitudinal modes of the laser are ideally phase-locked.

Nevertheless pulses as short as 3 psecs have been observed in the output from a mode-locked Nd: glass laser (59) and pulses of 5 psecs duration have been observed from a Rhodamine - 6G dye laser (71, 72).

The development of the Mode-locked laser however presented problems to researchers since even the fastest photodiode - oscilloscope combinations had risetimes of hundreds of picoseconds. Thus the presence of components in the laser output shorter than the rise time of the oscilloscope could be detected but not measured. To overcome this problem several new techniques were developed. These fall basically into two categories, the linear methods and the non-linear methods. The latter methods make extensive use of correlation functions to obtain information about the pulse temporal intensity profile, while the linear methods described in this chapter are mainly based upon the photoelectric effect. One linear method which also uses a correlation measurement is classified for convenience with non-linear correlation methods in section 1.2. Non-linear, ultra fast shutter methods are described in section 1.3 and linear methods are dealt with in section 1.4.

## 1.2. Correlation Techniques

All the techniques described in this section are based upon the measurement of a correlation function. All the techniques described except one are non-linear and this linear correlation technique is described primarily as an introduction to the other methods.

### 1.2.1 A Linear Correlation Technique

This method makes use of Michelson's interferometer (FIG.1). An incoming optical pulse of electric field amplitude  $E_0(t)$  is split into two identical pulses of amplitude  $E_0(t) / \sqrt{2}$  by the beamsplitter. A relative delay  $\tau$  is introduced between the two pulses by means of an adjustable position mirror. The pulses are recombined at a square law detector such as a photographic plate, photodetector, etc.

For  $D_1 \neq D_2$  the pulses can be represented as (1)

$$E_1(t) = E_0(t) / \sqrt{2} \cdot e^{j\omega t} \quad (1.1)$$

$$E_2(t) = E_0(t - \tau) / \sqrt{2} \cdot e^{j\omega(t-\tau)} \quad (1.2)$$

The intensity incident upon the detector is

$$I(t, \tau) = \frac{1}{2} |E_0(t) + E_0(t - \tau)|^2 \quad (1.3)$$

Assuming the detector response is slow compared to the pulse duration or  $\tau$ , the detector output signal  $S(\tau)$  is given by,

$$S(\tau) = \int_{-\infty}^{\infty} I(t, \tau) dt \quad (1.4)$$

$$= \frac{W}{W(1 + A(\tau))} \quad (1.5)$$

where  $W = \int_{-\infty}^{\infty} E_0^2(t) dt$  is the pulse energy and  $A(\tau)$  is the pulse amplitude autocorrelation function

$$A(\tau) = \frac{\int_{-\infty}^{\infty} E_0(t) E_0(t - \tau) dt}{\int_{-\infty}^{\infty} E_0^2(t) dt} \quad (1.6)$$

$A(\tau)$  is related through the Fourier transform to  $|P(W)|^2$ , the power density spectrum of the original optical pulse.  $A(\tau)$  and  $|P(W)|^2$  are in fact a Fourier pair and thus knowledge of one defines the other.  $|P(W)|^2$  is the function measured by a spectrometer, while  $A(\tau)$  is measured by an interferometer.

At the plane of the detector interference fringes are obtained. The difference in path length  $\Delta D = D_1 - D_2$ , over which these fringes are visible is called the coherence length. The coherence length is related to the pulse coherence time  $\Delta \tau_c$  and the spectral bandwidth of the pulse  $\Delta W$  by

$$\Delta \tau_c = 2\pi / \Delta W = 2\Delta D / c \quad (1.7)$$

Hence measurements of the coherence length  $\Delta D$  yield values for the pulse coherence time  $\Delta \tau_c$ . However only in the special case when the entire spectral content of the pulse is due to its short duration envelope will  $\Delta \tau_c$  be equal to the actual pulse duration. Thus this method can only yield a lower limit for the pulse duration since it cannot distinguish between pulses for which  $\Delta \tau_p = 2\pi / \Delta W$  and pulses for which  $\Delta \tau_p > 2\pi / \Delta W$ .

Experiments based upon this method have been carried out (2, 3) and it is found to be a useful method for studying the similarity between the pulses in a mode-locked train of pulses, (4).

### 1.2.2 Non-Linear Correlation by Second Harmonic Generation

Clearly the linear interferometric method is of little value if the actual pulse duration is required. A method proposed by Weber (5) converts the output pulses of the interferometer into their second harmonic by passage through a non-linear crystal. The amount of second harmonic radiation produced being a function of the delay  $\tau$ , between the two pulses.

If  $E_1(t)$  and  $E_2(t - \tau)$  are the output pulses from the interferometer of FIG.1 then the second harmonic output from the crystal is given by,

$$2W E(t) = (E_1(t) + E_2(t - \tau))^2 \quad (1.8)$$

neglecting the constant for the second harmonic generation efficiency. The output of a detector whose response is slow compared to  $W$  and  $\tau$  is given by

$$S(\tau) = \int_{-\infty}^{\infty} |2W E(t)|^2 dt \quad (1.9)$$

$$= 2W W(1 + 2G(\tau)) \quad (1.10)$$

where  $2W W = \int_{-\infty}^{\infty} E^4(t) dt \quad (1.11)$

is the energy in the pulse and  $G(\tau)$ , the pulse intensity autocorrelation function is given by,

$$G(\tau) = \int_{-\infty}^{\infty} E^2(t) E^2(t - \tau) dt / \int_{-\infty}^{\infty} E^4(t) dt \quad (1.12)$$

Measurement of the second harmonic intensity as a function of delay gives the time over which the pulse energy is spread. For large values of  $\tau$  for which no overlap of the pulses within the crystal occurs, then from eqn. (1.10)

$$S(\tau) / 2W W = 1$$

and similarly for  $\tau = 0$  when the pulses are coincident

$$S(\tau) / 2W W = 3$$

Hence in this experiment there is a peak signal to background ratio of 3:1. This is second harmonic generation (SHG) of the first kind.

An experiment for which there is theoretically zero background signal is.

$$S(\tau) / I^2 = 0$$

was also proposed by Weber (20). In this case second harmonic generation of the second kind is used. In the experiment the non-linear crystal is set at an angle, called the phase matching angle (20), such that two orthogonally polarised pulses from a Michelson arrangement propagating as ordinary and extraordinary rays through the crystal cause second harmonic generation only when they overlap within the crystal. Neither pulse acting alone causes appreciable second harmonic generation. The pulse width is obtained from the dependence of the second harmonic intensity upon the relative delay of the pulses.

A typical apparatus for second harmonic generation measurements due to Weber (7) is shown in FIG.2. The two orthogonally polarised pulses are produced by Glan-Thompson prisms (G) and polarisers (P) in each arm of the interferometer. A relative delay  $\tau$ , between the two pulses is introduced by means of a movable mirror ( $M_1$ ). The second harmonic signal is generated by the overlap of the two pulses in the non-linear KDP crystal (XTAL). A reference second harmonic signal, to allow for the variation of the laser output from shot to shot, is generated in another non-linear crystal, and used to normalize the output of the KDP crystal.

A plot of the normalised second harmonic output from the interferometer as a function of difference in path length of the pulses,  $\Delta l$  yields the required correlation function, (FIG.2).

The pulse full width at half maximum intensity (FWHM) is found using the relationship.

$$\Delta t_{\frac{1}{2}} = 2 \Delta l_{\frac{1}{2}} / K.C. \quad (1. 13)$$

where C represents the velocity of light in a vacuum and K is a constant whose value depends upon the assumed pulse shape, in this case  $K = 1.33$ .

Using this method Weber measured the duration of pulses from a mode-locked Neodymium: glass laser, and found them to be of duration 8 to 12.5 picoseconds.

The temporal resolution limit of the method, if an ideally mode-locked laser is used and a KDP crystal of  $\sim 1$  mm thickness is used, is of the order of 1 psec, (20). The resolution time is found to be inversely proportional to the crystal thickness. However the efficiency of second harmonic generation decreases as crystal thickness decreases and hence the sensitivity of the detector will set a limit to the resolution of the method.

Only the average duration of pulses can be measured by this method since to plot each point on the correlation function requires at least one firing of the laser, and to plot the whole function requires many shots with the attendant variation of the laser output from shot to shot. It must also be pointed out that no inference as to the shape of the pulses can be made using this technique. This is because the back transform of an autocorrelation function is not unique. Many different pulse shapes may give the same autocorrelation function when transformed. Also information about the symmetry or asymmetry of the pulse shape is lost since the autocorrelation function plotted is by definition always symmetrical.

At the same time as Weber proposed this second harmonic method a similar method for the measurement of the duration of pulses in a Nd: glass laser was used by Armstrong (6). He also used orthogonally polarised pulses to generate second harmonic radiation by their overlapping at the surface of a gallium arsenide crystal. Results of 4-6 picoseconds were obtained for the average pulse durations compared to Weber's 8-12.5 picoseconds.

Second harmonic generation techniques have also been used to measure the duration of pulses from continuous working dye lasers (8, 9). The durations of these pulses have been found to be as short as 1.5 - 2.3 psecs and some observations of pulses of 0.5 - 0.7 psecs have been reported (9).

A variation on the harmonic generation method has been used also to measure the pulse durations of a mode-locked Nd: glass laser. The method is based upon the fact that linearly polarised laser radiation produces third harmonic generation in an isotropic medium while circularly polarised radiation does not (11). In an experiment by Eckardt and Lee (10) each pulse from the laser was converted into two pulses circularly polarised in the opposite sense. A relative delay was introduced between the pulses and they were made to collinearly enter a cell containing a solution of fuchsin red in hexa-fluoroisopropanol. When the delay is of such a value that portions of the pulses overlap then a linear polarisation results in the region of overlap. This linear polarisation produces third harmonic generation in the fuchsin red solution.

By varying the relative delay and monitoring the third harmonic output a third order correlation curve was plotted, from which average pulse widths of the order of 0.73 psecs (FWHM) were inferred. This very short duration "spike" was however superimposed on a broad base  $\sim$  40 picoseconds wide at the 5% level. This method had an advantage in that careful preparation and orientation of a crystal were not required and it also exhibited zero background radiation.

The main disadvantage of harmonic generation measurements is that plotting of the correlation profile requires many laser shots with the associated variation of laser characteristics from shot to shot. Also in the case of second harmonic techniques the preparation of the crystal is both critical and time consuming. For these reasons SHG techniques became less popular and were generally replaced by the method of two Photon Fluorescence (TPF) which is discussed in the following section.

### 1.2.3. The Method of Two Photon Fluorescence

This method can be used to perform either cross-correlation or auto-correlation measurements of picosecond optical pulses. The most common experimental arrangements are illustrated in FIG 3. In both cases (a) and (b) each pulse travelling in the medium causes a two photon absorption process which is followed by fluorescence along the path of the pulse in the medium. In regions where the pulse overlaps with, in case (a) a neighbouring

pulse and in case (b) a replica of itself, an enhanced fluorescence is produced.

Consider the centre of the cell to be the origin  $Z = 0$ , and let pulses approaching from left and right be,

$$E_1(t - Z/C) \sin(KZ - Wt) \text{ and}$$

$$E_2(t + Z/C) \sin(-KZ - Wt)$$

The intensity in the cell  $C$ , is then given by (1),

$$I_W = (E_1(t - Z/C) \sin(KZ - Wt) + E_2(t + Z/C) \sin(-KZ - Wt)) \quad (1. 14)$$

Assuming the fluorescent intensity  $I_F$  is proportional to the intensity squared, then

$$I_F \propto I_W^2 \quad (1. 15)$$

From the above the fluorescent intensity is proportional to the fourth power of the instantaneous electric field. The spatial distribution of fluorescence is usually recorded photographically. The value recorded is however the time averaged value of  $I_F$  and because of the limited resolution of the film the recorded value is spatially averaged over several optical wavelengths. The value recorded by the film is then,

$$S(\tau) \propto \int_{-\infty}^{\infty} E_1^4(t - Z/C) dt + \int_{-\infty}^{\infty} E_2^4(t + Z/C) dt + 4 \int_{-\infty}^{\infty} E_1^2(t - Z/C) E_2^2(t + Z/C) dt \quad (1. 16)$$

Normalisation of  $S(\tau)$  gives

$$S(\tau)/W \propto 1 + 2G(\tau) \quad (1. 17)$$

where  $G(\tau)$  is the second order correlation function (eqn. (1. 12)). The spatial distribution of fluorescence is thus directly related to  $G(\tau)$  and the complete correlation profile is displayed simultaneously as a function of distance  $Z$ , from the centre of the overlap region. The observed fluorescence resembles a narrow bright region superimposed on a uniform background. From eqn. (1. 17) the ratio of peak fluorescence intensity, occurring when  $\tau = 0$  at  $Z = 0$ , to the background intensity far away from  $Z = 0$  so that no overlap occurs, is 3: 1.

The duration of pulses may be deduced from microdensitometer traces of the fluorescent intensity profile. FIG.4 shows a typical

TPF microdensitometer profile (upper trace). From the width  $\Delta Z$  (FWHM) of the profile, the pulse duration  $\Delta t$  (FWHM) may be obtained using the relationship

$$\Delta t = Kn \Delta Z / C$$

where  $n$  is the refractive index of the fluorescent medium,  $C$  is the velocity of light and  $K$  a constant whose value depends on the assumed pulse shape. For Lorentzian pulses  $K = 1$ , for Gaussian pulses  $K = 2^{\frac{1}{2}}$ .

The TPF method has been treated extensively both experimentally (14 - 17), and theoretically (12, 13) by several authors. The first reported measurement of picosecond pulses using TPF was by Giordmaine et al (16). They used the experimental configuration of FIG. 3(a) to produce a fluorescent track in a solution of dibenzanthracene (DBA) in benzene and other solutions. The pulses were generated by a mode-locked Nd: glass laser. From the fluorescent profiles pulses of 1-2 psecs were inferred. The peak fluorescent intensity to background intensity was however only  $\sim 2:1$ . This contrast ratio (CR) as it was called was less than the theoretically predicted value of 3:1.

In a similar experiment (17) Rentzepis and Duguay attempted to improve the contrast ratio over that observed by Giordmaine. In their experiment they produced pulses of wavelength 0.53  $\mu\text{m}$ , by second harmonic generation in a KDP crystal, from a mode-locked Nd: glass laser (fundamental wavelength 1.06  $\mu\text{m}$ ). The crystal output thus consisted of pulses at 0.53  $\mu\text{m}$  and at 1.06  $\mu\text{m}$  coincident in space and time. A relative delay between the 1.06  $\mu\text{m}$  and 0.53  $\mu\text{m}$  pulses was introduced by passage through a cell containing bromobenzene. Normal dispersion causing the 1.06  $\mu\text{m}$  pulse to emerge ahead of the 0.53  $\mu\text{m}$  pulse. From this point the experiment was essentially the same as Giordmaine's. Normal reflection of the pulses at a mirror, which formed the end wall of a cell of diphenylcyclopentadiene, caused the overlap of pulses within the cell producing the TPF track. The brightness of the overlap spot was proportional to the product of the pulse intensities, i.e.

$$I_F \propto I_{0.53 \mu\text{m}} I_{1.06 \mu\text{m}}$$

The 0.53  $\mu\text{m}$  pulses alone caused a weak fluorescence because of their low intensity, due to the inefficiency of SHG, while the 1.06  $\mu\text{m}$  pulses although of higher intensity were of the wrong wavelength to cause fluorescence. The sum frequency of the two however caused strong fluorescence.

Therefore by detuning the KDP crystal the amount of 0.53  $\mu\text{m}$  radiation produced, and hence the background fluorescence, could be reduced, while maintaining the product  $I[0.53 \mu\text{m}]I[1.06 \mu\text{m}]$ . Using this method the authors obtained contrast ratios of 10:1. The pulse durations were found to be  $\sim 3$  psecs. The advantage of this method lay in the fact that weak pulses or faint interpulse structure would not be lost in a high background radiation.

It was pointed out by Weber (14) that care must be taken in interpreting the results of a TPF experiment, because a similar fluorescence structure is obtained from the radiation of an ideally mode-locked laser and from a free running laser with the same oscillating bandwidth. He showed that a distinction could be made between the two cases by careful measurement of the contrast ratio, since for the ideally mode-locked laser the contrast ratio should be  $\sim 3:1$  and for the free running laser  $\sim 1.5:1$ .

Bradley et al (22) measured the output from a free running Nd: glass laser using a Rhodamine 6G (R6G) solution as the fluorescent medium, placed in a cell inside the laser cavity. The output was observed to consist of "spikes" of duration typically  $\sim 0.3$  psecs. The measured contrast ratio was found to be always less than 1.5:1.

The discrepancy between theoretical and experimentally observed contrast ratios was removed by Shapiro and Duguay (18). They used a triangular TPF configuration placed outside the laser cavity (FIG. 3(b)).

The cell containing the fluorescent medium was very thin  $\sim 28 \mu\text{m}$ , and fluorescence was monitored using a photomultiplier. As the cell was so thin its position had to be adjusted after each laser shot to enable complete plotting of the autocorrelation profile, since each single shot corresponded to only one value of the relative delay between the pulses, i.e. when the cell is positioned at the origin  $Z = 0$ , the relative delay between pulses is zero.

The experiment thus suffered the disadvantage of being multishot, and a function of the reproducibility of the laser.

In the experiment the outputs of both the mode-locked and free running Nd: glass laser were monitored. For the mode-locked laser, pulse durations of  $\sim 0.25$  psecs were observed with a contrast ratio of  $2.95 \pm 0.25:1$  compared to the theoretical value of  $3:1$ . For the free running case the contrast ratio was found to be  $1.4:1$  also in good agreement with the theory.

Bradley et al (23) showed that similar results could be obtained in a single shot using the triangular configuration outside the laser cavity. A 2cm cell was used containing a solution of R6G dye as the fluorescent medium and the resulting fluorescence profile was recorded photographically. The profile obtained is the upper microdensitometer trace of FIG.4 (NORMAL TPF). The width of the fine central spike was very sharp  $\sim 50$   $\mu\text{m}$  and approached the spatial resolution limit of the camera. A mode-locked Nd: glass laser was used and from the width of the TPF profile it was found that the output consisted of structure  $\sim 0.2 - 1.0$  psecs. The intensity step of X2.6 to the right of the trace of FIG.4 represents that portion of the field of view of the camera that was not covered by a neutral density filter of attenuation X2.6. From this result the contrast ratio was estimated to be  $\sim 2.5:1$  in fair agreement with theory. This experiment showed that the photographic process was not the reason why difficulty had been encountered previously in recording fine structure, and contrast ratios in agreement with theory, although as stated previously the spatial resolution limit of the camera was approached.

An experiment has also been described where a third order correlation function has been measured. This three Photon Fluorescence (3PF) experiment proposed by Rentzepis et al (21) measured the pulses from a mode-locked Nd: glass laser and found them to be in the range  $0.3 - 1.0$  psecs. In this case the

theoretical contrast ratios are 10: 1 for the ideally mode-locked laser and 2.5: 1 for the free running laser, (24, 25). The authors found that for their laser the contrast ratio was  $\sim 9: 1$  and that by reducing the intensity of the pulses background could be virtually eliminated.

Care must be taken in both the setting up and interpretation of TPF results. It has been suggested that small misalignments in setting up of TPF experiments which cause imperfect overlapping of the laser pulses may be responsible for low values of the contrast ratio, (15). Focussing and alignment of the recording camera in photographic TPF experiments is also critical since it may be required to focus on a region as narrow as 50  $\mu\text{m}$  (23).

The theory of TPF measurements states that the observed fluorescence is proportional to the square of the intensity of the optical pulse, however an intensity dependant quenching of the fluorescence profile peak has been observed causing marked reductions in contrast (19).

This quenching effect is shown in FIG.4 where a microdensitometer trace from a time integrated TPF display is shown to have its central spike reversed. The intensity step to the right is X2 and is used for contrast measurements. This reversal was observed by Bradley et al (19) when investigating the output of a mode-locked ruby laser using R6G and 9-10 diphenylanthracene (DPA) as the fluorescent media. Examination of the TPF patterns of DPA with a high speed TRW streak camera capable of 50 psec time resolution (26) showed the reversal to be most marked for the high intensity pulses near the centre of the train, with the normal TPF profile returning as the train neared its end where the intensity of the pulses is lower. For the R6G solution the profile was reversed in all cases. From this it was concluded that the effect was intensity dependant, and that the pulse intensity should be kept as low as is consistent with obtaining usable TPF records.

Because TPF measurements employ the recording of a correlation function of the pulse they also suffer from the loss of information about the original pulse shape which occurs with SHG techniques, and thus a pulse shape needs to be assumed before an estimate of the pulse duration may be obtained. While the TPF experiment is simpler to perform than the SHG measurement of pulse width, it suffers from a low contrast ratio which may obscure fine or interpulse structure, and care must be taken in the interpretation of results.

### 1.3. Ultra Fast Shutters

Other non-linear pulse measurement techniques based upon the optical Kerr effect and saturable absorption are essentially ultra fast shutters. Although the main application of ultra fast shutters has been in the measurement of excited state lifetimes (27, 28, 29), these techniques have also been used to measure the duration of laser pulses (30, 36, 37). Both the optical Kerr effect shutter and the saturable absorber shutter are based upon the 'excite and probe' technique in which a powerful optical pulse induces a time dependant variation in some characteristic of the medium employed, and this time dependant variation is monitored by the transmission of a weaker probe pulse through the medium.

#### 1.3.1 The Optical Kerr Effect

The optical Kerr effect is the birefringence induced in many isotropic media by an intense optical frequency field. That is the media exhibit different refractive indices in directions parallel and perpendicular to the electric field component of the optical pulse. The effect was first demonstrated by Mayer and Gires (32), and is particularly strong in liquids containing anisotropic molecules (31).

The essential experimental configurations for optical Kerr effect investigations are shown in FIG.5. In the configuration of FIG.5(a) the Kerr cell shutter K is opened by an intense gating beam, G, and simultaneously probed by a weaker portion of the same beam.  $P_1$  and  $P_2$  are crossed polarisers such that there is zero transmission to the detector D, before the arrival of the gating pulse G. Similarly there is zero transmission to D at

a time  $T_r$  after the gating pulse has passed.  $T_r$  is the characteristic relaxation time of the Kerr active medium used. Polariser  $P_1$  and  $P_2$  are oriented to transmit light polarised at  $45^\circ$  to the plane of polarisation of the gate beam. The transmission of the probe signal is then (33).

$$S = \frac{1}{2} \sin^2 (d\theta/2) \quad (1. 18)$$

$$\text{where } d\theta = (2 \pi L / \lambda_0) \cdot |\eta_{\parallel} - \eta_{\perp}| \quad (1. 19)$$

and  $\eta_{\parallel}$  and  $\eta_{\perp}$  are the refractive indices for probe light polarised parallel and perpendicular to the gating pulse.  $d\theta$  is the phase shift between probe light polarised in these directions,  $\lambda_0$  is the mean vacuum wavelength of the probe beam and  $L$  is the path length in the Kerr medium.

If the phase shift  $d\theta$  is small and the shutter relaxation time  $T_r$  is much shorter than  $T_g$  the gate pulse duration, then the shutter transmission  $S(t)$  is related to the temporal intensity  $I_g(t)$ , of the gate pulse by

$$S(t) = \frac{1}{2} \left( \pi n_2 / 2 \lambda_0 \right)^2 \cdot I_g^2(t) \quad (1. 20)$$

where  $n_2$  is the optical frequency Kerr coefficient.

The time integrated signal recorded by the detector  $D$ , is the convolution,

$$G(t) = \int_{-\infty}^{\infty} S(t) I_p(t) dt \quad (1. 21)$$

where  $I_p(t)$  is the intensity profile of the probe pulse. Thus in order to record the complete profile relative delays between the arrival of probe and gating pulses at the Kerr cell are introduced by means of the movable prism of FIG.5(a). The experiment is therefore multishot and a function of laser reproducibility. The time resolution of the method depends on the width of the function  $S(t)$  and ideally  $S(t)$  should be shorter than any pulse in the probe beam. In experiments using the configuration of FIG.5(a) however,  $I_g(t)$  and  $I_p(t)$  are from the same source and the signal actually recorded is proportional to the third order correlation function.

$$G^3(0, \tau) = \int_{-\infty}^{\infty} I^2(t) I(t+\tau) dt \quad (1.22)$$

where  $\tau$  is the relative time displacement between the two beams.

With a similar experimental arrangement to that of FIG.5(a) Dughey and Hansen (29) performed Kerr effect measurements on carbon disulphide ( $\text{CS}_2$ ) and nitrobenzene using a mode-locked Nd: glass laser of known pulse duration  $\sim 5$  psecs (FWHM). With  $\text{CS}_2$  as the Kerr medium they plotted the transmission of the cell as a function of the relative delay between gate and probe pulses. A sharp symmetrical curve of FWHM  $\sim 8$  psecs was obtained. Since the relaxation time of the Kerr effect in  $\text{CS}_2$  is less than 2 psecs (34) this represented the prompt response of the system. For nitrobenzene however a curve with an exponential tail was observed, which allowed an estimate of  $T_r$  to be made, of the order  $32 \pm 6$  psecs. The problem of light scattered from the intense gating pulse, on its passage through the cell, reaching the detector was overcome in the above experiment by converting the probe pulse to the second harmonic frequency of the gate pulse and using an appropriate filter. This however resulted in the duration of the probe pulse becoming less than that of the gate pulse.

The big disadvantage of the experiment of FIG.5(a) is that it is multishot. A more convenient arrangement whereby the profile may be obtained in a single shot is shown in FIG.5(b). In this case probe and gate beams intersect orthogonally in the Kerr medium. The gating beam whose depth is kept as small as possible so as not to impair time resolution creates a region of birefringence as it traverses the cell. This is equivalent to a narrow slit moving across the cell at the velocity of light in the medium. The probe beam is expanded so that its intensity is spatially uniform across the whole cell. The travelling shutter moving across the Kerr cell converts the temporal variation of the probe pulse intensity into a spatial variation which is recorded by the camera. The scattering of gate pulse light is also a problem with this method but less so than the previous case.

Using an arrangement similar to this the duration of pulses from a mode-locked dye laser has been measured (35). Pulse half widths of  $\sim 7$  psecs were obtained. Similar arrangements have been utilised to measure both relaxation times and the durations of light pulses which are long compared to laser pulses (27, 30).

In an experiment due to Duguay et al (36) the Kerr cell has been used as the shutter for a conventional camera, allowing the photograph of a picosecond pulse propagating through a diffusing cell to be taken. The experimental arrangement is shown in FIG.6. The second harmonic radiation of the Nd: glass laser is passed through a cell C, containing a colloidal suspension of milk particles. The fundamental frequency radiation of the laser is used to gate the Kerr cell containing CS<sub>2</sub>. By adjustment of the position of the prism the gate pulses can be synchronised to the incidence of the scattered radiation from C, and photographs of the picosecond pulses may be directly taken using an ordinary camera. Here again the operation of transforming the temporal profile of the pulses into a spatial profile is carried out, this time by passage of the pulses through a diffusing cell. The finite depth of the beam in the diffusing cell causes shearing of the image recorded in the final photographs. This as well as the finite angular aperture of the rays passing through the Kerr cell must be taken into account when an evaluation of the time resolution of the method is made. As the shutter time of the Kerr cell depends on the squared intensity of the gate pulse, eqn. (1.20), then for a 10 psec pulse the exposure time is ~ 7 psecs. Using this method Duguay has measured pulses of duration 7 - 15 psecs.

### 1.3.2 Saturable Absorber Shutters

Methods of picosecond pulse measurements using saturable absorber shutters are very similar to the Optical Kerr effect methods. The experimental arrangement is that of FIG.5(a) with the polarisers removed and the Kerr cell replaced by a cell containing a saturable absorber. The method is a good example of the 'excite and probe' technique. An intense gating pulse is used to deplete the ground state population of the absorber raising the molecules to higher excited electronic energy states. In this condition the absorber transmission for a probe pulse is high, and the transmission decreases as the ground state repopulates. The shutter time of the absorber is defined as the time for the transmission to fall to 1/e of its peak value. Provided the gating pulse is sufficiently intense the aperture time of the shutter may be made substantially shorter than the relaxation time of the absorber.

Mourou et al (38) used DDI in methanol as a saturable absorber to measure the pulses from a mode-locked ruby laser, which indicated that the pulses were of  $\sim 10$  psecs duration. As the absorber had a relaxation time  $\sim 10$  psecs the shutter time was  $\sim 2$  psecs (33) and so the shutter action could be assumed to be prompt.

#### 1.4. Linear Measurement Techniques

A linear measurement technique has been described previously (1.2(1)) utilising a Michelson interferometer. This method however only yields a lower limit for the pulse duration in contrast to the linear methods in this section which directly yield estimates of the actual pulse duration, providing the pulse duration exceeds the resolution limit of the measuring system.

The methods described are all based upon the response of a photocathode to a pulse of light. While it has been shown that the response time of the photoelectric effect is  $\sim 10^{-14}$  secs (39), the temporal resolution of methods based upon this effect is  $\sim 10^2 - 10^4$  times greater.

##### 1.4.1. Photodiode - Oscilloscope Combinations

Presently available photodiodes typically have rise times of 100 psecs (65, 66). The relatively slow response being due to the many different paths taken by electrons, liberated from the photocathode, to reach the anode. A prompt electron signal at the photocathode will be considerably extended in time when it reaches the anode due to this spread in path lengths. The same limitation to the risetime occurs in photomultipliers, but in their case the risetime is further limited by a delay in the secondary emission process and also the path distance between the photocathode of the photomultiplier and its anode is greater than that of the photodiode.

The fastest oscilloscopes available have bandwidths  $\sim 5$ GHZ, corresponding to risetimes  $\sim 70$  psecs (40, 41). The photodiode - oscilloscope combination thus provides a convenient method of pulse measurement with  $\sim 150$  psec temporal resolution. A recently

reported 10 GHz bandwidth photodiode and 5GHz oscilloscope of sensitivity 3v/cm together provide a risetime of  $\sim 70-80$  psecs (41). The limitation to oscilloscope risetimes lies in the need for very fast timebase sweeps if these short duration events are to be satisfactorily displayed. Very fast timebase sweeps mean that the electrons exciting the phosphor screen must be of high energy since the current which can be drawn from the electron gun is limited. High energy electrons necessitate a high accelerating voltage and this in turn leads to a reduction in the deflection sensitivity of the oscilloscope. To restore the deflection sensitivity an amplifier must be used and it is the bandwidth of the amplifier which sets the risetime limit of the oscilloscope. The Tektronix 519 oscilloscope which does not use a vertical amplifier has a bandwidth  $\sim 1$  GHz. The bandwidth in this case is limited by the bandwidth of the co-axial cable, used to transport the photodiode voltage pulse to the oscilloscope, and that of the deflection circuitry.

If the source of the ultra short pulses is continuous, as is the case with continuous working (CW) lasers, then a sampling oscilloscope may be used. A sampling oscilloscope unit may have a rise time as short as 25 psecs and in this case the rise time of the combined system is limited by that of the photodiode to around 100 psecs (42, 43).

A picosecond optical sampling oscilloscope has also been reported (44). The pulse to be displayed is optically sampled and each sample relayed via a different length of fibre-optic line to a photomultiplier - oscilloscope combination. The envelope of the displayed samples represents the profile of the laser pulse. The delay between each optical sample was 3.9 psecs and from the real time display, via the 3 nsecs rise time photomultiplier, on the 0.8 ns risetime oscilloscope the pulse duration could be estimated. In the experiment a mode-locked Nd: glass laser was estimated to have a pulse duration  $\sim 17$  psecs.

#### 1.4.2. Electron - Optical Chronography

While photodiode - oscilloscope combinations provide a convenient means of studying events of  $\sim 100$  psecs duration, in order to accurately study events lasting less than  $\sim 10$  psecs it is

necessary to use a device whose temporal resolution limit is considerably lower. This order of resolution may be achieved using the method of electron-optical chronography or high speed photography.

The basis of the method is that an optical signal may be readily converted into an electron image of that signal by use of a suitable photocathode. The electron signal may then be conveniently focussed, deflected, accelerated, and switched on or off by the application of an electric or magnetic field. The original optical signal may be faithfully reproduced by accelerating and focussing the electron image onto a phosphor screen.

The manipulation of the electron signal is carried out in a device known as an image tube. The image tube derives from the image convertor tube used to convert infra-red radiation to visible radiation by the use of an infra-red sensitive photocathode and a phosphor emitting light in the visible region.

The use of the image tube in electron-optical chronography was first proposed in 1956 by Zavoiskii and Fanchenko (45). Since then the image tube has been used in two distinct modes, a) the framing mode and b) the streak mode. When nanosecond time resolution is adequate the image tube may be operated in the framing mode, but for picosecond resolution the image tube must be used in the streak mode.

An image tube camera designed for operation on a nanosecond time scale and developed by Huston is shown in FIG.7 (46).

Electron images of the light incident upon the photocathode P/C are electrostatically focussed by means of voltages applied to the cone C and the anode A onto the output phosphor screen, P. To shut off the image at the phosphor a sinusoidal voltage is applied to the shutter plates SP to deflect the electron image away from the aperture AP. The time the electron image spends in the aperture region is the frame or exposure duration. To enable stationary images to appear on the output phosphor an opposing sinusoidal voltage is applied to the compensating plates CP. During the

time when the image is off the screen a staircase voltage is applied to the deflection plates DP such that when the beam next sweeps across the aperture region the electron image is deflected to a different portion of the phosphor screen.

Huston's camera was capable of recording between eight and sixteen sequential images each with an exposure or resolution time of  $\sim 10$  nsecs at a framing rate of  $2 \times 10^7$  frames per second. The exposure or resolution time was limited by the bandwidth of the voltage deflection circuitry. More recently a framing camera having an exposure duration of  $\sim 1$  nsec and a framing rate of  $6 \times 10^8$  frames per second has been reported (47).

Image tube cameras operated in the framing mode are useful for the study of luminous events such as spark discharges (39) which occur on a nanosecond time scale, however for the study of sub nanosecond events such as mode-locked laser pulses the image tube camera must be operated in the streak mode.

The essential components of an image tube streak camera are shown in FIG.8. Light from the event under study illuminates a narrow slit at the front of the camera. The lens focusses the image of the slit onto the photocathode of the image tube. The number of photoelectrons liberated by the photocathode is proportional to the intensity of the optical signal, and because of the prompt response of the photocathode the electron signal accurately reproduces the temporal intensity variation of the original signal.

Acceleration and focussing of the electron signal is carried out by the application of voltages to the electrodes C and A as in the framing mode. In the static case with equal voltages applied to the deflection plates DP (originally the shutter plates in the framing mode) a focussed image of the slit appears at the centre of the phosphor screen. In streak mode operation a very fast risetime high voltage ramp is applied to the deflection plates causing the electron beam to be swept or streaked across the face of the phosphor screen at velocities approaching that of light. The temporal intensity variation of the original light signal is

thus converted to a spatial intensity variation at the output phosphor. Photographic records of this streaked slit image may then be made and from these the duration of the luminous event may be determined.

The ultimate time resolution of image tube streak cameras has been shown to be limited by the initial electron energy spread near the photocathode (45, 39), which leads to a photoelectron transit time dispersion in the image tube. The transit time distribution has a half width  $\Delta\tau_d$  given by

$$\Delta\tau_d = m \Delta U / eE \text{ secs} \quad (1. 23)$$

where  $\Delta U$  is the half width of the initial electron velocity distribution and  $e$  and  $m$  are the electronic charge and mass. From eqn. (1. 23) it is clear that the electric field strength  $E$  near the photocathode must be maximised in order to reduce  $\Delta\tau_d$ . In other words the electrons need to be accelerated quickly to a velocity sufficient to make their small initial velocity differences negligible. Also it can be seen that reduction of the initial electron velocity spread  $\Delta U$  will reduce the value of  $\Delta\tau_d$ .

The value of  $\Delta U$  for a particular photocathode depends upon the wavelength of the illuminating light. The variation of  $\Delta U$  with wavelength for a Ag-O-Cs (S1) photocathode is shown in FIG.9 (48). For cathode illumination by 1.06  $\mu\text{m}$  radiation the electron energy spread has a half width  $\sim 0.3$  ev. If the desired limit on the transit time dispersion  $\Delta\tau_d$  is  $\sim 10^{-12}$  secs then the value of the field  $E$ , required near the photocathode may be found using the relationship below (45) which is another form of eqn. (1. 23).

$$\Delta\tau_d = 7.8 \times 10^{-11} \cdot \left( \frac{\Delta E_n}{E} \right)^{\frac{1}{2}} \text{secs} \quad (1. 23a)$$

where  $\Delta E_n$  is the halfwidth of the photoelectron energy distribution in electron volts, and  $E$  is the electric field strength in CGSE units. The above expression yields a value of  $\sim 40$  esu or 12kv/cm for the field near the photocathode. Such a high value field may be achieved by positioning a fine mesh planar electrode near the photocathode to which a high voltage may be applied. A fine mesh electrode  $M_1$  is shown in the image tube sketch of FIG.8. As can be seen from FIG.9 if the wavelength of the illuminating radiation is tuned so that the photocathode operates near cut off then the electron energy distribution is reduced and a further reduction in the value of  $\Delta\tau_d$

may be achieved.

Thus it can be seen that to produce an image tube streak camera capable of operating with picosecond resolution it is necessary to produce a high extraction field near the photocathode. In practice the value of the extraction field which can be used is limited by insulation breakdown between the mesh and photocathode. It is also helpful to match the wavelength of the illuminating radiation to near the long wavelength cut off value of the photocathode to further reduce the limit set by photoelectron transit time spread.

The temporal resolution of a streak camera does not however depend only upon the value of  $\Delta T_d$ , although this is a major factor, but also upon the streak resolution limit  $\Delta T_s$ . The streak resolution limit is the time taken to displace the image by one resolution element at the output phosphor, in streak mode operation. If the dynamic spatial resolution under streak conditions is  $\delta$  where  $\delta$  is expressed in line pairs per cm (Lp/cm) and the sweep velocity of the electron image across the phosphor screen is  $v$  cm/sec, then  $\Delta T_s$  is given by,

$$\Delta T_s = 1/v \delta \quad \text{secs} \quad (1.24)$$

For the camera pictured in FIG.8 typical values for  $v$  and  $\delta$  are  $10^{10}$  cm/sec and 50 Lp/cm respectively. These values yield a streak resolution limit of  $\sim 2$  psecs (49, 61). From eqn.(1.24) an increase in the streak writing speed and the dynamic spatial resolution should lead to a reduction of the limit set by  $\Delta T_s$ . The value of  $\delta$  however is a constant for a particular image tube, and a limit to the value of  $v$  which can be used is set by the sensitivity of the image recording process. Beyond a velocity of  $10^{10}$  cm/sec there arises the problem of obtaining sufficient light output from the image tube phosphor to enable photographic records of the streaked slit image to be made. This can not be overcome simply by drawing more current from the photocathode since at values of current well below the photocathode saturation current

the image is found to blur or saturate. In this case the spatial resolution of the camera deteriorates appreciably. Also at high photocurrents the response of the photocathode is no longer linear and space charge effects begin to limit the temporal resolution (54 - 56).

In order to overcome these problems an image intensifier (61) is used to boost the light output from the image tube phosphor and thus enable the photocurrent drawn to be reduced. It is only necessary for the intensifier to preserve the spatial resolution of the original signal and to relay it without distortion, at a greater intensity to the recording camera.

From the photographic record of the streaked slit image microdensitometer traces may be made. If the event under study is a laser pulse then the recorded half width (FWHM)  $\Delta\tau_r$  of the microdensitometer trace is related to the transit time dispersion  $\Delta\tau_d$  and the streak resolution limit,  $\Delta\tau_s$  by,

$$\Delta\tau_r^2 = \Delta\tau_d^2 + \Delta\tau_s^2 + \Delta\tau_p^2 \quad (1. 25)$$

where  $\Delta\tau_p$  is the actual pulse half width (51), and the pulses are assumed to be of Gaussian shape. The width of the input slit to the camera is always set such that it is less than a spatial resolution element and hence the time to scan the slit is negligible compared to the time to scan a resolution element. Hence the limit set by the slit width is neglected in the above expression.

The function  $(\Delta\tau_s^2 + \Delta\tau_d^2)^{\frac{1}{2}}$  is known as the camera instrumental function and it is the half width of this function which defines the camera temporal resolution limit. For accurate recording of pulse durations it is necessary for  $(\Delta\tau_s^2 + \Delta\tau_d^2)^{\frac{1}{2}} \ll \Delta\tau_p$ . Early streak cameras had half widths in the range 20-60 psecs mainly because of the low value of electric field near the photocathode (51 - 53). With the introduction of the planar mesh electrode near the photocathode half widths of less than 10 psecs became possible (49, 50). Presently available cameras have half widths in the range 2-3 psecs (59, 62) and the camera of FIG.8 due to Bradley et al (57, 59, 61)

operated with an extraction field of  $\sim 7000$  v/cm and with  $v$  and  $\delta$   $10^{10}$  cm/sec and 50 Lp/cm has a half width  $\sim 2.5$  psecs. Therefore at present it is not possible to accurately measure pulse durations less than  $\sim 2$  psecs with electron-optical streak cameras because of the limitations due to transit time dispersion and streak resolution. In chapter 2 an improved version of the image tube camera of FIG.8, with a lower transit time dispersion and greater streak resolution will be described.

Streak cameras have been used extensively to measure the durations of pulses from several sources. Pulses from mode-locked, ruby, Nd: glass, CW dye and pulsed dye lasers have been measured (49, 50, 58-61) using a camera similar to that of FIG.8. Other designs of streak cameras have been used in the measurement of pulses from mode-locked Nd: glass lasers. Schelev et al (48) employed a camera based upon an RCA C73435 image tube for this purpose. However a combination of low extraction field (3600 v/cm) and dynamic spatial resolution (1.3 Lp/mm) meant that the camera half width was  $\sim 5$  psecs. Basov, et al (62) and Frolov and Fanchenko (63) have reported a camera using a helical sweep, produced by an X band microwave resonant cavity system and a simultaneous linear sweep, which gives a long total recording time of 15 - 20 ns (c.f. the camera of FIG.8 which with a 5 cm sweep length at  $10^{10}$  cm/sec gives a recording time  $\sim 0.5$  ns), with a writing speed of  $(4.5 - 6) \times 10^{10}$  cm/sec. A low extraction field value however limits the instrumental resolution to  $\sim 2$  psecs, and the use of a point image instead of a slit reduces the information available making microdensitometry and the interpretation of results difficult. Butslav et al have more recently reported a streak camera with a linear sweep velocity  $\sim 2 \times 10^{10}$  cm/sec and an extraction field of  $\sim 20$  kv/cm (67). The dynamic spatial resolution of the image tube was the limiting factor in this case and the authors claimed a resolution limit of  $\sim 1$  psec with this device.

#### 1.5. Summary of Ultra Short Pulse Measurement Techniques

In conclusion to this chapter it is helpful to summarize the relative merits of the most commonly employed techniques mentioned

in previous sections. The most popular non linear methods are those of SHG and TPF together with the optical Kerr effect. The SHG technique is very sensitive and has found its most valuable application in the study of CW laser pulses (8, 9). It has the drawback however of being multishot and hence a function of laser reproducibility. The preparation of SHG crystals is time consuming and their orientation critical. SHG methods have a potential resolution limit  $\sim 1$  psec (20).

Optical Kerr effect methods are simpler, but to obtain an appreciable degree of birefringence it is necessary to use a medium such as  $\text{CS}_2$  which has a large Kerr coefficient but a relaxation time of  $\sim 2$  psec, and this therefore limits the resolution of the method (28).

TPF methods have the advantage of being easier to perform and if carried out carefully have the capability of  $\sim 0.2$  psec resolution (23). The interpretation of TPF results however depends greatly on the accurate measurement of the contrast ratio.

All three methods, TPF, SHG and the optical Kerr effect suffer from the disadvantage of requiring high power pulses for their efficient operation and are thus relatively insensitive to weakly luminous phenomena. They are all also based upon the measurement of a higher order correlation function which means that information about the original pulse envelope is lost in the measuring process.

The method of electron optical chronography, the streak camera in particular, provides a linear method for the direct observation of ultra short optical events of high or low intensity. The streak camera has been used to measure low intensity fluorescence (35,58), and interpulse energy in laser pulse trains  $\sim 10^4$  times less than that in the pulse (64).

The temporal resolution of presently available streak cameras of  $\sim 2$  psec (59, 62) makes the device an attractive diagnostic tool for the direct and unambiguous recording of ultra short pulses of varying intensities. Methods by which the temporal resolution of the instrument may be further reduced to enable the recording of pulses of durations less than  $\sim 2$  psecs will be discussed in the next chapter.

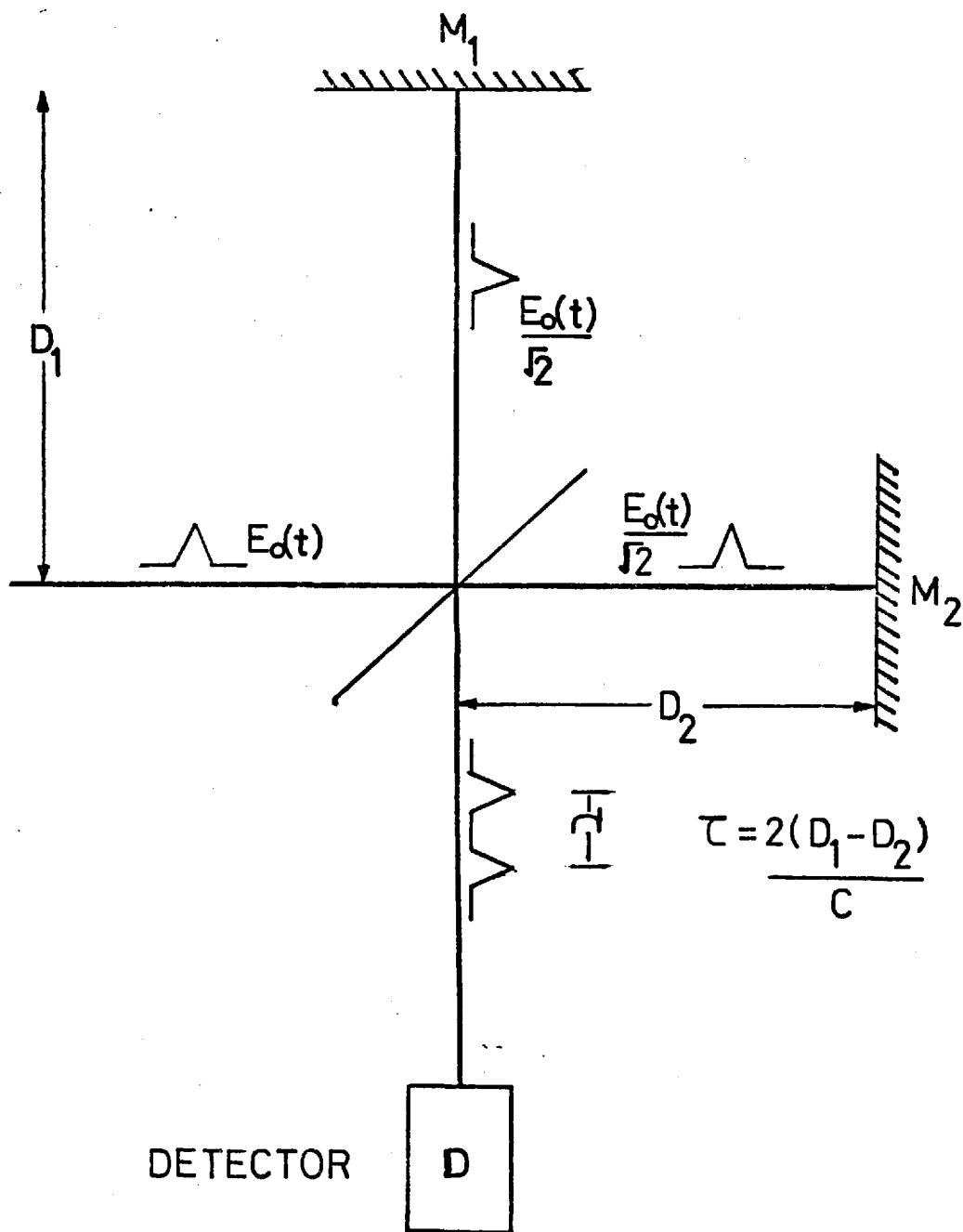


FIG. 1

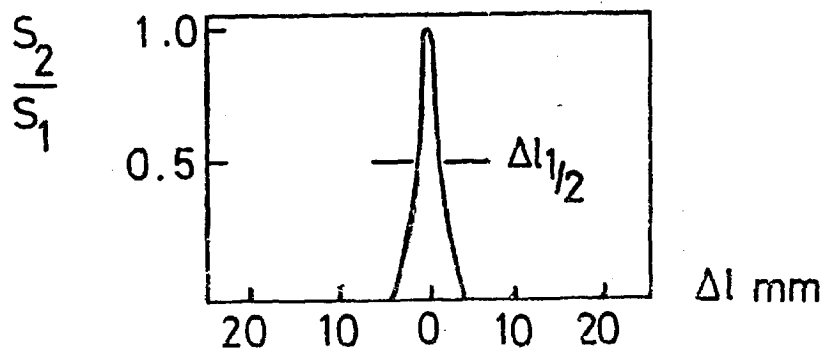
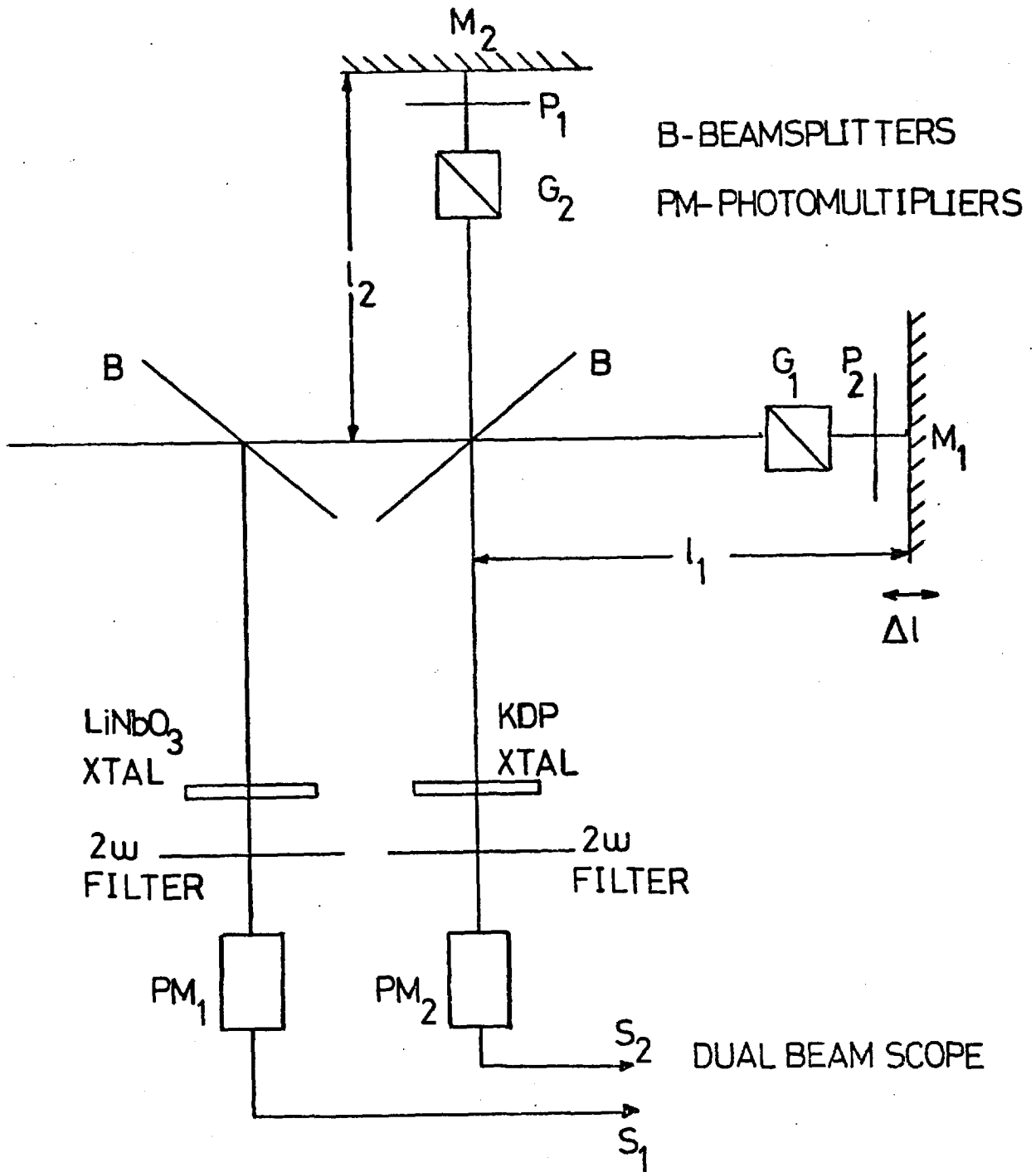
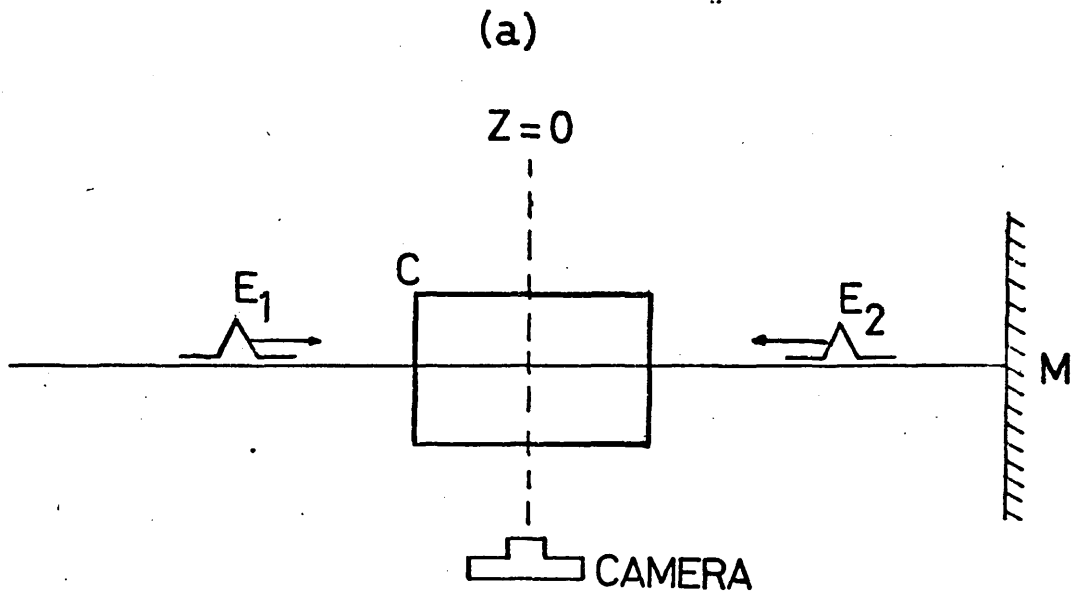


FIG. 2



C-CELL CONTAINING FLUORESCENT MEDIUM

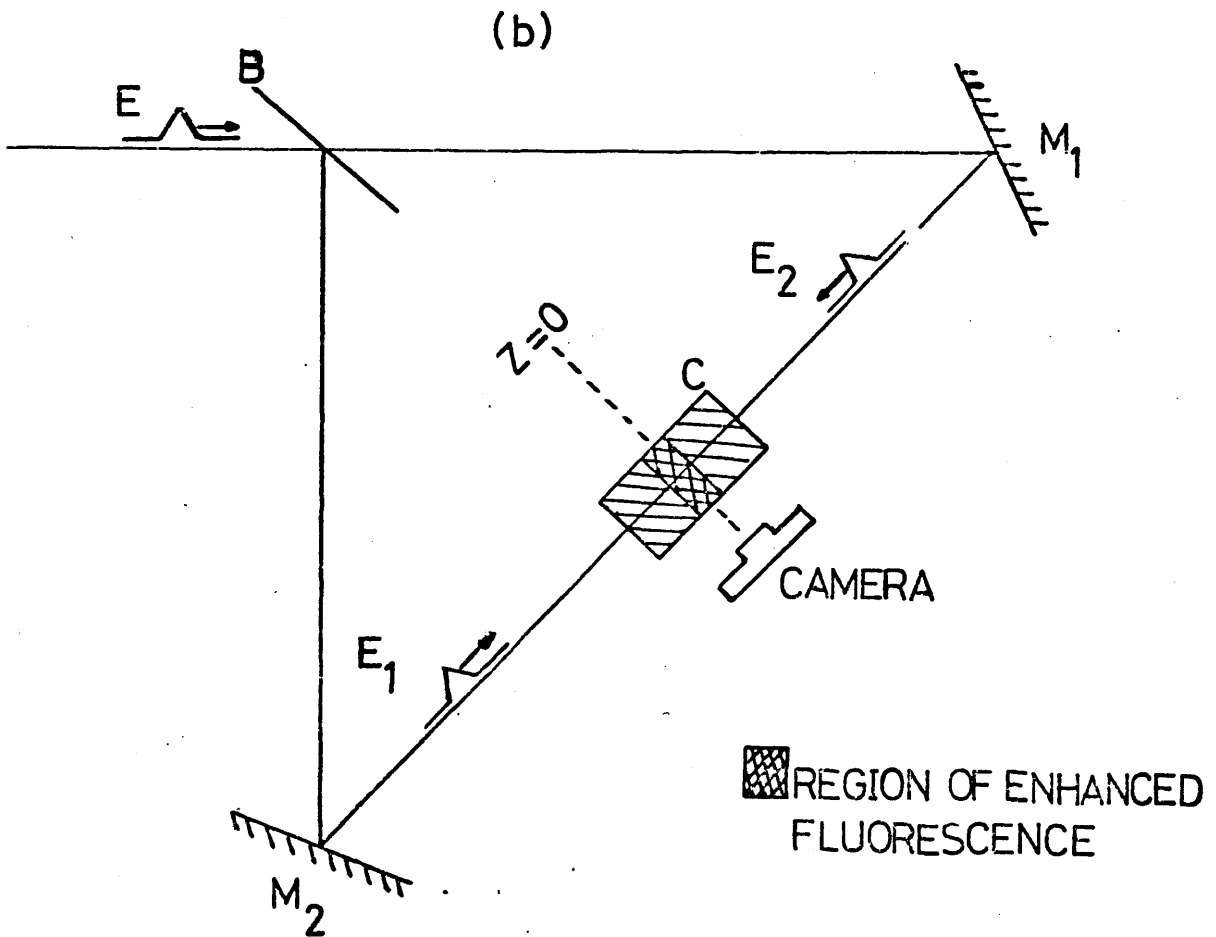
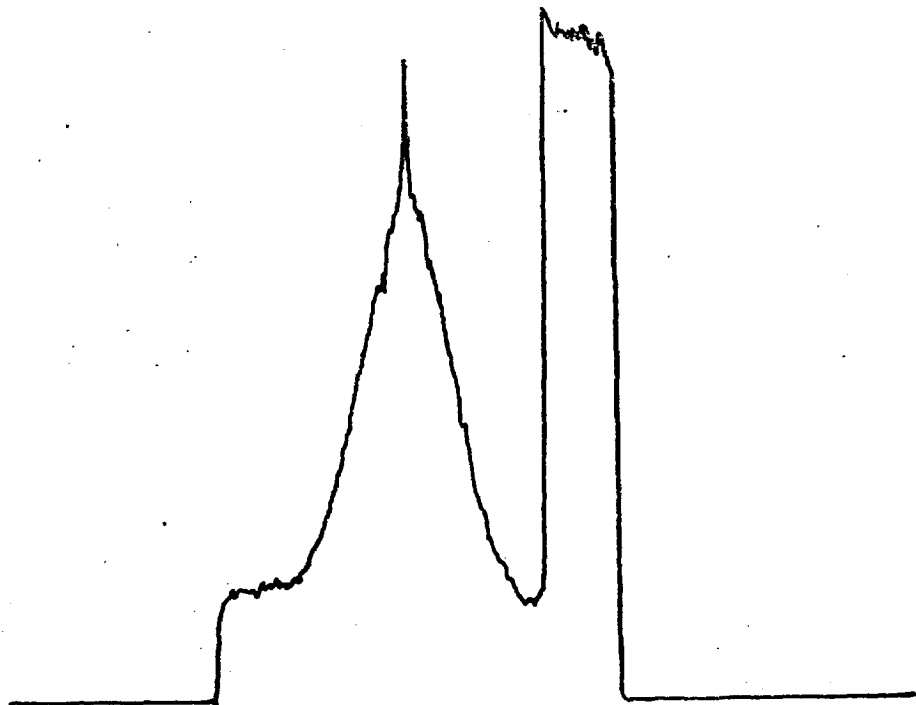
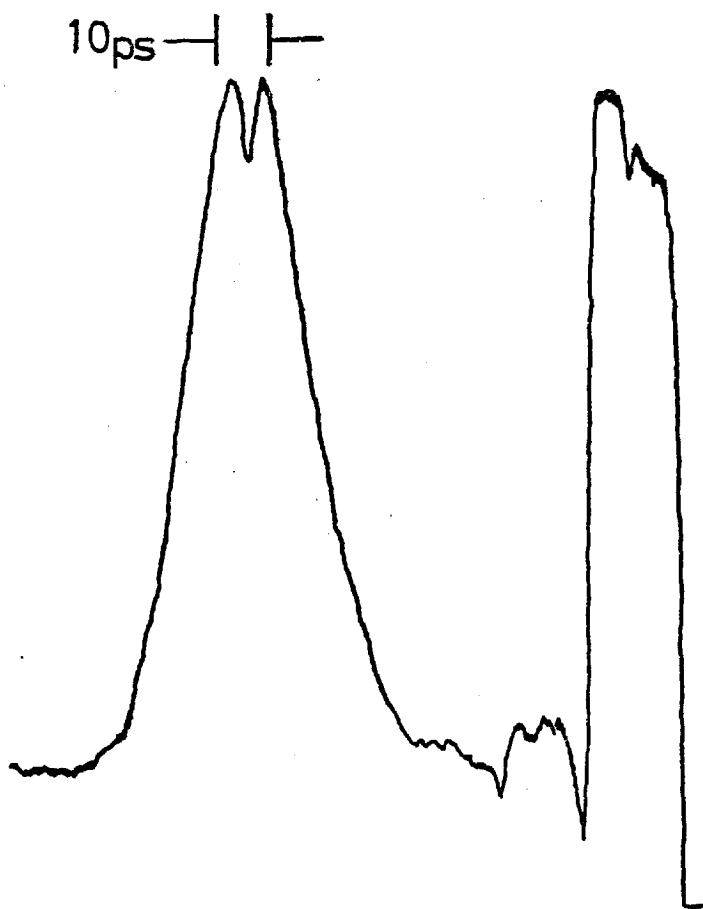


FIG. 3



NORMAL TPF



QUENCHED TPF

FIG. 4

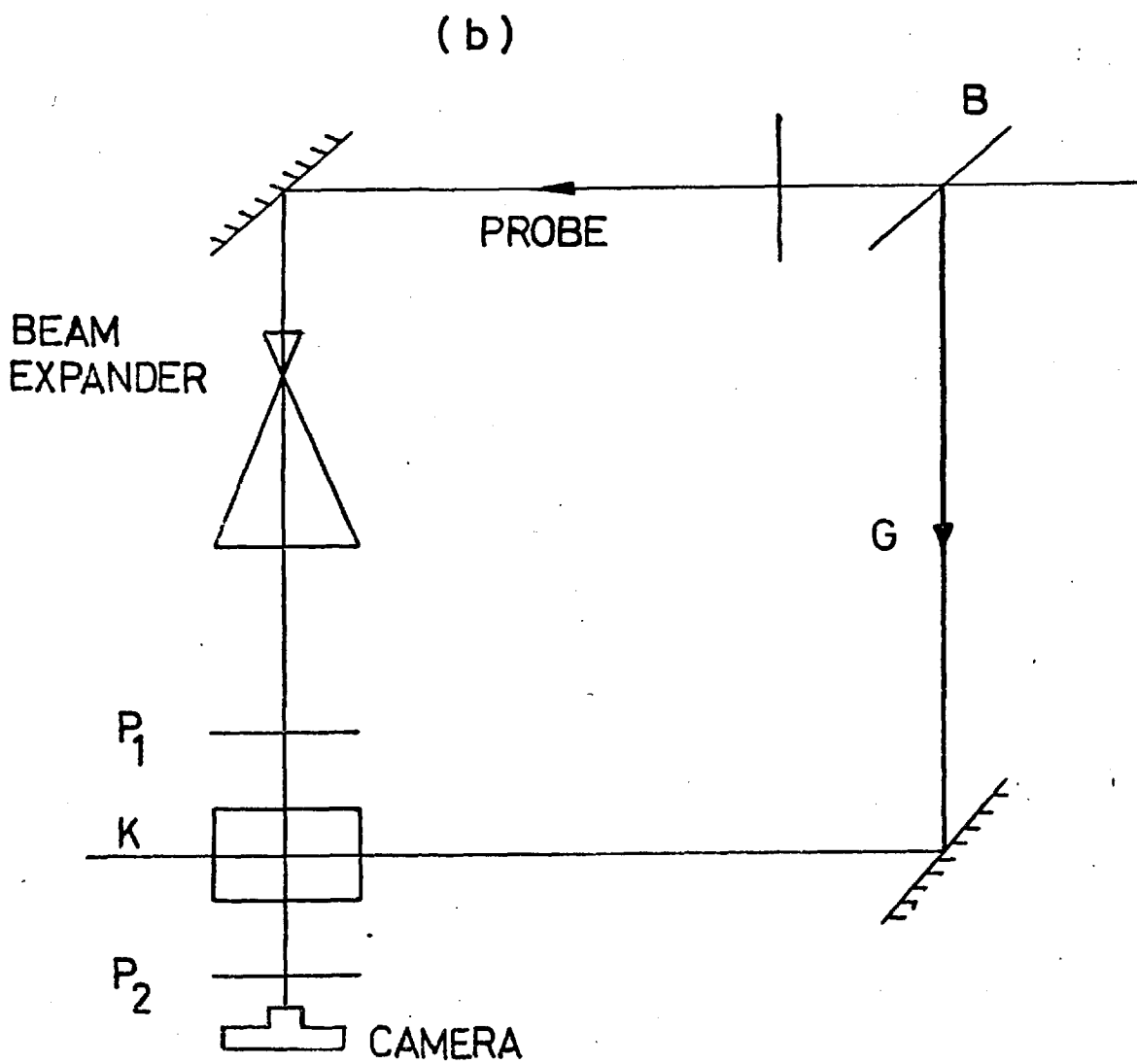
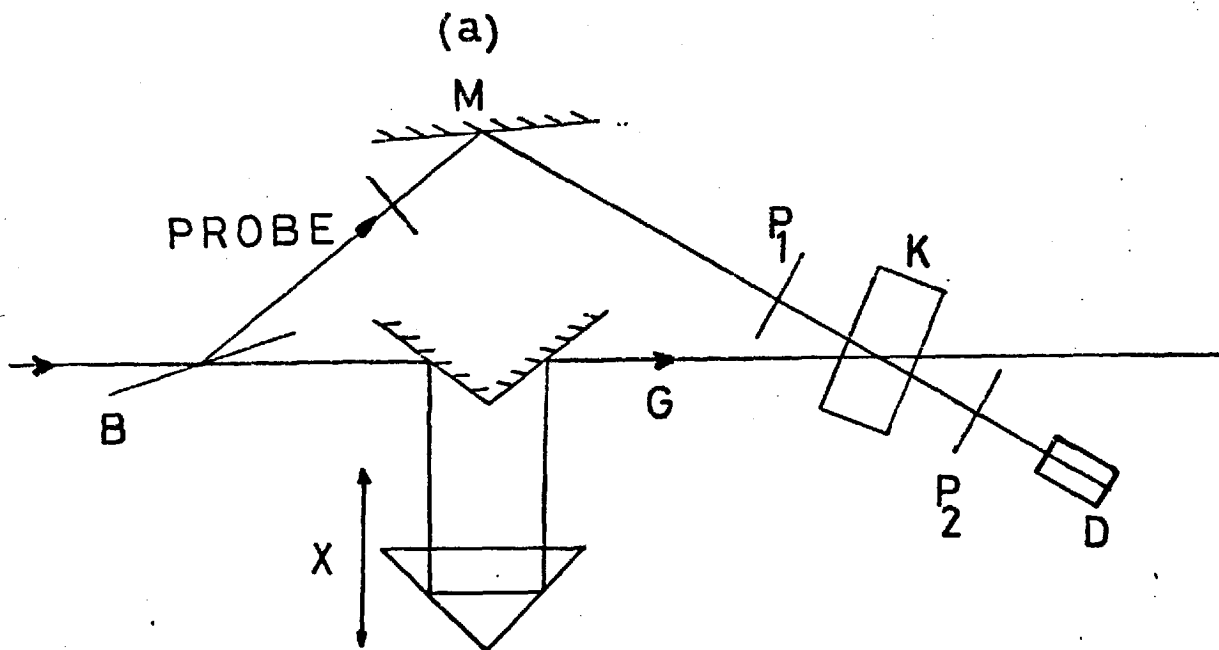
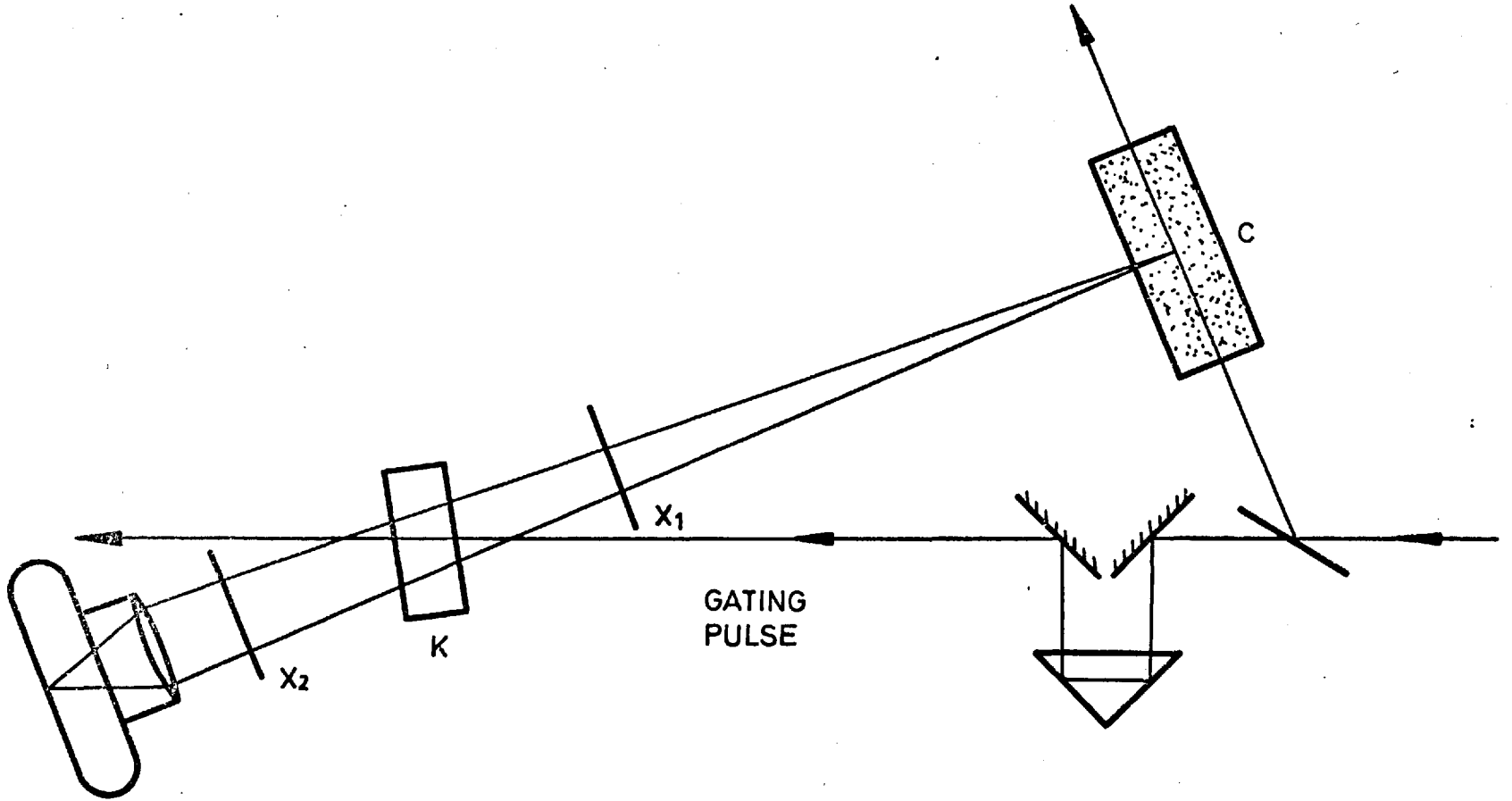
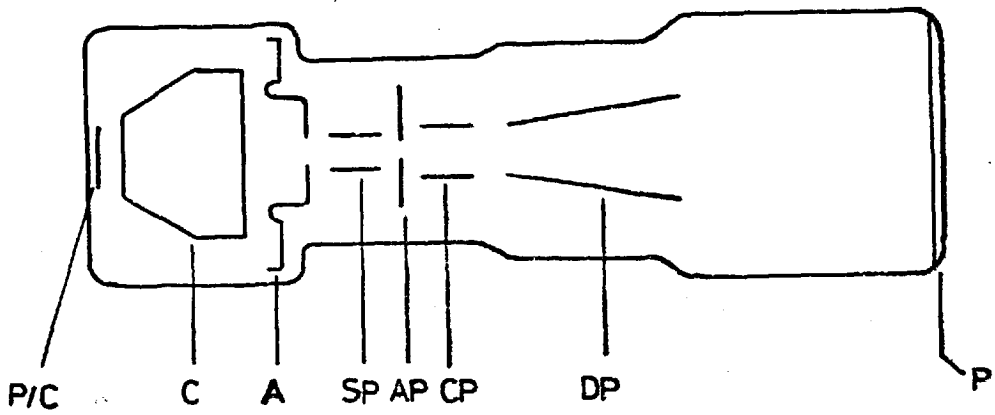


FIG. 5

FIG. 6

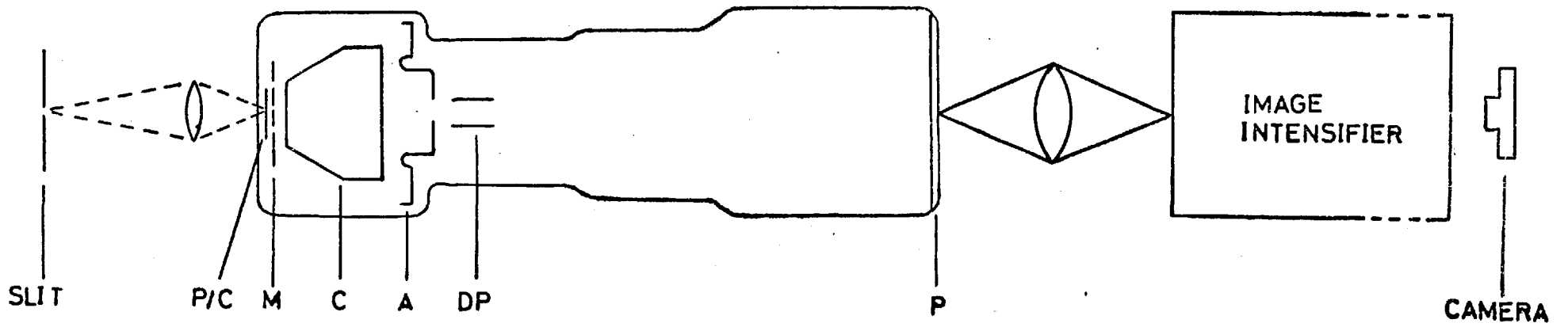




DP - DEFLECTION PLATES SHOWN 90° OUT OF POSITION

FIG. 7

FIG. 8



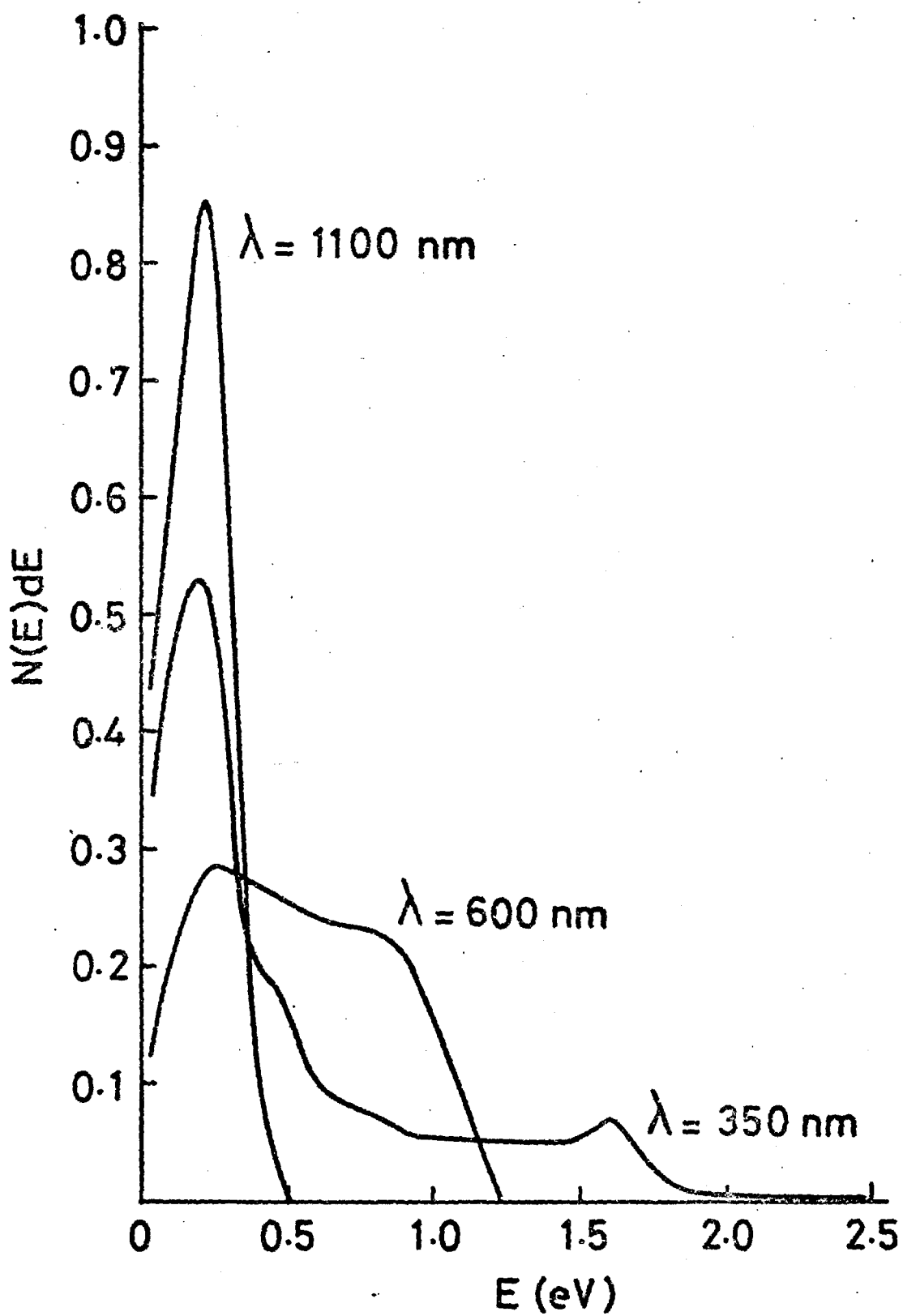


FIG. 9

## CHAPTER 2

### THE PHOTOCRON I STREAK CAMERA

#### 2.1. INTRODUCTION

It was shown in Chapter 1 that electron-optical chronography provides a direct and unambiguous method for the measurement of ultra short light pulses. A camera has been developed from the framing camera of section 1.4.2, capable of resolving events on a picosecond timescale and this camera is described in more detail in this chapter.

The static and dynamic characteristics of the streak camera system are discussed, and the methods of providing the necessary focussing and deflection voltages are described. Image intensification is needed when streak cameras are operated for picosecond time resolution and the reasons for and the methods whereby this is provided are also described in greater detail.

Experiments carried out using this streak camera have shown it to be capable of a temporal resolution of  $\sim 2$  psecs (59, 62) and demonstrated its value as a diagnostic tool in laser pulse measurements. The streak camera described in this chapter will be called the Photochron I streak camera. In chapter 3 a streak camera, the Photochron II, a modified version of Photochron I and capable of a lower temporal resolution will be described.

#### 2.2. The Photochron I Image Tube

The image tube of the Photochron I streak camera evolved from the framing camera of FIG.7. This framing camera could also double as a streak camera (46) by applying a fast risetime voltage ramp to the deflection plates, D.P. to streak the image across the phosphor screen. Bradley et al (73) modified the image tube of the framing camera by the insertion of a fine mesh electrode close to the photocathode ( $\sim 3\text{mm}$ ) to which a voltage  $\sim 1$  Kv could be applied. The deflection voltage ramp

was provided by a laser triggered spark gap, which gave a streak writing speed of  $\sim 3.5 \times 10^9$  cm/sec at the phosphor screen. These modifications allowed the streak camera to operate with a temporal resolution of less than 10 psecs.

This image tube was further modified (49) by removal of the aperture, AP, compensating plates, CP, and the use of the smaller shutter plates SP, as the deflection plates (FIG.8). The smaller shutter plate dimensions (2.0 cm long by 2.5 cm wide with 0.5 mm separation) gave a faster response to the applied voltage, thus increasing the writing speed at the phosphor. In addition the position of these plates further back in the tube increased the deflection sensitivity by  $\sim 40\%$ . By replacing the laser triggered spark gap by an avalanche transistor - krytron switch to generate the ramp voltage, the streak writing speed was increased to  $\sim 10^{10}$  cm/sec. This together with a 2 Kv potential at the fine mesh electrode enabled the camera instrumental function to be reduced to  $\sim 3.5$  psecs. The image tube in this form is the Photochron I image tube of FIG.8.

The photocathode of the Photochron I is located a few mm behind the front face of the image tube's glass envelope. The photocathode consists of photoemissive material deposited on a suitable substrate which allows transmission of the illuminating radiation. A metal ring  $\sim 3$  cm in diameter supports the substrate and electrical contact to the cathode is made via this ring. The fine mesh electrode (300 mesh/cm) is similarly supported so that the distance between the mesh and cathode emissive surface is  $\sim 3$  mm. An effective cathode emissive surface diameter of  $\sim 1$  cm and a mesh diameter of  $\sim 2.5$  cm ensures a uniform electric field over the cathode area. The mesh is situated  $\sim 2.5$  mm from the cone of the image tube (FIG. 23 (a)).

The cone and anode electrodes of the tube are electrically isolated and the interior tube walls are coated with a thin

layer of aluminium from the anode back to the phosphor screen. This ensures that the anode to phosphor screen is an equipotential region, or drift space as far as electrons are concerned. The anode aperture is  $\sim 4\text{mm}$  in diameter and the deflection or streak plates are situated  $\sim 5\text{mm}$  from the anode in the drift space. Both deflection plates are electrically isolated from the drift space. Connections to these electrodes are made via metal pins in the tube glass walls, and in the case of the phosphor screen and cone via metal flanges. A silver activated zinc sulphide P11, phosphor screen is used which has a thin backing of aluminium to prevent back scattering of phosphorescence and to encourage forward light emission. The whole tube is evacuated to a pressure of  $\sim 10^{-8}$  Torr.

Equal anode and screen potentials of 18 Kv are used in the Photocron I image tube. For tube operation under static conditions the same potential (18 Kv) is applied to both deflection plates and the image thus appears at the centre of the phosphor screen. With the cone at earth potential it is found that for each value of mesh potential only one photocathode potential will give a focussed image on the phosphor screen. To determine the focussing conditions of the tube a resolution test pattern consisting of pairs of bright and dark lines of increasing spatial frequency was imaged onto the photocathode, and the mesh and cathode potentials were varied for optimum focussing. The focussing characteristic obtained with anode to screen potential  $\sim 18$  Kv and cone 0v is shown in FIG. 10 (a) (61).

It was also noted that as the mesh potential increased so did the size of the image at the output phosphor. This result is consistent with one obtained by Driard et al (74), who using a fine mesh electrode placed close to a photocathode could control the size of the image at the output by variation of the mesh potential alone. The electron-optical magnification in the Photochron I image tube from cathode to phosphor as a function of mesh voltage (for corresponding values of cathode potential at focus) is shown in FIG. 10 (b). The spatial resolution at

the photocathode was approximately constant at 30 Lp/mm for mesh voltages in the range 500 - 2000 volts. Thus at a mesh voltage of 2000 volts the spatial resolution at the output phosphor was between 8 and 9 Lp/mm since 30 Lp at the photocathode now occupied 3.5 mm at the phosphor. When the focussed image was deflected across that part of the phosphor screen used in streak operation the loss in spatial resolution was negligible.

In Huston's original framing image tube (46) the electron-optical magnification was  $\sim 1.8$  and in this design with a mesh potential of  $\sim 2000$  volts the magnification is  $\sim 3.5$  and thus the increase in image size is due mainly to the inclusion of the mesh close to the cathode.

### 2.3 Image Tube Electronics

The voltages required for focussing and biasing of the Photochron I are supplied via a resistive potential divider chain from a stabilised high voltage D.C. power supply. A schematic diagram of the image tube and its voltage supply is shown in FIG.11. With the switch in the focus position both deflection plates are at 18 Kv and thus the image will appear at the centre of the screen. Fine adjustments to the image focus may be made by varying the potentiometer control, which supplies the cathode voltage. In operation the mesh potential is  $\sim 2$  Kv to provide an electric (extraction) field value near the photocathode of  $\sim 7000$  v/cm. With this value of extraction field the transit time dispersion limit  $\Delta T_d$ , for a tube with an S11 photocathode and light of wavelength  $\sim 600$  nm is  $\sim 2$  psecs, (49).

When the tube is in streak operation the switch is set to bias. This deflects the image to a position off the phosphor screen since the upper deflection plate is now at a potential 2.5 Kv above that of the lower plate. The deflection sensitivity of the streak plates measured at the phosphor screen is  $\sim 330$  v/cm. The phosphor screen which is  $\sim 10$  cm in diameter is masked such that a rectangular portion 4 cm x 2 cm only is visible (4 cm in streak direction). Thus at bias voltages substantially less

than 2.5 Kv the image is effectively switched or shuttered off. To deflect the image across the screen a fast risetime ( $\sim 1\text{nsec}$ ), high voltage ( $\sim 5\text{Kv}$ ) negative going ramp is applied to the upper deflection plate via the coupling capacitor  $C_d$  (50pF, 20Kv). The voltage on the upper plate thus changes from 20.5 to 15.5 Kv in  $\sim 1\text{ nsec}$  and the image is swept across the phosphor screen at velocities of the order  $1.0$  to  $2.0 \times 10^{10}$  cm/sec.

This fast negative going ramp is supplied by an avalanche transistor - krytron switch, the circuit diagram of which is shown in FIG.12. The component values are listed below.

$R_1$ - 39 Ohms	$R_5$ - 100 MO
$R_2$ - 2.7 MO	$R_6$ - 50 MO
$R_3$ - 10 MO	$R_7, R_8, R_9, R_{11}$ - 4.7 MO
$R_4$ - 470 Ohms	$R_{10}$ - 10 KO
$C_1$ - 20 pF, 20v	$R_t$ - 50 Ohms
$C_2$ - 470 pF, 750v	VRI - 5MO Lin. Pot.
$C_3$ - 0.01 $\mu\text{F}$ , 1000v	$D_1$ - OA202
$C_t$ - 500 pF	

T1 - 6 Mullard BSX61 NPN

Min. Co-ax Cable RG/174U (16")

Krytron - KN22, EG & G.

The Central Component of the circuit is the krytron switch. This is a gas filled tube containing four control electrodes, the anode A, the cathode C, the grid G and keep alive KA. The switch tube will come into conduction when triggered by a minimum gate voltage pulse of  $\sim 750\text{v}$ . In the krytron the delay between triggering and the valve coming into conduction is reduced by the use of the keep alive electrode. This is essentially a beta emitter and requires a current of  $\sim 300\text{ uA}$  to maintain a plasma near the cathode. By using this keep alive

electrode the delay time is 30 - 40 nsecs. For the type KN22 the maximum recommended anode - cathode voltage is  $\sim 5\text{Kv}$  (76), and risetimes of  $\sim 0.7$  nsecs can be obtained when operating near this voltage. The trigger pulse for the krytron is derived from an avalanche transistor stack. Each transistor when operated in the avalanche mode (77, 78) is capable of holding off  $\sim 100\text{v}$  (collector - emitter). The potentiometer VR1 is adjusted so that the potential drop across the transistor stack is  $\sim 600\text{v}$ . Transistor T1 is non-conducting until triggered via C1 by a fast rising positive going pulse of amplitude  $\sim 10\text{V}$ . This trigger pulse is usually derived from the delayed gate output of a Tektronix 519 oscilloscope, which is itself triggered by the laser under investigation, via a photodiode. When T1 comes into conduction the potential drop across each of the transistors T2 - T6 now exceeds  $\sim 100\text{v}$ , the breakdown voltage. These transistors turn on very fast or avalanche ( 1 - 2 nsecs risetime) and a voltage pulse  $\sim 600\text{v}$  amplitude is injected into the miniature 50 ohm co-axial cable. At the unterminated (open circuit) end of the cable the voltage is doubled to provide a trigger pulse greater than 1 Kv at the grid of the krytron. The krytron switches on after a delay of 30 - 40 nsecs and the voltage at the output, O/P falls from 5Kv - 0v in  $\sim 1$  nsec.

The speed of this voltage ramp has been investigated at the krytron output, using a capacitive attenuator (x300) which introduced little distortion to the pulse shape (75, 79). The output pulse was displayed on a Tektronix 519 scope and the measured fall time between 10% and 90% of full amplitude was  $\sim 1$  nsec. Repetitive triggering of the krytron to give 20 superimposed oscillograms of the ramp showed that jitter was subnanosecond.

This fast voltage ramp is then relayed along a short, straight length of 50 ohm co-axial cable (RS UR43) to the streak plate of the image tube. To prevent electrical ringing at the streak plate a termination is used, consisting of a capacitor Ct, and a

resistor  $R_t$ , at the end of a section of 50 ohm co-axial cable. The cable is 400 cm long so that any reflections which may occur at the termination return to the streak plate a comparatively long time after the application of the voltage ramp.

To ensure that the deflection ramp is linear, only the central 1.5 Kv portion of the 5Kv ramp is used. This is achieved by adjusting the bias off voltage (FIG.11) so that when streaking, the central 1.5 Kv portion is responsible for deflecting the image across the unmasked section of the phosphor. By using this portion the departure from linearity is less than 10%.

The voltage at the upper streak plate drops to 15.5Kv when the tube is streaked. If this voltage was allowed to return to its original value of  $\sim 20.5$ Kv while radiation was still illuminating the camera input slit, then a second set of streak images would be superimposed on the first. This problem is overcome by choosing the value of the resistor, through which charging of the streak plate capacitor takes place, to be large enough to ensure it is hundreds of microseconds before the upper plate voltage returns to its original value.

If the output of the krytron is applied directly to the streak plates then streak velocities of the order of  $(1.5 - 2.0) \times 10^{10}$  cm/sec are obtained at the phosphor screen. At these streak velocities it is necessary to draw a large photocurrent to ensure an adequate intensity at the camera output is obtained, to allow microdensitometry of the recorded images (2.4). However even with image intensification, streak velocities in excess of  $1.5 \times 10^{10}$  cm/sec require a very large photocurrent, and the magnitude of this current is such that unwanted effects such as image degradation, and loss of temporal resolution occur (1.4(2), 2.4). Therefore the streak velocity must be limited to  $\sim (1.0 - 1.2) \times 10^{10}$  cm/sec.

In order to achieve a variable but slower streak velocity, integrators of the type shown in FIG.12 were used. These consisted of an RLC circuit housed in a dural box to which 50 ohm BNC connectors were attached. The integrating units

were thus interchangeable between the krytron circuit output and the streak plate capacitor. A range of such integrators was constructed to give streak writing speeds between  $10^8$  and  $10^{10}$  cm/sec.

The dynamic spatial resolution of the Photochron I streak camera at these streak velocities was also estimated (61) by illuminating a resolution test pattern with pulses from a Rhodamine 6G dye laser and streaking the image. From the recorded image at the output a dynamic spatial resolution of  $\sim 4$  Lp/mm at a streak velocity of  $10^{10}$  cm/sec was estimated, and under more favourable conditions (61) a dynamic resolution of 5 Lp/mm was inferred. If the dynamic spatial resolution is taken as 50 Lp/cm then the camera streak resolution limit  $\Delta\tau_s$  in this case (eqn. 1.24) was  $\sim 2$  psecs. When this is combined with a transit time dispersion  $\Delta\tau_d$  of  $\sim 2$  psecs then the camera instrumental function,  $(\Delta\tau_s^2 + \Delta\tau_d^2)^{\frac{1}{2}}$ , is of the order of  $\sim 2.8$  psecs. Thus the Photochron I streak camera is capable of resolution of less than 3 psecs.

#### 2.4. The Image Intensifier

As noted in the previous section, the limited photocurrent which can be drawn in the image tube prevents the use of streak velocities greater than  $10^{10}$  cm/sec. Even at these velocities image intensification is still required.

With the image tube operating at an anode potential of 18 Kv then each photoelectron incident upon the phosphor screen causes the emission of  $\sim 500$  blue photons of energy  $\sim 2.8$  ev (80). If every photon emitted can be collected and relayed to the recording film at a 1:1 magnification, then it has been estimated that for Polaroid type 47 film (3000 ASA) that an energy density of  $10^9$  photons/cm<sup>2</sup> (81) is required to produce a unit change in density. Thus the corresponding number of photoelectrons required is  $\sim 2 \times 10^6$  per cm<sup>2</sup>. This requires a current density at the photocathode of

$$ipc = n e m^2 / t \quad A / cm^2$$

where  $n$  is the number of photoelectrons,  $e$  is the electronic charge,  $m$  is the electron-optical magnification and  $t$  the tube conduction time. The current density at the photocathode is thus  $\sim 2.8 \text{ A/cm}^2$ , and this is derived from a slit area of  $17 \text{ microns} \times 3\text{mm}$ , giving a total tube current of  $\sim 1.5 \text{ mA}$ .

However a lens must be used to relay the image onto the film and this introduces a loss since the lenses used are only  $\sim 2\%$  efficient. Hence the total tube current required to give an exposure would be  $\sim 75 \text{ mA}$ . Numerous problems arise if a photocurrent of this magnitude is drawn. It has been shown by Key et al (56) that under streak conditions the maximum increase in potential at the centre of a photocathode of surface resistivity  $\rho$  from which a current density  $i_{pc}$  is drawn is given by,

$$\Delta V = i_{pc} \rho (W_c W_s - \frac{1}{2} W_s^2)$$

where  $2W_c$  is the cathode width and  $2W_s$  the width of the slit illumination. The input slit to the image tube is  $50 \text{ microns}$  wide,  $1\text{cm}$  long and the illuminated slit image is relayed via a  $3:1$  demagnifying,  $f/1.5$ ,  $75 \text{ mm}$  lens to the photocathode which is  $\sim 1 \text{ cm}$  in diameter. With a required photocurrent of  $\sim 150 \text{ A/cm}^2$ , and a surface resistivity  $\sim 100 \text{ ohms}/\square$  then  $\Delta V \sim 6\text{v}$ . Since the focussing of the image tube may be carried out by varying the photocathode potential, then it is important to know this value of  $\Delta V$ , as the spatial resolution of the tube may be affected if too high a photocurrent is drawn. It is however evident from FIG.10 (a) that the tube focussing is not seriously affected by changes of less than  $\pm 10\text{v}$  in the cathode potential. The use of a high gain image intensifier permits a lower photocurrent to be drawn and thus this is no longer a problem. Other effects which limit the tube performance at high values of photocurrent are space charge and coulombic repulsion between electrons. If high photocurrents are drawn a build up of electrons occurs near the photocathode surface and this effectively reduces the value of the mesh extraction field. Thus the transit time dispersion limit  $\Delta \tau d$  is increased and

the temporal resolution of the camera suffers. A further increase in photocurrent will only lead to saturation of the photocathode (83) and in this event the response of the cathode is no longer linear and the interpretation of results would become difficult.

The method of electron focussing in the tube causes an inverted image of the slit to appear at the phosphor. Therefore inside the tube the electrons cross the electron-optical axis. The electron beam waist diameter is a minimum at the cross over point and the charge density is therefore a maximum. At high photocurrents therefore mutual repulsion between electrons in this area could lead to image distortion and loss of spatial resolution. As pointed out previously a high photocurrent needs to be drawn if sufficient light for photographic records is to be obtained. This could however lead to the problems outlined. The use of an image intensifier eliminates the need to draw a large photocurrent while providing sufficient light amplification to enable photographic records to be obtained.

A suitable image intensifier with a blue light gain of  $\sim 10^6$  is the EMI 9693 or 9694 model. The intensifier consists of an input photocathode (S11, to match the P11 phosphor of the image tube) followed by three P11/S11 phosphor - photocathode sandwiches, and an output P11 phosphor. The device is thus essentially four stages. A water cooled solenoid surrounding the intensifier provides an axial magnetic field for electron focussing. When operated at a current of  $\sim 5A$ , i.e. "two loop" focus the magnification in the intensifier is 1:1. A large potential difference between the input photocathode and the first sandwich accelerates the electrons liberated from the photocathode onto the phosphor of the first sandwich. Photons from this phosphor liberate electrons from the photocathode of the first sandwich and the process repeats itself to the output phosphor. At an overall operating potential difference of  $\sim 35$  Kv the gain per stage is  $\sim 30$  giving an overall gain of  $10^6$ . The spatial resolution of the image intensifier is  $\sim 25$  Lp/mm and is constant over a central area of  $\sim 25$  mm (84). At the maximum gain the background noise level of the intensifier is negligible.

If like the photocathode the response of the image tube phosphor to the incident electronic image was prompt ( $< 10^{-12}$  secs) then

photocurrent saturation effects would occur in the intensifier also. However the decay time of a P11 phosphor is  $\sim 80$  microseconds to 10% of its peak emission (85) and because of the integrating effect of the phosphor for exposure times substantially less than the decay time, the first stage current of the intensifier will be hundreds of times smaller than that of the image tube. The transfer of the spatial and temporal information at the image tube phosphor to the intensifier input is carried out using an  $f/1.5$ , 80 mm focal length, Ilex lens at a demagnification of  $\times 0.7$ . The intensifier output is relayed to the recording film via an  $f/1.5$ , 80 mm, Ilex lens operating at unit magnification. For setting up tests Polaroid type 47 film is used but for quantitative results Ilford HP4 film is used (35 mm, 450 ASA). The use of even such wide aperture lenses introduces a loss of  $\sim 2\%$  per lens, into the recording system. Thus the effective gain of the intensifier is reduced to  $\sim 4 \times 10^2$ . If Polaroid type 47 is used for recording, then  $10^9$  photons/cm<sup>2</sup> are required to produce a unit density change (56, 81). At a streak velocity of  $10^{10}$  cm/sec the dynamic spatial resolution is  $\sim 5$  Lp/mm (2.3) and considering one 18 Kev electron produces 500 2.8 ev photons (80) then these photons are contained in an area  $8 \times 10^{-5}$  cm<sup>2</sup>. Since there is a net demagnification of  $\times 0.7$  between the image tube phosphor and the recording film the photon density incident upon the film is  $\sim 5 \times 10^9$  photons/cm<sup>2</sup>. This would imply that the camera system is capable of recording a single photoelectron. However to take account of the statistical fluctuation in the recorded streak of  $N^{\frac{1}{2}}$  where  $N$  is the number of photoelectrons, then  $N$  should be  $\geq 100$ .

## 2.5 Evaluation of the Photochron I Performance

Before the experimental evaluation of the camera performance can be made the system must be focussed for optimum spatial resolution. As previously described (2.4) the image of the input slit (Hilger and Watts, 2 cm long precision spectrograph slit adjustable from 5 microns to 2 mm) is relayed via an  $f/1.5$ , 75 mm focal length lens to the photocathode at a demagnification of  $\times 3$ . The image at the tube phosphor is then relayed via another lens, the coupling lens (2.4) to the intensifier and from the intensifier output via a third lens (2.4) to the recording film. The image tube and the intensifier are normally adjusted separately for optimum focus

before the camera system is assembled. To focus the camera system the input slit is fully opened to a width of 2mm, and a resolution test pattern is placed against it. The test pattern is illuminated by a variable intensity projection lamp. With the image tube set for focus the image of the test pattern appears at the centre of the intensifier phosphor. A microscope is used to view this image so that best focus can be judged more easily.

With the input lens fully open at  $f/1.5$  and the coupling lens stopped down to  $f/32$ , the position of the input lens is adjusted for best focus. The input lens is then stopped down to  $f/32$ , the coupling lens is opened to  $f/1.5$  and the coupling lens adjusted for best focus. This routine is repeated until stopping down the lenses, to increase their depth of focus, no longer produces an improvement in the spatial resolution observed at the phosphor of the intensifier.

With both lenses stopped down to  $f/32$  the electrostatic focus of the image tube and the electromagnetic focus of the intensifier are checked. The optical focussing procedure is then repeated and when satisfied that the best focus possible has been achieved the recording camera is focussed on the image at the intensifier phosphor.

In operation the input lens is normally at  $f/4$  while the coupling and camera lenses are at  $f/1.5$ . The best observable spatial resolution under these conditions is limited to that of the image tube at  $\sim 8-9$  Lp/mm (2.2), corresponding to a dynamic spatial resolution of  $\sim 5$  Lp/mm.

The experimental evaluation of the Photochron I performance was carried out by Sibbett (61) using a R6G dye laser, mode-locked, and tuned to 605 nm by an intra-cavity Fabry-Perot etalon. This laser was capable of producing transform limited pulses (i.e. pulses whose time bandwidth product  $\Delta\nu\Delta t \sim 0.5$  for Gaussian profiles) of duration  $\sim 2 - 4$  psecs (86). The image tube had an S11 photocathode for which the electric field strength close to its surface was  $\sim 7000$  v/cm, thus the transit time spread is  $\sim 1.4$  psecs since  $\Delta E_n \sim 0.15$  ev (eqn. 1.23 a). Also

with a streak speed of  $\sim 10^{10}$  cm/sec and a dynamic spatial resolution of  $\sim 5$  lp/mm the streak resolution limit was 2 psecs (eqn. 1.24). These factors imply a camera instrumental function of less than 3 psecs.

The experimental arrangement for testing the camera performance is shown in FIG.13. The beam splitters  $B_1$  and  $B_3$  directed a portion of the laser output onto a TPF set up, and a biplanar vacuum photodiode. The signal from the diode was used to trigger the Tektronix 519 scope, which displayed the laser pulse train on a nanosecond time scale. The oscilloscope when triggered also produced a trigger output of  $\sim 10$ v at a variable delay of 0 - 30 nsecs after the diode signal. This was used to trigger the krytron ramp deflection circuit. The remainder of the laser pulse train was optically delayed by a series of uncoated parallel plate beam splitters. These generated from each single laser pulse a series of sub-pulses separated in time by an amount corresponding to the distance between, and the thickness of the glass discs. The generated sub-pulses were then directed onto a diffuser in front of the camera slit. The optical delay line provides a means of calibrating the camera since by measuring the distance between sub-pulses on the streak records, an estimate of the streak velocity and streak durations may be made.

Initially the delay line consisted of two 6mm thick glass discs separated by 2.8 cm. Thus generating from each laser pulse four sub-pulses of relative delays 60 psecs, 190 psecs, and 60 psecs.

The total streak duration, at a velocity of  $10^{10}$  cm/sec with a phosphor 'window' of  $\sim 4$  cm, is only  $\sim 400$  psecs. Then without the optical delay line providing a set of sub-pulses over a period of  $\sim 300$  psecs, the synchronisation of the streak deflection ramp with the arrival of a pulse at the streak plates would be very difficult, since a pulse of 2-4 psecs duration would be arriving only once every  $\sim 4$ nsecs (the cavity round trip time). In practice synchronisation is effected by varying the internal electronic delay of the oscilloscope producing the trigger pulse and also by varying the length of the cable along which the trigger pulse passes to the trigger input of the krytron circuit.

The photodiode signal was optically and electronically attenuated and the scope trigger level adjusted so that a pulse near the peak of the laser train envelope was streaked. The streak record shown in plate 1 (a) was obtained. From this result the streak velocity was estimated to be  $\sim 10^{10}$  cm/sec, and the non-linearity of the streak was less than 10%. The microdensitometer trace of the streaks obtained is shown in plate 1 (b), and from these a recorded half width of  $\sim 5$  psecs was estimated. The background scintillations of plate 1 (a) show the effect of the scattering which occurs in the image tube, when the electron beam is biased off the phosphor before and after streaking. The patchy appearance of the streak records is due to the limited photocurrent which can be drawn at streak velocities of  $\sim 10^{10}$  cm/sec. When a microdensitometer trace of such a record is made the analysing slit averages over the bright scintillations and the dark gaps in between. Thus the microdensitometer reading is less than the peak value due to the bright scintillations, and pulse half widths estimated from such a trace are likely to be inaccurate.

Before microdensitometer traces can be used to estimate pulse widths it is essential to know the film characteristic or  $\gamma$  so that the density corresponding to half the peak intensity can be deduced. Since the  $\gamma$  of the emulsion depends on the development conditions and the possibility of reciprocity failure at very short exposure times ( $< 10^{-6}$  secs) it is necessary to calibrate each film. To do this the camera is operated in the focus mode with the slit fully open and a wedge consisting of neutral density filters of increasing values is placed against it. The wedge is uniformly illuminated with white light from a projection lamp and photographed. The negative is microdensitometered and from a plot of density versus  $\log_{10}$  intensity the value of the  $\gamma$  of the film is found. To find the pulse half width it is only necessary to measure the width of the density profile at a point  $0.3 \gamma$  below the peak.

However for reasons outlined before, the use of microdensitometry to estimate half widths can be inaccurate. It was therefore decided to use the criterion that two pulses were said to be resolved when the modulation between their partially overlapping profiles was  $\sim 20\%$ . In the case where Gaussian pulses are

are assumed this requires that the pulses are separated by  $1.14 \Delta\tau_r$  where  $\Delta\tau_r$  is the width (FWHM) of the recorded pulse profile. From the microdensitometer trace the two pulses are said to be resolved if the difference between the measured peak density  $D_p$ , and the density at the saddle of the profile  $D_s$  is (61).

$$D_p - D_s = 0.1 \gamma$$

In this case their half intensity width is approximately equal to the separation of their peaks.

To perform this experiment the delay line was adjusted to generate sub-pulses separated in time by the estimated combined width of the camera instrumental function and laser pulse duration. The delay units now comprised two flat glass discs  $\sim 6$  mm thick spaced by a glass washer to give an air gap of  $\sim 1$  mm over three quarters of their diameter. A microdensitometer trace of streaks obtained using such an arrangement is shown in FIG.14 (a), the central pair being separated by 6.6 psecs with a modulation of  $\sim 40\%$ . This implied recorded pulse half widths of  $\sim 5$  psecs. From simultaneous TPF measurements the average pulse duration was estimated to be  $\sim 3.5$  psecs. and using this and eqn. 1.25, the camera instrumental function was estimated to be  $\sim 3.6$  psecs.

Further deconvolution of the transit time spread limit ( $\Delta\tau_d \sim 1.4$  psecs) and the slit width limit of 0.5 psecs inferred a streak resolution limit  $\Delta\tau_s$ , of  $\sim 3$  psecs. To check this value of  $\Delta\tau_s$  the image of a resolution test pattern was streaked and a dynamic spatial resolution of 3-4 Lp/mm was observed. This combined with a streak velocity of  $10^{10}$  cm/sec gave a value of  $\Delta\tau_s$  of  $\sim 3$  psecs in good agreement with the deconvolved value. These results indicated that the theoretical expression (eqn. 1.25) for the camera instrumental function did indeed agree with experimental results and gave sufficiently accurate results.

In subsequent experiments to measure the duration of the mode-locked dye laser pulses, the extraction field near the photocathode was raised to  $\sim 8000$  v/cm and under these conditions the dynamic spatial resolution was estimated to be  $\sim 5$  Lp/mm, giving a streak

resolution limit at  $v \sim 10^{10}$  cm/sec of  $\Delta\tau_s \sim 2$  psecs. With the laser tuned to 615 nm the transit time dispersion limit was  $\sim 0.9$  psecs. The streaks obtained are shown in plate 2. From the recorded pulse widths of 3.5 psecs and taking the slitwidth limit of 0.5 psecs into account, laser pulse widths of  $\sim 2.6$  psecs were estimated.

Closer examination of the pulses of plate 2 showed that each apparently single pulse was in fact a pair of pulses separated by 2.5 psecs. The microdensitometer trace of this pulse pair is shown in FIG. 14 (b). A modulation of  $\sim 20\%$  is shown which just satisfies the criterion for resolution. The recorded pulse duration from this trace is  $\sim 2.3$  psecs, at the half intensity level. Deconvolving from this a streak resolution limit  $\Delta\tau_s \sim 1.8$  psecs, a transit time spread  $\Delta\tau_d \sim 0.9$  psecs and the slit width limit of  $\sim 0.5$  psecs, then the pulse duration is  $\sim 1$  psec. This result clearly demonstrated the capability of the camera to resolve events of the order of  $\sim 2$  psecs duration.

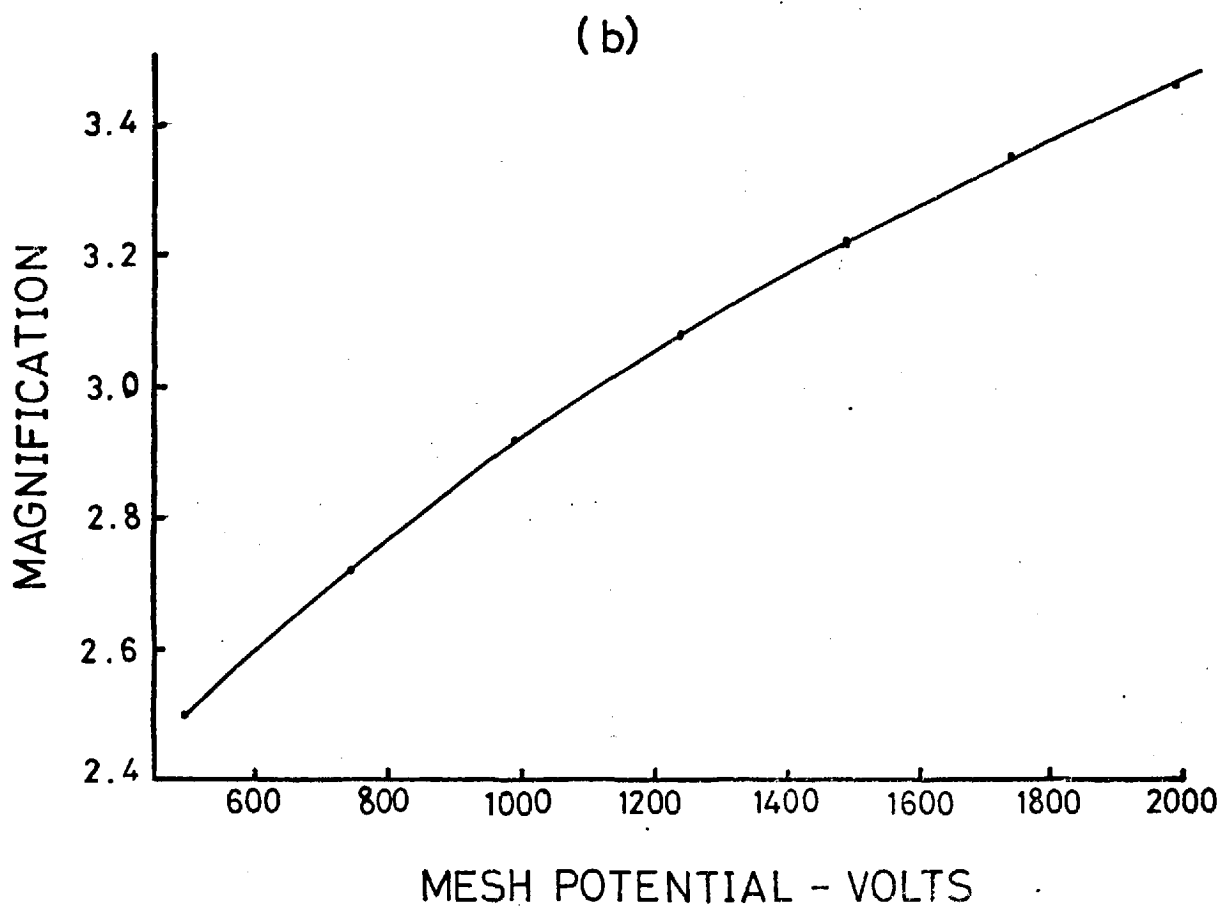
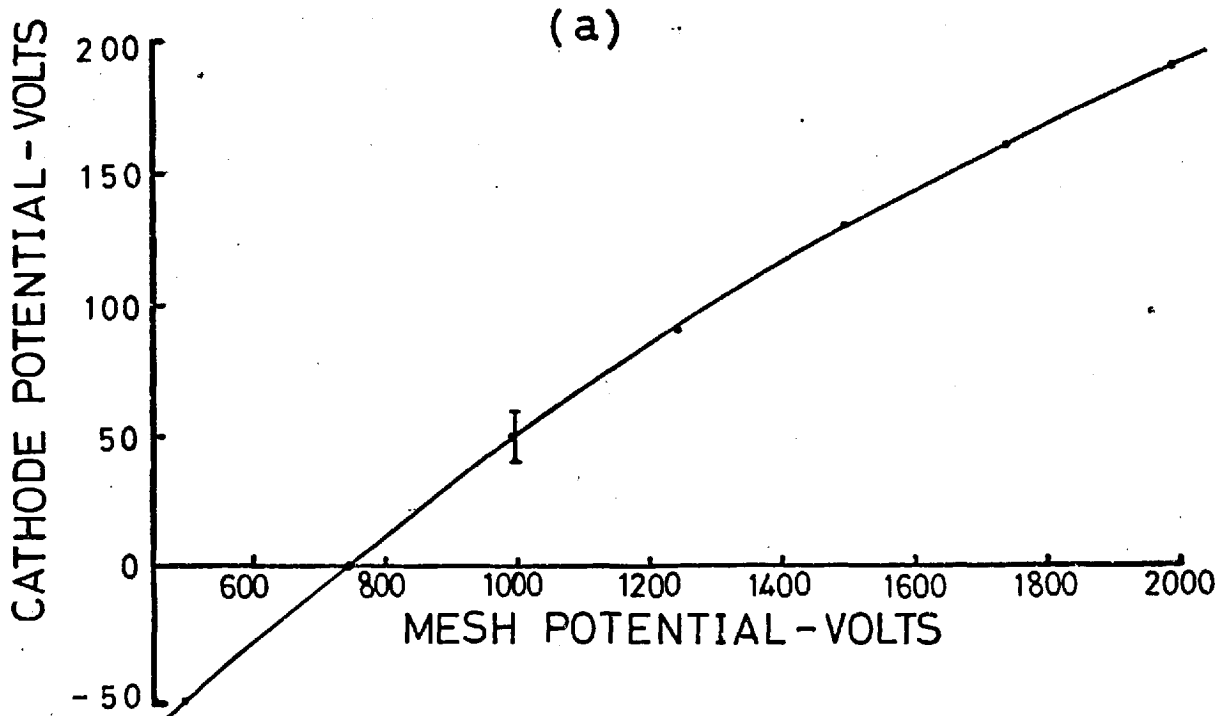


FIG. 10

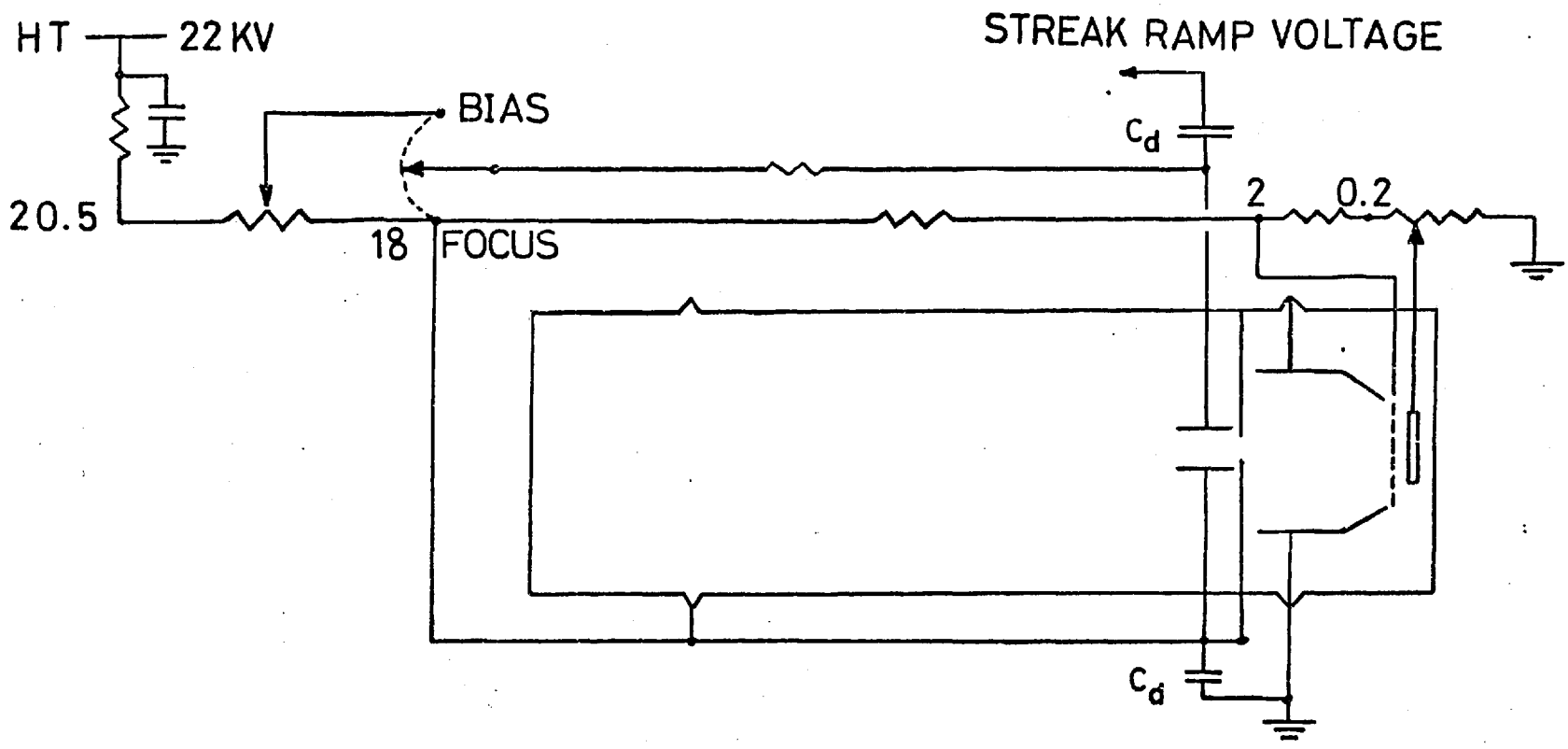


FIG.11

FIG.12

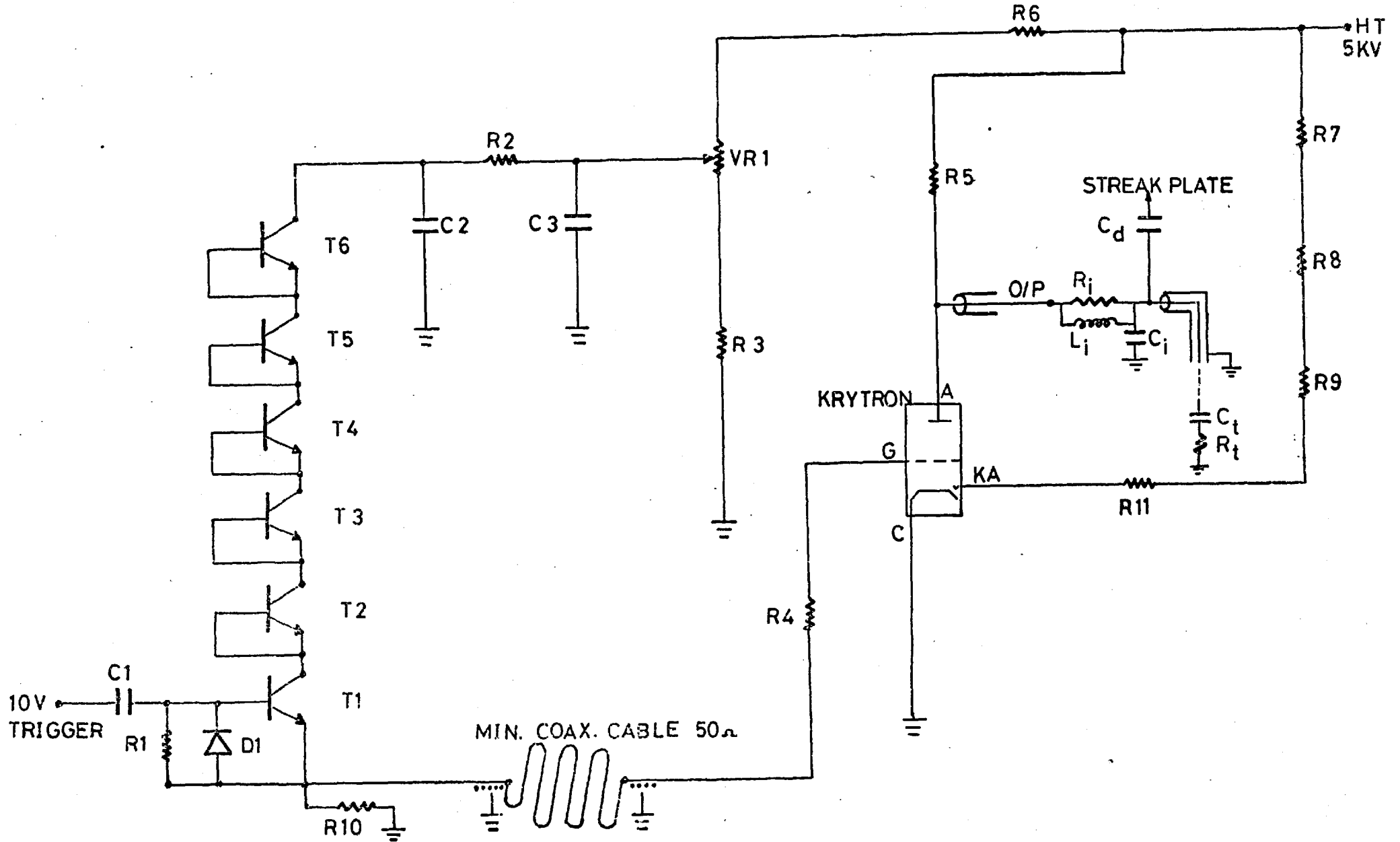
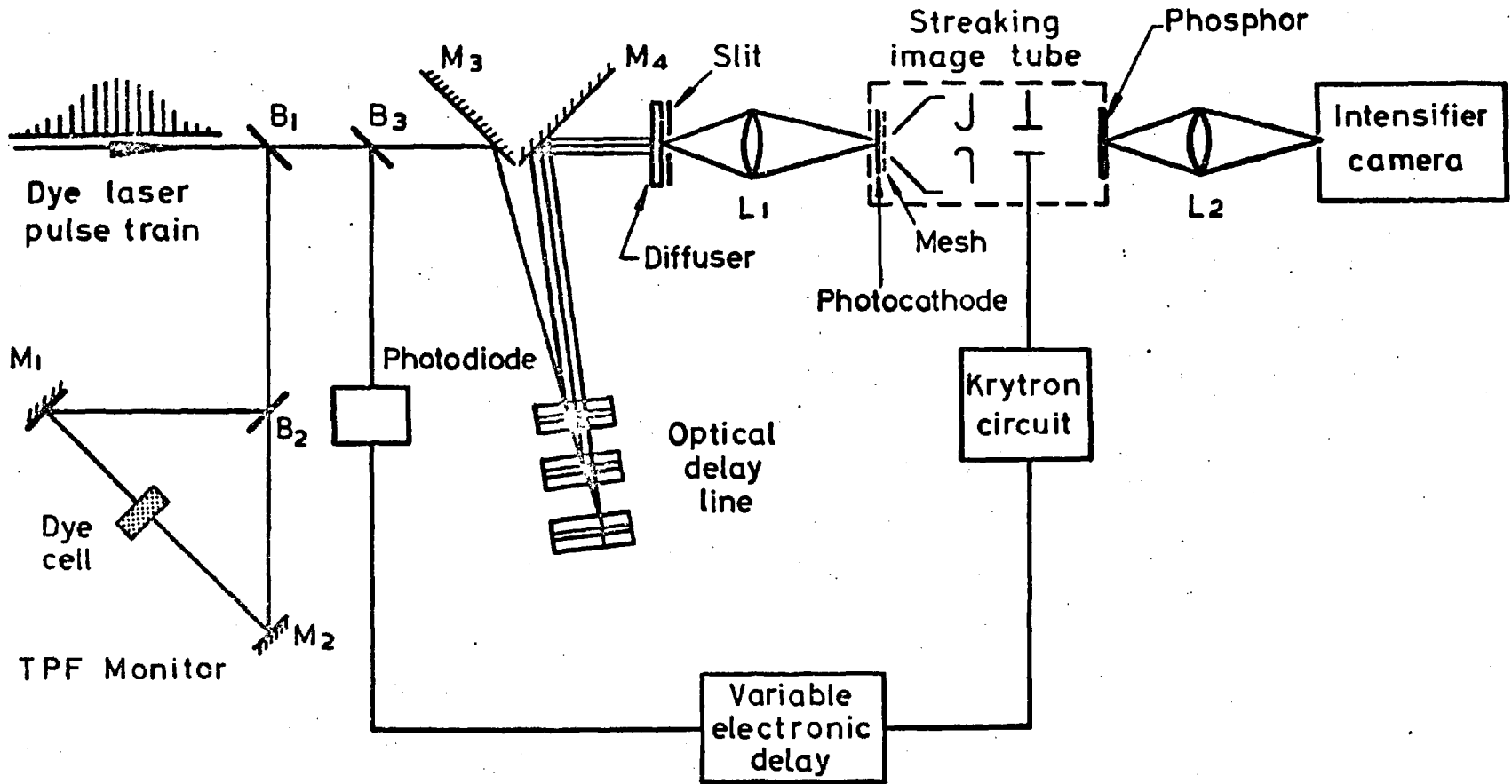
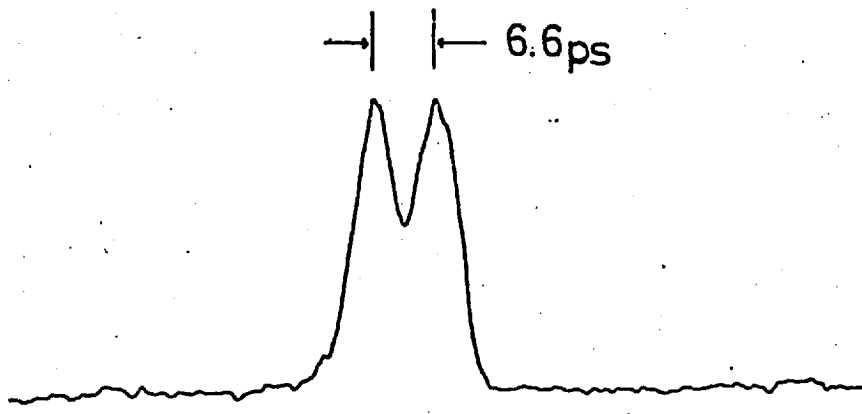


FIG.13





(a)

(b)

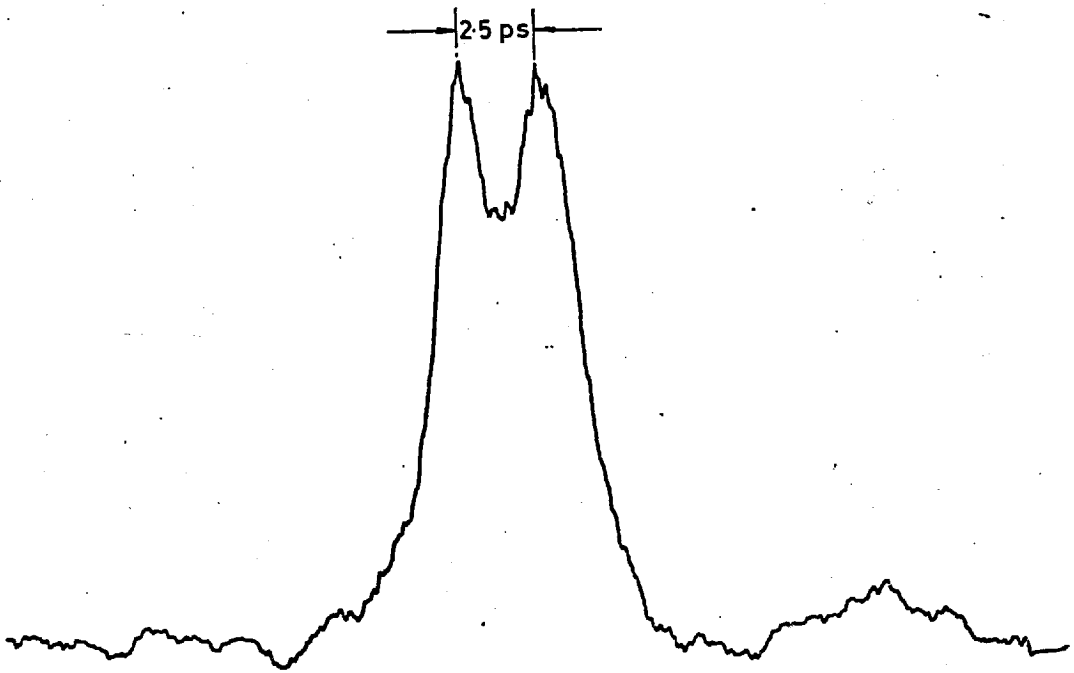


FIG. 14

Plate 1

(a)

Dye laser pulses separated by  
60 psecs and 190 psecs

(b)

Microdensitometer trace of above

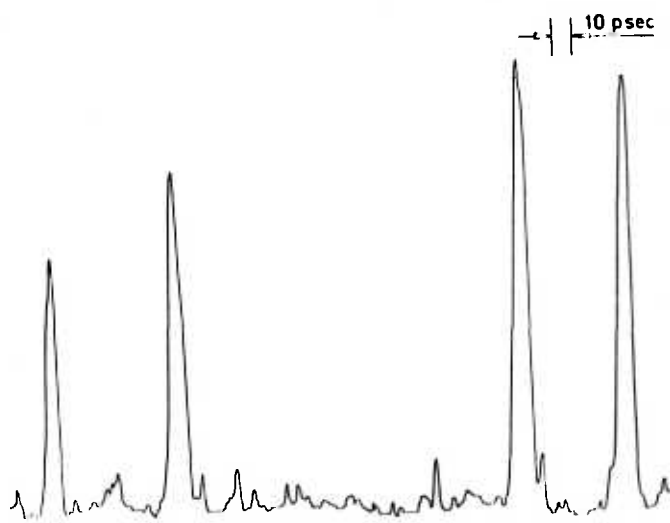
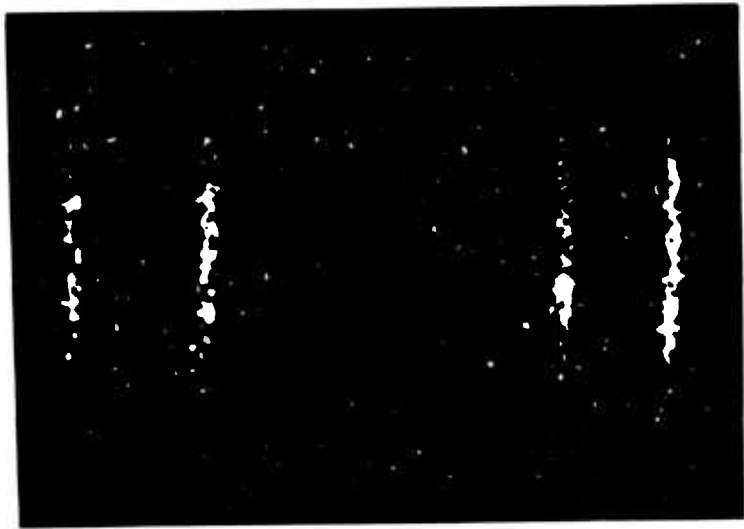


Plate 2

Four sub-pulses separated by  
6.6 psecs. and 60 psecs

The pulse to the right shows each  
sub-pulse to be two pulses of  
separation 2.5 psecs.



## CHAPTER 3

### THE PHOTOCHRON II IMAGE TUBE

#### 3.1. Introduction

The Photochron I image tube of Chapter 2 had a temporal resolution limit of  $\sim 2$  psecs (2.5). The main limitations on the achievement of a lower temporal resolution being the transit time spread in the image tube, and the limited values of the dynamic spatial resolution and streak velocity.

This chapter describes the design of a new image tube, with a subpicosecond resolution capability, the Photochron II. The methods by which this could be achieved were suggested in eqn. 1.23(a) and eqn. 1.24. By increasing the electric field strength near the photocathode the transit time spread may be reduced, and by increasing the static spatial resolution of the image tube the capability of an increased dynamic spatial resolution may be provided. However to increase the extraction field near the photocathode by simply raising the mesh voltage has two disadvantages. Firstly the increase in electron-optical magnification as the mesh voltage is raised (FIG.10(b)) effectively reduces the static resolution at the image tube phosphor. As the resolution at the photocathode is constant for a particular image tube the increase in image size at the phosphor means that the same number of line pairs (as was visible at the photocathode) are now contained in a greater area at the phosphor and the resolution in terms of lp/mm is reduced. Secondly the greater voltage at the mesh increases the possibility of electrical breakdown to the photocathode. Since the resolution of the Photochron I image tube is constant at  $\sim 30$  lp/mm at the photocathode, to improve the static resolution at the phosphor the magnification must be reduced while maintaining 30 lp/mm at the cathode.

It is shown in this chapter how the static spatial resolution at the image tube phosphor may be increased by a decrease in the electron-optical magnification while a simultaneous increase in the value of the electric field at the photocathode is made.

A method by which signal induced background may be reduced is also proposed and it is indicated how these modifications effectively increase the sensitivity of the image tube.

### 3.2. Electron - Optical Magnification

Electron-optics deals with the application of optical laws to electron motion. Instead of considering the shape of the electron orbits as caused by accelerations due to electric forces, the orbits are considered to be the result of refractions of the electron ray by a series of refracting surfaces such as the equipotential surfaces in the electrostatic field. All electrostatic fields with circular or two dimensional symmetry possess the properties of an optical lens i.e. they can project electron - optical images.

An illustration of the way in which an equipotential surface may refract an electron ray is shown in FIG.15(a). The electron travels with velocity  $u$  in a space of constant potential  $V_1$ , and is transmitted through a potential step into a space of potential  $V_2$ . If  $V_2$  is more positive than  $V_1$  then the horizontal velocity component  $u_h$  is increased while  $u_v$  remains constant. The electron ray is thus refracted at the potential step. A sudden change in potential does not however occur in electron - optical lenses but rather the potential varies continuously along the path of the electron.

A sketch of some of the equipotentials in the cone-anode region of the Photochron I image tube is shown in FIG.15(b). Using the criterion that electrons travelling from a region of higher potential to one of lower potential are refracted away from the normal to the equipotential surface and vice versa then the mesh - cone region and the cone-anode region form positive converging lenses. This result is consistent with the observation that an electron ray travelling from a high field region into a region of lower electric field will 'see' a converging lens (74). Both lenses are 'thin' lenses and the mesh-cone lens does not extend axially towards the photocathode, but only in the direction towards the cone.

With the operating voltages shown in FIG.15(b) the mesh-cone lens is of short focal length and the proximity of the photocathode to the mesh ensures that the object of the mesh - cone lens lies within its focal length. The optical analogy of the electrostatic lens system is shown in FIG.16, where  $L_1$  is the mesh-cone lens of focal length  $F_1$  and  $L_2$  is the cone-anode lens of focal length  $F_2$ . Lens  $L_1$  forms a virtual magnified image,  $I$  of the object,  $O$  at a point to the left of the photocathode plane. This virtual image forms the object for lens  $L_2$  which produces a magnified real image  $I_p$  of the object  $O$ , at the output phosphor plane. It was noted from FIG.10(b) that as the mesh potential was increased the electron-optical magnification at the phosphor increased also. The increase in mesh potential leads to an increase in the value of the electric field in the mesh-cone region and thus increases the converging power of the lens by shortening its focal length.

From FIG.16, if the focal length of  $L_1$  is decreased to  $F'$  by increasing the field between the mesh and cone then a virtual image  $I'$  of  $O$  is formed, again magnified and to the left of the object plane. The increased size of the virtual image  $I'$  leads to an increased image size  $I_p'$  at the output phosphor plane. Thus if the electron-optical magnification at the output phosphor can be increased by increasing the strength of the mesh-cone field then conversely by decreasing the mesh-cone field strength a reduction in electron-optical magnification may be obtained.

In order to investigate the electron-optical focussing of the image convertor experimentally, an image tube in which the constituent parts i.e. the mesh, photocathode, deflection plates, etc. were demountable from the glass body of the tube was obtained (95). Experiments were carried out with the image tube positioned on an optical bench assembly situated inside a chamber which could be conveniently evacuated. The apparatus is shown in plate 3 and consists of a glass T piece (QVF Jobling,  $1\frac{1}{2}$ " thick), 18" long with horizontal entry and exit ports 14" in diameter. The third port was  $6\frac{1}{2}$ " in diameter and was connected to the vacuum system, an Edwards coating unit type 18E4/286, comprising a rotary pump and

a 9" oil diffusion pump. This system could evacuate the glass T piece to a pressure of less than  $10^{-4}$  Torr in approximately 30 minutes. The horizontal ports were closed by 'O' ring sealed dural plates. A quartz window was let into one of these plates, and into the other a plain glass window through which the image tube phosphor could be viewed.

In the image tube proper the photocathode be it S1, S11 or S20 is formed on the substrate inside the image tube while it is under vacuum. Therefore in the demountable system such cathodes could not be used as they would be readily poisoned upon letting down the system to atmospheric pressure. Therefore in the vacuum system a gold photocathode on a quartz substrate was used in conjunction with an ultra-violet lamp (HPK, 125W, Philips). The image tube body comprising the cone, anode and phosphor was supported with dural rings upon two optical bench mounts. The gold photocathode and the mesh were supported on separate movable mounts, so that the separations of the mesh, photocathode and cone could be easily varied.

These separations could be varied while the system was evacuated, by the use of push rods, sealed by 'O' rings in the end plates of the T piece, which moved the mesh and photocathode mounts up and down the optical bench. The ultra-violet light source was placed outside the vacuum system and its light focussed by a 10 cm focal length quartz lens through the quartz window in the dural end plate onto the gold photocathode. Electrical contact to the image tube electrodes was made through insulated high voltage connectors in the dural end plate which contained the plain glass window. Such a system could reproduce the static performance of the image tube proper.

In preliminary investigations of the electron-optical magnification a gold photocathode cum resolution chart was used. The cathode consisted of a resolution test pattern (maximum resolution  $\sim 10$  lp/mm) on a quartz substrate overlaid with gold. The maximum resolution at the photocathode was thus  $\sim 10$  lp/mm. With both deflection plates at the anode to phosphor potential

of 18 Kv the variation of electron-optical magnification with mesh to cone separation was investigated, at three distinct values of photocathode to mesh separation. The results of this investigation are shown in FIG.17(a). Curve A shows the results for the standard Photochron I, mesh to photocathode separation of 3mm. In this case the mesh voltage was  $\sim 2500V$  and the cathode was earthed corresponding to an electric field of  $8300 \text{ v/cm}$  near the cathode.

In order to further reduce the magnification the mesh voltage was lowered, however to maintain the extraction field value the mesh to cathode separation was reduced. Curve B shows the results for a mesh to cathode separation of 1.5mm and an applied mesh voltage of 1250v. Curve C shows the results for a mesh to cathode separation of 1mm and a mesh voltage of 830v. Curves B and C show that the electron-optical magnification may be substantially lowered while maintaining the extraction mesh field value at  $\sim 8300 \text{ v/cm}$ .

At each value of mesh to cone separation the cone voltage was adjusted for best focus of the image at the phosphor. When satisfied that best focus was achieved the image size at the phosphor was measured using a travelling microscope. The focussing characteristic for each of the curves A, B and C is shown in FIG. 17(b). Since the resolution at the photocathode was only  $\sim 10 \text{ lp/mm}$  no inference as to the resolution capability of the image tube under these conditions could be made. It was noted however that the resolution at the photocathode was maintained as the mesh to cone separation was increased to  $\sim 3.5 \text{ cm}$ , beyond which point the resolution started to fall off. No results were taken for separations greater than 5.0 cm since distortion of the image began to occur.

These preliminary results showed how the electron-optical magnification could be reduced simply and effectively. The results of FIG.17 curve C showed that a minimum magnification could be obtained by both increasing the mesh to cone separation and reducing the mesh voltage. Since the purpose of these tests was also to increase the extraction mesh field it was decided to maintain the mesh voltage at  $\sim 830-1000v$  while decreasing further to 0.5 mm the mesh to photocathode separation. At such a mesh

voltage the magnification should not vary greatly from that of curve C, but the extraction mesh field would be a factor of  $\sim 2.5 - 3$  times greater than that previously used. Also in order to test the resolution capability of the tube more thoroughly an NBS resolution test chart with line frequencies up to  $\sim 80$  lp/mm, overlaid on a quartz substrate, was obtained (Graticules Ltd). This substrate was gold coated and thus formed the photocathode. Tests were carried out in the demountable system described for the preliminary investigations.

The variation of magnification with mesh to cone separation is shown in FIG.18(a) for the mesh to photocathode separation constant at 0.5 mm. The mesh voltage was set at 1000 volts with the photocathode earthed and no electrical breakdown was observed for mesh voltages up to  $\sim 1300$ v. From FIG.18(a) it can be seen that the magnification follows the general trend of FIG.17(a), but in this case the value of the extraction field is  $\sim 2.5$  times greater. As before magnification measurements were made with the cone voltage adjusted for best focus of the image at the phosphor screen. The focussing characteristic of cone voltage versus mesh to cone separation is shown in FIG.18(c). At each value of mesh to cone separation the resolution at the phosphor was observed using a x10 microscope and a plot of resolution versus mesh to cone separation is shown in FIG.18(b). The observed number of line pairs at the phosphor (i.e. resolution at the photocathode) divided by the electron-optical magnification gives the resolution at the phosphor screen in terms of lp/mm. In FIG.18(b) both the resolution at the photocathode (P/C) and at the phosphor (PH) are plotted. As the observed number of line pairs at the phosphor decreases with increasing mesh to cone separation, the resolution remains fairly constant at  $\sim 15$  lp/mm since the magnification also decreases. However at separations greater than 3.0 cm this resolution began to decrease and so no further points were plotted.

The Photochron I image tube had a constant resolution at the photocathode of  $\sim 30$  lp/mm (2.2). It can be seen from FIG.18(b) however that the resolution at the photocathode is now  $\sim 40$  lp/mm at mesh to cone separations of  $\sim 1.0$  cm. Plate 4(a) shows the

resolution test chart photographed at the image tube phosphor with an Exacta 35 mm camera with an  $f/1.5$ , 75 mm focal length lens, and using Ilford FP4 film. Plate 4(b) and 4(c) shows the photographed resolution test chart at mesh to cone separations of 2.0 cm and 3.0 cm respectively. The increased resolution at a 1.0 cm separation is due to the stronger and more uniform field near the photocathode, which eliminates field curvature and distortion. The photographed resolution charts of plate 4 indicate how the size of the image is reduced with increasing mesh to cone separation (the charts are not actual size), and how the resolution is maintained.

From the result of FIG.18(b) it can be seen that the image tube resolution at the phosphor may be increased from  $\sim 8-9$  lp/mm to  $\sim 15$  lp/mm by increasing the mesh to cone separation to either 1.0, 2.0 or 3.0 cm. However at separations of 1.0 and 2.0 cm electron-optical magnification is still fairly high, while at 3.0 cm it has fallen to 1.75 a factor of  $\sim 2$  times down on that of the Photochron I (FIG.10 b)). It has been shown (2.4) that the streak velocity at which the image tube camera may be operated is limited by the photocurrent which is drawn. At high streak velocities a large photocurrent must be drawn in order to produce a large enough photon density to cause a unit density change on the recording film. The current density which must be drawn is  $ipc$  where  $ipc \propto m^2$ , where  $m$  is the electron - optical magnification. Thus if the magnification is reduced by a factor of  $\sim 2$ , the photocurrent required to produce the same density change on a film is  $\sim 4$  times less and hence the camera sensitivity is increased by a factory of  $\sim 4$ . With an image tube of low electron-optical magnification it would thus be possible to increase the streak velocity above  $10^{10}$  cm/sec (2.4) without drawing too high a photocurrent. For this reason a mesh to cone separation of 3.0 cm giving an increased spatial resolution and an electron-optical magnification of  $\sim 1.75$  is an attractive modification.

To summarise it is useful to list the modifications which have taken place to the electron-optics, and the advantages of these modifications. The decrease in the mesh to photocathode separation from 3mm to 0.5 mm has increased the spatial resolution at the photocathode from 30 lp/mm to 40 lp/mm. Maintaining

the mesh voltage at  $\sim 1000\text{v}$  has produced a field value near the photocathode of  $\sim 20,000\text{ v/cm}$ , an increase of  $\sim 2.5\text{-}3$  times that used previously. With an S11 photocathode and light of wavelength  $\sim 615\text{ nm}$  the photoelectron energy spread  $\Delta E_n$  is  $\sim 0.15\text{ ev}$  and with an extraction field of  $20,000\text{ v/cm}$  the transit time dispersion  $\Delta T_d$  is only  $\sim 0.4\text{ psecs}$ . The increased mesh to cone separation of  $\sim 3.0\text{ cm}$  has reduced the electron-optical magnification from  $\sim 3.6$  to  $\sim 1.75$ , a factor of  $\sim 2$ . This has led to an increase in camera sensitivity of  $\sim 4$ . The reduction in magnification together with a resolution at the photocathode of  $\sim 30\text{ lp/mm}$  has led to an increased spatial resolution at the phosphor of  $\sim 15\text{ lp/mm}$ . With a static resolution of  $\sim 8\text{-}9\text{ lp/mm}$  (2.2) the Photochron I has a dynamic spatial resolution of  $\sim 5\text{ lp/mm}$  (2.5). It would therefore be reasonable to assume that the Photochron II would have a dynamic spatial resolution of  $\sim 9\text{-}10\text{ lp/mm}$ . This together with an increased streak writing speed of  $\sim 2.10^{10}\text{ cm/sec}$ , (which can be provided by a krytron circuit (2.3)), would lead to a streak resolution limit  $\Delta T_s$  of  $\sim 0.5\text{ psecs}$ .

With a streak resolution limit of  $\sim 0.5\text{ psecs}$  and a transit time spread of  $\sim 0.4\text{ psecs}$  the camera instrumental function would have a half width of  $\sim 0.6\text{ psecs}$ . Hence with these modifications it should be possible to produce a streak camera capable of subpicosecond resolution.

### 3.3. Signal Induced Noise

A problem arising in the Photochron I image tube is the signal induced noise due to scattering of the electron beam in the image tube before and after streaking. A mode-locked laser train is typically of the order of  $1\text{-}2\text{ microseconds}$  long and therefore the pulses before and after the one selected for streaking give rise to the background noise seen on the streaks of plates 1 and 2.

In the Photochron I the streak deflection plates were  $20\text{ mm}$  long by  $25\text{ mm}$  and were  $4.0\text{ mm}$  apart. The maximum potential difference between these plates occurs at the beginning and end of the streak

operation, and is  $\sim 2.5$  Kv (2.3). With the usual accelerating voltage at the anode of  $\sim 18$  Kv, the deflection of an electron which enters at the centre of the plates is given by (87)

$$y = \frac{x^2}{4d} \frac{V_d}{V_a} \quad (3.1)$$

where  $V_d$  is the potential difference between the plates,  $d$  the plate separation,  $V_a$  the electron accelerating potential and  $x$  the distance travelled between the plates. Thus at the beginning and end of the streak operation the maximum electron deflection at the exit of the plates is  $\sim 3.5$  mm. However since the plate separation is only  $\sim 4$  mm then the electron beam must strike the plates before it exits, causing scattering of the beam towards the phosphor (FIG 19(a)). Also it can be seen that at potential differences less than 2.5Kv the electron beam will collide with the wall of the image tube and again scattering towards the phosphor will occur (19(b)). To remedy these causes of scattering it was proposed to flare the plates so that they did not interrupt the deflected electron beam at potential differences of  $\sim 2.5$  Kv and also to insert apertures in the image tube drift space to prevent scattering from the tube walls onto the phosphor screen.

From eqn. (3.1) it is evident that the electron beam deflection will be  $\sim 2$  mm at a point  $\sim 15$  mm from the start of the deflection plates, and the beam will thus strike the plates at this point. These calculations are only approximate however since they take no account of the finite electron beam width. With this in mind a new set of flared deflection plates were manufactured, (FIG.20(a)). The plates were 25 mm wide and 20 mm long, they were parallel at a separation of  $\sim 4.5$  mm to 12 mm where they flared to a final separation of 11.5 mm at 20 mm. These were inserted in place of the usual streak plates in the demountable image tube. Two apertures were also constructed and inserted in position in the demountable image tube as shown in FIG.20(b). Aperture 1 was circular of diameter 1.5 cm and aperture 2 was also circular and of diameter 4.0 cm. These still allowed a phosphor scan of  $\sim 8.0$  cm.

Tests upon the remodelled tube were carried out in the evacuated chamber described earlier (3.2). In this case a thermionic electron source providing a slit image was used since the gold photocathode did not provide sufficient electrons for noise performance tests. The potential of the lower deflection plate was set at 18Kv and the potential of the upper plate was varied above and below the value at the lower plate. The noise at the image tube phosphor as the slit image was deflected was recorded photographically. The regions of most interest in these recordings were those for which the upper plate voltage was between 2.5 Kv above and 2.5Kv below that of the lower plate. This corresponded to the 5Kv scan generated by the krytron deflection circuit. No records were taken at voltages (on the upper plate) for which the slit image appeared on the phosphor screen. To reproduce the conditions of operation of the streak camera, an image intensifier (EMI type 9694) was coupled externally to the output phosphor of the demountable image tube via the plain glass window of the vacuum system. The intensifier was operated at full gain and the noise at the intensifier output recorded on HP4 35mm film. The noise due to the intensifier itself was negligible compared to that arising in the image tube.

The noise in the image tube as the slit was deflected was recorded for three image tube configurations. In the first, the noise with the flared deflection plates and both apertures in position was recorded. In the second the noise with the flare plates in position and no apertures was recorded, and in the third the noise with the original parallel plates in position and the apertures also was recorded. So that comparisons of the noise in each configuration could be made the photographs were all taken with identical exposure times and f numbers, and on the same film to ensure the same  $\gamma$  and development times. Each film used was calibrated with a neutral density step wedge and the film  $\gamma$  was estimated (2.5). From microdensitometer traces of the noise levels a mean value of the recorded sensity DR was estimated. The

recorded density is related to the intensity I, incident upon the film by,

$$DR = \gamma / W \text{ Log}_{10} It$$

where t is the exposure time and W the density step wedge range. From the values of DR, values for the noise intensity I were obtained. The noise intensity as a function of the voltage on the upper deflection plate was plotted for each of the three image tube configurations. The results are shown in FIG.21 and these indicate that the system with the least noise is that using both the flared plates and the apertures (FIG.21(a)). The flared plates minus the apertures show a marked increase in noise suggesting that the apertures do play an important role in noise suppression (FIG.21(b)). The performance of the parallel plates plus apertures is shown in FIG.21(c)) and here again the noise is higher than that of FIG.21(a) showing this time the effect of using flared plates.

To investigate the effect of removing the apertures while using the parallel deflection plates the experiment was repeated. FIG.22(a) shows the noise performance of the parallel plates plus apertures and FIG. 22(b) the noise performance with the apertures removed. The noise with the apertures removed was once again greater than that with the apertures in place confirming the role of the apertures in noise reduction. No comparison of the results in FIG.21 and FIG.22 may be made since they were carried out under different experimental conditions.

The conclusion which may be drawn however from these results is that the use of flared plates and apertures in the drift space of the image tube allows a reduction in the background noise level arising when the signal is deflected.

The major drawback to the use of flared plates however is the loss in deflection sensitivity. The parallel deflection plates had a sensitivity of ~ 330v/cm. The flared plates sensitivity was measured to be ~ 400v/cm. With a sensitivity of ~ 330v/cm the 4 cm length of the phosphor used in streak mode operation is swept by a voltage difference of 1320 volts. This voltage is provided by the central 1.5 Kv of the krytron ramp (2.3). For a sensitivity of 400 v/cm however, 1600 volts are required to sweep

the phosphor segment, and this means an increased sweep time at the phosphor. Since the ramp generated by the krytron circuit has a nonlinearity of less than 10% over the central 1.5 kv portion then the streak velocity at the phosphor should be reduced in the ratio of the deflection sensitivities.

Thus the use of the flared plates would mean that the maximum attainable streak velocity would be ~ 80% of that obtained using the parallel deflection plates. This in turn would lead to a reduction in the temporal resolution of the tube since the streak limited resolution  $\Delta\tau_s$  would be increased (eqn.1.24) as  $\Delta\tau_s = 1/v\delta$ . Thus for an image tube of streak velocity  $10^{10}$  cm/sec and with a dynamic spatial resolution of 50 Lp/cm, the use of flared streak plates would increase the value of  $\Delta\tau_s$  from 2.0 psecs to 2.5 psecs.

#### 3.4. The S1 Image Tube Streak Camera

A Photochron II design image tube incorporating the features of high photocathode field, lower electron-optical magnification (3.2), flared deflection plates and aperture stops (3.3) was manufactured (95). The tube had an S1 (Ag-o-Cs) photocathode so that its performance could be evaluated using a Nd: glass laser.

In the manufacture of S1 photocathodes the process of caesiation (88) lowers the work function at the surface of the cathode and with the high field values near the photocathode of the Photochron II the possibility of electrical breakdown is enhanced. A new photocathode shape was therefore designed to reduce this possibility. The Photochron I mesh and cathode assemblies and the new design cathode of the Photochron II are shown in FIG.23(a) and (b) respectively. The design of the Photochron I prevented simply bringing the mesh M and photocathode P/C assemblies closer together to achieve the required separation of 0.5 mm, since at such a mesh to cathode separation the supporting rings would be in contact. The design of FIG. 23(b) was therefore used. A more detailed view of the new cathode substrate is shown in FIG. 23(c). The cathode edges were all made with a large radius of curvature to eliminate high field

values at these points. The useful area of the plateau on which the cathode material was deposited was  $\sim 9$  mm in diameter and the plateau was  $\sim 4$  mm above the substrate base. Electrical contact was made by evaporating a chromium layer on the sloping edge of the cathode and contact to this was made by way of the supporting ring at the substrate base.

This design ensured that the highest electric field values were at the plateau of the photocathode and that no extreme values of field were present where the electrical contacts were made. Thus the possibilities of electrical breakdown were minimised.

In order to test the static performance of the image tube a resolution test pattern was imaged onto the photocathode. With the image tube operated in the focus mode the resolution at the phosphor and the electron-optical magnification were observed for different mesh voltages. The results are as shown in FIG.24(a) and (b) respectively. The focussing characteristic of cone voltage at each particular mesh voltage is also shown in FIG.24(c). The observed spatial resolution at the phosphor was slightly higher in the manufactured image tube, than that observed in the demountable system (3.2). This is most likely due to the more precise location of the manufactured tube's electrodes, and the more uniform electric field near the photocathode. The greater sensitivity of the S1 photocathode compared to the gold cathode used previously also helps to increase the contrast in the image observed. However the plot of magnification versus mesh voltage showed a slight increase at a mesh voltage of  $\sim 1$ kv. The magnification value now being  $\sim 1.95$  compared to  $\sim 1.8$  observed in the demountable experiments. This higher value probably arises due to a more accurate location of the mesh nearer to the photocathode than was attained previously. No points were plotted for mesh voltages below 500v since the resolution began to worsen and distortion to appear at lower voltages.

The values of cone voltage for which the image at the phosphor was in best focus (FIG.24(c)) show only a variation of  $\sim 20$  volts for

mesh voltages in the range 500v to 1000v. From FIG 24(c) it can be seen that at a mesh voltage of  $\sim 860$ v the cone voltage to focus the image tube is also  $\sim 860$ v. The electric field between the mesh and the cone in this case is almost zero and therefore the mesh to cone lens  $L_1$  of FIG.16 is much weakened. In this case the magnification at the phosphor should be due mainly to the action of the cone-anode lens  $L_2$ . The magnification in this case should therefore be of the same order as that of the image tube before insertion of the mesh electrode was made (2.2). From the plot of mesh voltage versus electron - optical magnification (FIG.24(b)), the magnification at 860 volts is  $\sim 1.9$  compared to 1.8 before insertion of the mesh electrode (46). Thus in this case the image tube combines the low magnification of the pre-mesh tube with the advantages of a much lower transit time spread.

To investigate the dynamic performance of the Photochron II streak camera a mode-locked Nd: glass laser was employed. The radiant sensitivity of the S1 photocathode of the streak camera image tube was low  $\sim 0.25$  mA/watt (more usually  $\sim 1$  mA/watt) at 1.04 microns. The experimental system employed in the investigation is shown in FIG.25. The laser active medium consisted of a  $3/8$ " by 6" Nd: glass rod (Owens Illinois ED-2) with Brewster angled end faces, optically pumped using a helical xenon filled flashlamp.

Distilled water flowing in a co-axial quartz sheath about the rod was used for cooling purposes. A concave, 35 cm focal length, dielectric coated mirror of 99% reflectivity formed one end reflector of the cavity while at the other end a 70% reflectivity plane dielectric mirror was used as the output coupler. The laser was mode locked using a saturable absorber in contact with the 70% output mirror (89,90). The absorber was a solution of Eastman Kodak 9860 Q switch dye, in a solution of 1, 2 - dichloroethane. A red filter F prevented decomposition of the dye by U.V. flashlight. The concave mirror was used with a concave lens L (focal length 10 cm) to compensate for thermal lensing effects (92) of the optically pumped rod. The output of this laser was monitored using an S1 biplanar vacuum photodiode and a Tektronix 519 oscilloscope, and was found to consist of a train of picosecond pulses (61), of total

duration  $\sim 1$  microsecond, with each pulse separated by  $\sim 8$  nanoseconds.

A portion of the laser output was selected by the beamsplitter B and directed into the optical delay line (2.5) which was set to give subpulses separated by 60 psecs. The synchronisation of the streak ramp voltage with the arrival of a pulse at the deflection plates was effected by the use of the variable internal electronic delay of the 519 oscilloscope used to generate the trigger pulse (2.5). The width of the camera input slit was set at 50  $\mu\text{m}$  (16  $\mu\text{m}$  at the photocathode) and the input lens was set at  $f/4$ . The intensifier was operated at full gain (i.e. input lens at  $f/1.5$ , and voltage  $\sim 35$  Kv). For initial tests the krytron circuit was operated at an anode voltage of 5Kv and two integrators were used, (2.3). The same integrators when used with the Photochron I image tube camera gave velocities at the phosphor of  $\sim 3.3 \times 10^9$  cm/sec and  $9 \times 10^9$  cm/sec. These integrators used with the Photochron II design gave streak writing speeds at the phosphor of  $\sim 2.8 \times 10^9$  cm/sec and  $6.6 \times 10^9$  cm/sec respectively. Thus the Photochron II design exhibited a streak velocity  $\sim 75 - 80\%$  of that of the Photochron I. This reduction in the streak velocity being of the same order as the reduction in the deflection sensitivity due to the use of the flared plates (3.3). The noise background of the streak photographs was fairly low, however at such slow streak speeds the photocurrent drawn is also low and consequently the background noise is lower than at higher streak velocities.

Without an integrator between the krytron output and the streak plate capacitor the observed streak velocity was  $\sim 1.2 \times 10^{10}$  cm/sec. There was a noticeable increase in the background noise in this case due to the higher streak velocity. The noise however showed an improvement over the noise at high streak velocities ( $\sim 10^{10}$  cm/sec) in the Photochron I. The degree of improvement was however not as much as might have been expected from the preliminary results (3.3). The conclusion to be drawn is that at the high streak velocities needed for good temporal resolution the noise improvement is not so marked as at the lower streak velocities. Further noise reduction

may perhaps be achieved by reducing the aperture diameters and moving them further back in the image tube towards the streak plates, such that the effective phosphor scan, although reduced, is still great enough for streak operation (i.e. 4 cm). Refinements to the streak plate shape may still be necessary although it is doubtful whether the loss in streak velocity due to increased flaring of the plates is offset by the improved noise performance.

In order to test the temporal resolution capability of the camera it was necessary to increase the streak speed in order to reduce the streak resolution limit  $\Delta T_s$  (3.3). In an attempt to increase the streak velocity the anode voltage of the krytron ramp generator was increased to  $\sim 6\text{Kv}$  by insertion of extra resistance in the keep-alive and avalanche transistor circuits (2.3). The optical delay line was adjusted to give sub-pulses separated by 60 psecs and 20 psecs. An integrator was not used, the ramp generator output being directly coupled to the streak deflection plates.

From streaks obtained on Polaroid type 47 film the streak velocity was measured to be  $\sim 1.5 \times 10^{10}$  cm/sec, showing that increase of the anode voltage reduced the krytron ramp rise time. The streaks obtained however were of quite high background noise, due to both the increased streak velocity and the increased voltage scan of  $\sim 6\text{Kv}$  at the upper deflection plate (3.3). It was therefore decided to electro-optically switch out several pulses from the laser train which contained typically 100 - 200 pulses. The selected pulses only would be incident upon the photocathode and therefore the number of pulses available for scattering, and hence the noise, would be reduced. A pockels cell arrangement (FIG.26) was used to select  $\sim 5$  pulses from the train. The pockels cells P.C., were placed between crossed Glan Kappa polarisers, G.K. The transmission of this arrangement is practically zero until the application of a high voltage pulse ( $V \lambda/2$  at 1060 nm  $\sim 9\text{Kv}$  for KDP)

to the pockels cells, when the transmission increases to  $\sim 60\%$ . A square voltage pulse of  $\sim 5\text{Kv}$  amplitude and duration  $\sim 40$  nsecs was provided by a krytron circuit and co-axial pulse forming network. This square pulse applied to both pockels cells rotated the polarisation of each by  $\sim 45^\circ$  so that the resultant polarisation was  $\sim 90^\circ$ . For the duration of the square pulse the arrangement was transmitting and thus selected  $\sim 5$  pulses from the laser train when the pockels cells gating pulses were synchronised correctly to the start of the laser train.

These switched out pulses were then directed into the delay line and the streak of plate 5 was obtained. The streak was recorded on Polaroid type 47, and shows sub-pulses separated by 20 psecs and 60 psecs. From this result the streak velocity was measured to be  $\sim 1.5 \times 10^{10}$  cm/sec and thus demonstrates the capability of the Photochron II design to operate at streak speeds in excess of  $10^{10}$  cm/sec without deterioration of temporal resolution due to the drawing of large photocurrents. The lower electron-optical magnification permits a lower photocurrent to be drawn (3.2), thus at streak velocities in excess of  $10^{10}$  cm/sec the photocurrent required is not of such a value as to cause image distortion and space charge effects (2.4).

The estimated recorded pulse full width of the central streak pair of plate 5 is  $\sim 3.3$  psecs. Measurements carried out previously on this same laser (59) have shown that the shortest duration pulses produced were  $\sim 3$  psecs. Other authors have also reported that the shortest observed pulses from similar lasers were  $\sim 3$  psecs (93,94). It is reasonable to assume therefore an actual pulse duration  $\Delta\tau_p$  of  $\sim 3$  psecs. Soboleva et al (91) have shown that the energy distribution  $\Delta E_n$  of an S1 photocathode illuminated by light of wavelength 1060 nm has a half width  $\sim 0.3$  ev. This corresponds to a transit time spread  $\Delta\tau_d \sim 0.7$  psecs for an electric field strength of 20,000 v/cm near the photocathode. Taking the slit width resolution limit of  $\sim 0.2$  psecs at  $1.5 \times 10^{10}$  cm/sec and assuming a dynamic spatial resolution of 10 Lp/mm then the camera instrumental function  $(\Delta\tau_s^2 + \Delta\tau_d^2)^{\frac{1}{2}}$  (1.4) is  $\sim 1$  psec. Using

the actual pulse width value of  $\Delta\tau_p \sim 3$  psecs then the recorded pulse width  $\Delta\tau_r$  is given by

$$\Delta\tau_r^2 = \Delta\tau_p^2 + (\Delta\tau_s^2 + \Delta\tau_d^2)$$

This yields a value of 3.2 psecs for  $\Delta\tau_r$ . Since the recorded pulse full width from the streaks of plate 4 is  $\sim 3.3$  psecs then this is in good agreement with a camera instrumental function of  $\sim 1$  psec and a dynamic spatial resolution of  $\sim 10$  Lp/mm.

Evaluation of the pulse duration of this same laser with the Photochron I streak camera (61) indicated that the camera had an instrumental function of 3 psecs. By using the same source of test pulses it is clearly demonstrated that the modifications incorporated in the Photochron II design streak camera have permitted the reduction of the camera instrumental function to  $\sim 1$  psec. Also the situation is now approached where the camera instrumental function may become negligible when compared to the laser pulse duration.

### 3.5. The S-20 Image tube Streak Camera

The image tube described in the previous section had an S1 photocathode and was thus most suited to measurements of the output of the infra-red Nd: glass laser. The shortest observed pulses from such a laser are of duration 3 psecs (59, 93, 94) and in order to further test the streak camera performance shorter pulses are required. Pulses of duration 2 psecs are reliably produced by the mode-locked R6G dye laser described in section 2. In order to use this laser as a source of test pulses a Photochron II design image tube was manufactured with an S20 photocathode (95). The image tube was this time made with parallel streak plates in order to increase the streak writing speed, (3.3).

The static characteristics of the image tube were tested and found to be similar to those of the S1 image tube (FIG.24(a) and (b)). For a photocathode extraction field value of 20Kv/cm the electron - optical magnification was x2 corresponding to a spatial resolution at the image tube phosphor of 18 Lp/mm. To complete the streak camera assembly the model 9694 image intensifier used in previous experiments (2.4) was replaced by a new system - EMI type 2001 which

was fitted with a four stage intensifier tube (type 9912) as before but was air cooled. The system gain was  $\sim 10^6$  and the maximum spatial resolution was  $\sim 35$  Lp/mm. The intensifier was operated at full gain (input lens at f/1.5, operating voltage 35Kv). The experimental arrangement was essentially that used with the SI image tube (3.4), FIG.25, only this time the Nd: glass laser arrangement was replaced by the twin flashlamp pumped R6G dye laser (61). The dye laser was passively mode-locked using a saturable absorber (DODCI in ethanol) placed in contact with the 100% reflectivity cavity mirror. A 60% reflectivity mirror served as the output coupler. An intra-cavity Fabry-Perot etalon was used to tune the laser output to 605 nm. The streak deflection ramp was generated by a krytron circuit (2.3) as before and the output of this circuit was directly connected to the streak plates of the camera. With the parallel streak plates the streak writing speed at the phosphor (for an anode voltage of 6Kv) was found to have increased from  $1.5 \times 10^{10}$  cm/sec to  $2.0 \times 10^{10}$  cm/sec. The laser output was monitored with a Tektronix 519 oscilloscope and the optical delay line was arranged to give sub pulses of separations 60 psecs.

Using this arrangement streaks as shown in plate 6 were obtained. The streaks were recorded on Ilford HP4 film and from the microdensitometer trace of FIG 27 (a) a recorded pulse half width  $\Delta\tau_r$  of  $\sim 2.0$  psecs was measured. Since the shortest pulses recorded in the output of this laser using the Photochron I streak camera (61, 96) had half widths ( $\Delta\tau_p$ ) of 2.0 psecs then it is reasonable to assume (eqn. 1.25) that the camera instrumental function of the Photochron II must be negligible when compared to the actual laser pulse durations.

When the ethanolic solution of DODCI used to mode - lock the laser was replaced with a solution of 1, 3' diethyl 4,2' quinoly - oxadicyanocyanine iodide (DQOCI) in ethanol and the laser tuned to 605 nm then recorded pulse widths (FWHM) of  $\sim 1.5$  psecs were measured. (The lifetime of DQOCI being an order of magnitude smaller than that of DODCI (102)). A microdensitometer trace of a pair of such pulses of separation 60 psecs is shown in FIG. 27(b). When the TPF method was used to measure the duration of

pulses from this laser when mode-locked with DQOCI no pulses shorter than 2.0 psecs were recorded (104). Even if an actual laser pulse duration of  $\sim 1.0$  psec is assumed then this implies a camera instrumental function of the order of 1.0 psec. However it is likely that the actual pulse durations  $\Delta T_p$  are somewhat greater than this value and thus this would give a camera instrumental function of less than one picosecond (eqn. 1.25).

During the investigation of the dye laser output (when mode locked with DQOCI) many streak records were taken and in some cases pulses composed of two nearly equal intensity components were observed. The microdensitometer trace of a streak record of a pair of such pulses is shown in FIG 27(c). Such pulses arise because of the manner in which the mode-locked dye laser output builds up from the initial intensity fluctuation pattern (96). The peaks of the sub pulses of FIG.27(c) are separated by 2.0 psecs and from this microdensitometer trace recorded half widths of the order of 1.0 psec are obtained. This result clearly demonstrates that the instrumental function of the Photochron II is less than one picosecond. With a transit time dispersion limit  $\Delta T_d$  of the order of 0.5 psecs (at a photocathode field value of 20Kv/cm) then the streak resolution limit  $\Delta T_s$  is also of the order of 0.5 psecs (eqn. 1.24).

These results thus show that the Photochron II streak camera has a subpicosecond resolution capability at dye laser wavelengths. The higher sensitivity of the Photochron II permits the use of an increased streaking velocity and the improved spatial resolution makes more information available to the observer. These factors coupled with the higher photocathode electric field have made possible this subpicosecond resolution capability.

### 3.6. Conclusions

It has been shown (3.4, 3.5) that the Photochron II streak camera provides a linear method for the measurement of ultra short light pulses from the infra-red to the visible region of the spectrum. Depending on the type of photocathode and the wavelength of the

illuminating radiation (1.4.2) the Photochron II camera may provide a diagnostic tool for laser pulse measurement which has the capability of subpicosecond temporal resolution (3.5).

Other streak cameras while employing streak velocities equal to or greater than that of the Photochron II have not achieved subpicosecond temporal resolution. The S1 streak camera developed by Schelev et al (48) has a streak writing speed of  $1.6 \times 10^{10}$  cm/sec however low values of extraction field (3600 v/cm) and dynamic spatial resolution (1.3 Lp/mm) meant that the camera had a half width of  $\sim 5$  psecs. Basov's helical sweep streak camera has a writing speed of 4.5 to  $6 \times 10^{10}$  cm/sec (63) and a dynamic spatial resolution of 5 Lp/mm corresponding to a value of  $\Delta\tau_s \sim 0.4$  psecs. Again, however the low extraction field value near the S1 photocathode (6000 v/cm) limits the transit time dispersion to  $\sim 2.0$  psecs and the camera instrumental function is therefore  $\sim 2.0$  psecs.

The Photochron II camera has a streak resolution limit  $\Delta\tau_s$  of  $\sim 0.5$  psecs. The ultimate limit for the streak resolution occurs when the streak ramp voltage  $V$  (5Kv) is applied as a step waveform. The streak limited resolution  $\Delta\tau_s$  is then given by (83).

$$\Delta\tau_s = \frac{t_d}{VD\delta}$$

where  $t_d$  is the transit time of an electron in the streak plates ( $\sim 0.25$  nsecs for 18Kev electrons and plates 2.0 cm long),  $D$  is the deflection sensitivity (330v/cm or  $\sim 3$  cm/Kv) and  $\delta$  is the dynamic spatial resolution (100 Lp/cm). Thus the limiting value of  $\Delta\tau_s$  is 0.17 psecs, and this limit is now being approached as streak velocities increase. Simply shortening the deflection plates reduces the limit but also reduces  $D$  and thus the streak velocity will suffer.

The limiting value of the transit time dispersion is set by the

value of electric field which may be applied near the photocathode and also by the electron energy distribution of the photocathode itself. At present the gallium arsenide photocathode appears to provide the lowest value of  $\Delta E_n$  of  $\sim 0.1$  ev when illuminated over the wide band from 200 - 900 nm (97). With the present value of extraction field of 20Kv/cm this would yield a value for  $\Delta \tau_d$  of  $\sim 0.3$  psecs. Combining these values of  $\Delta \tau_s$  and  $\Delta \tau_d$  it would therefore be possible to provide a streak camera with an instrumental function  $(\Delta \tau_s^2 + \Delta \tau_d^2)^{\frac{1}{2}}$  of  $\sim 0.35$  psecs, without radical redesign of the Photochron II image tube.

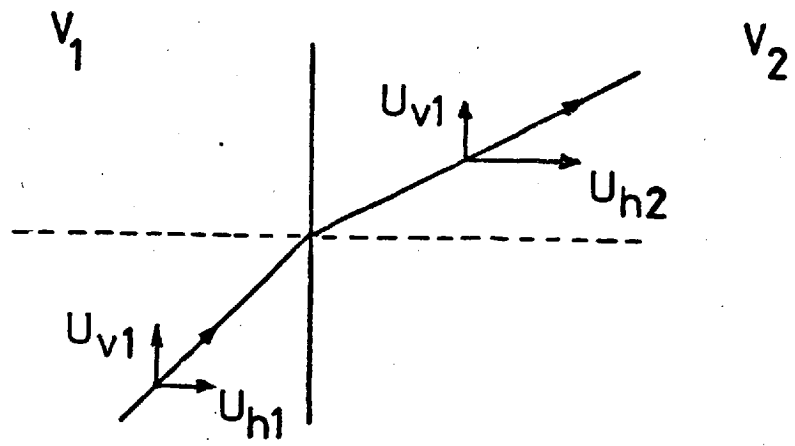
The position of the extraction mesh close to the cathode (0.5 mm) and the relatively low voltage (1Kv) at which it is held gives the Photochron II tube the facility of gated operation. It has been observed that a negative potential of 10 volts or more applied to the mesh will extinguish the image at the tube phosphor. In this condition the tube is non-conducting or gated off, and any information arriving at the photocathode while the mesh voltage is held at this negative value will not give rise to an output. If a square voltage pulse (amplitude  $\sim 1$ Kv) of fast rise and fall times ( $\sim 1$  nsec) and duration equal to several laser cavity round trip times, is applied to the mesh then the tube will conduct for the duration of the square pulse. Any information arriving at the photocathode during this gated on period will give rise to an output. Thus by providing such a pulse at the image tube mesh a portion of an incident laser pulse train could be switched out and a pulse in this portion selected for streaking. The background noise in this case would be much reduced since the number of pulses arriving during the tube 'ON' time would be smaller. Such a facility would make the pulse selecting arrangement of FIG.26 redundant. The attractiveness of this arrangement is that while only a relatively low amplitude gating pulse is required ( $\sim 1$ Kv) a high value of extraction field ( $\sim 20$ Kv/cm) is maintained.

While it has been demonstrated that the Photochron II streak camera is capable of subpicosecond temporal resolution, sources of such short duration pulses are required to accurately determine the

resolution limit of the camera. Pulses near the end of the mode - locked Nd: glass laser train have been shown to contain structure of subpicosecond duration (23), however discrete pulses of subpicosecond duration can not be obtained unless special techniques are adopted. These have included expanding the lasing bandwidth to produce pulses  $\sim 0.9$  psecs in duration (98) and the use of a ring amplifier and saturable absorber, again to broaden the spectrum, to produce pulses of  $\sim 1$  psec (99).

However for the production of pulses of duration much less than a picosecond, methods based on the Raman effect and beat signals from a dual frequency dye laser (101) are more promising. Colles (100) has demonstrated with a Raman oscillator (active medium - benzene) that pump pulses from a Nd: glass laser of  $\sim 3$  psecs duration may be converted to pulses  $\sim 0.3$  psecs in duration, and Russian workers (67, 103) have employed the beats technique extensively.

Thus by utilising pulses from the stimulated Raman effect and the beating of two dye laser frequencies a suitable test source will be available to enable the resolution limit of the Photochron II camera to be determined.



(a)

(b)

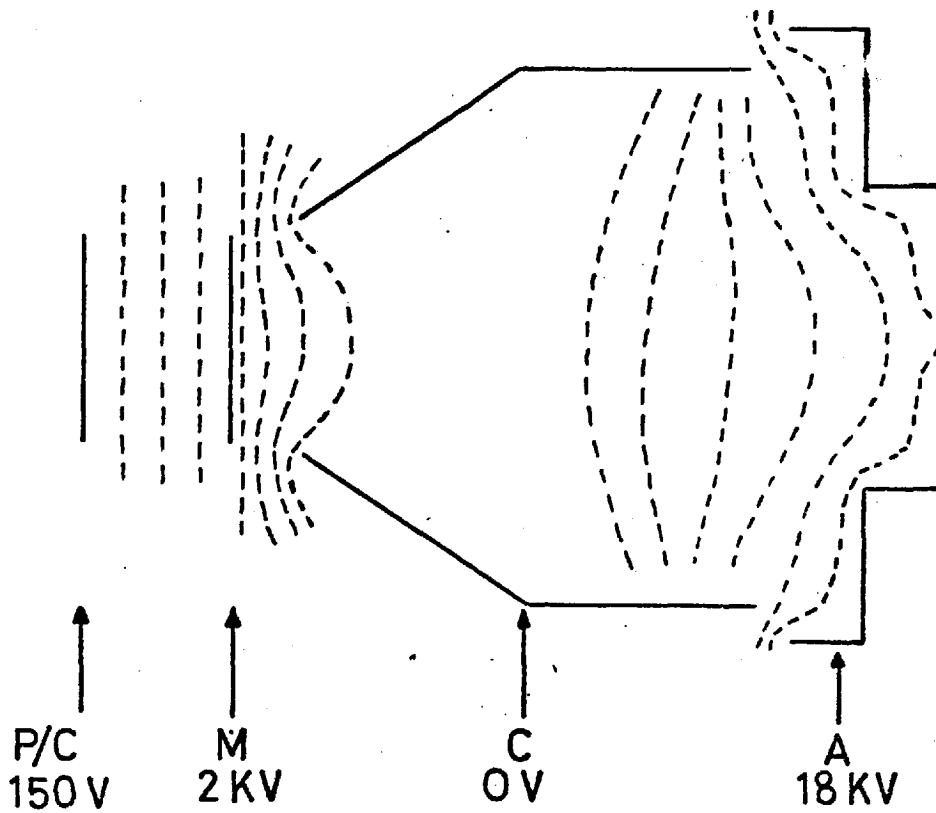
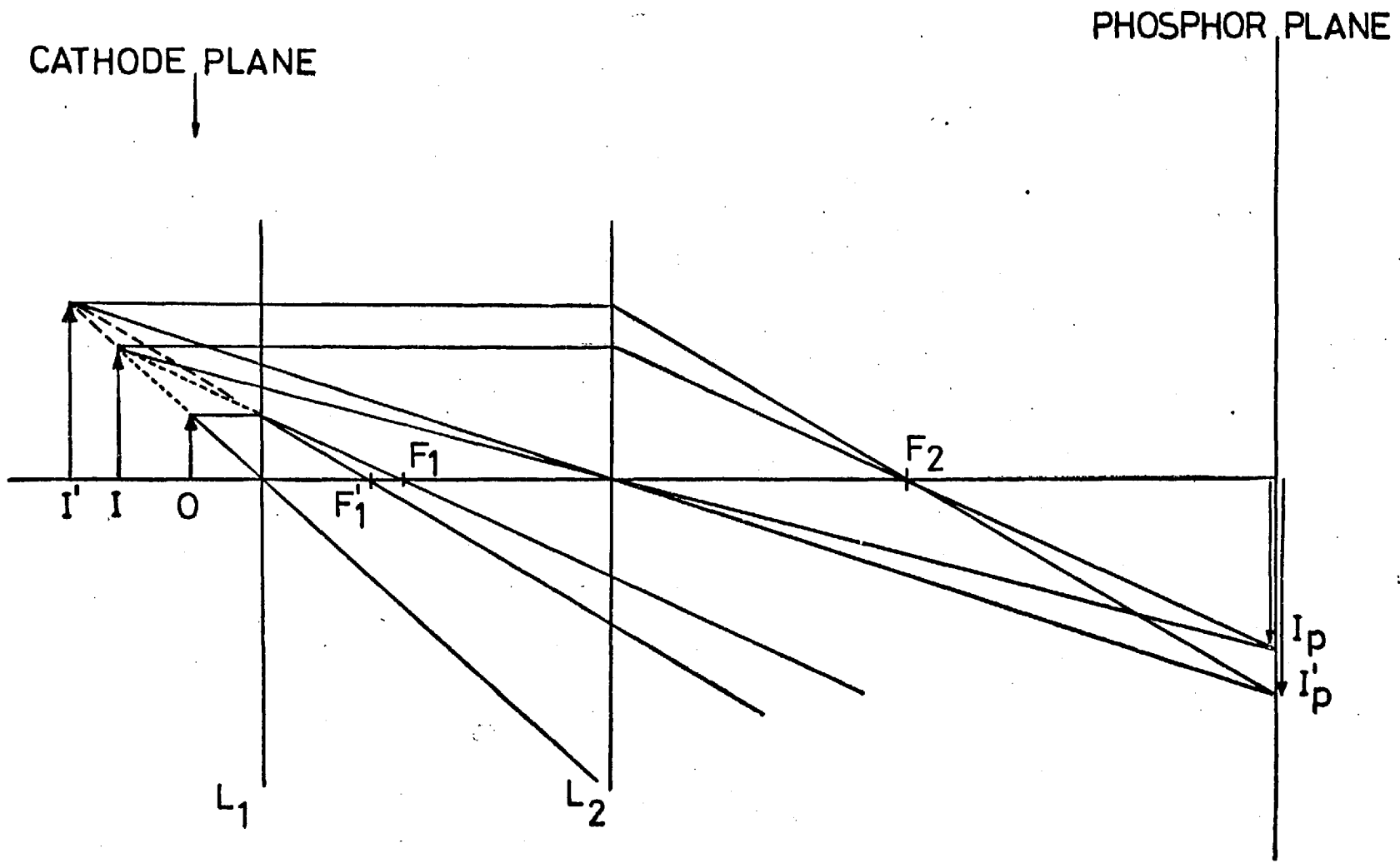


FIG. 15

FIG.16



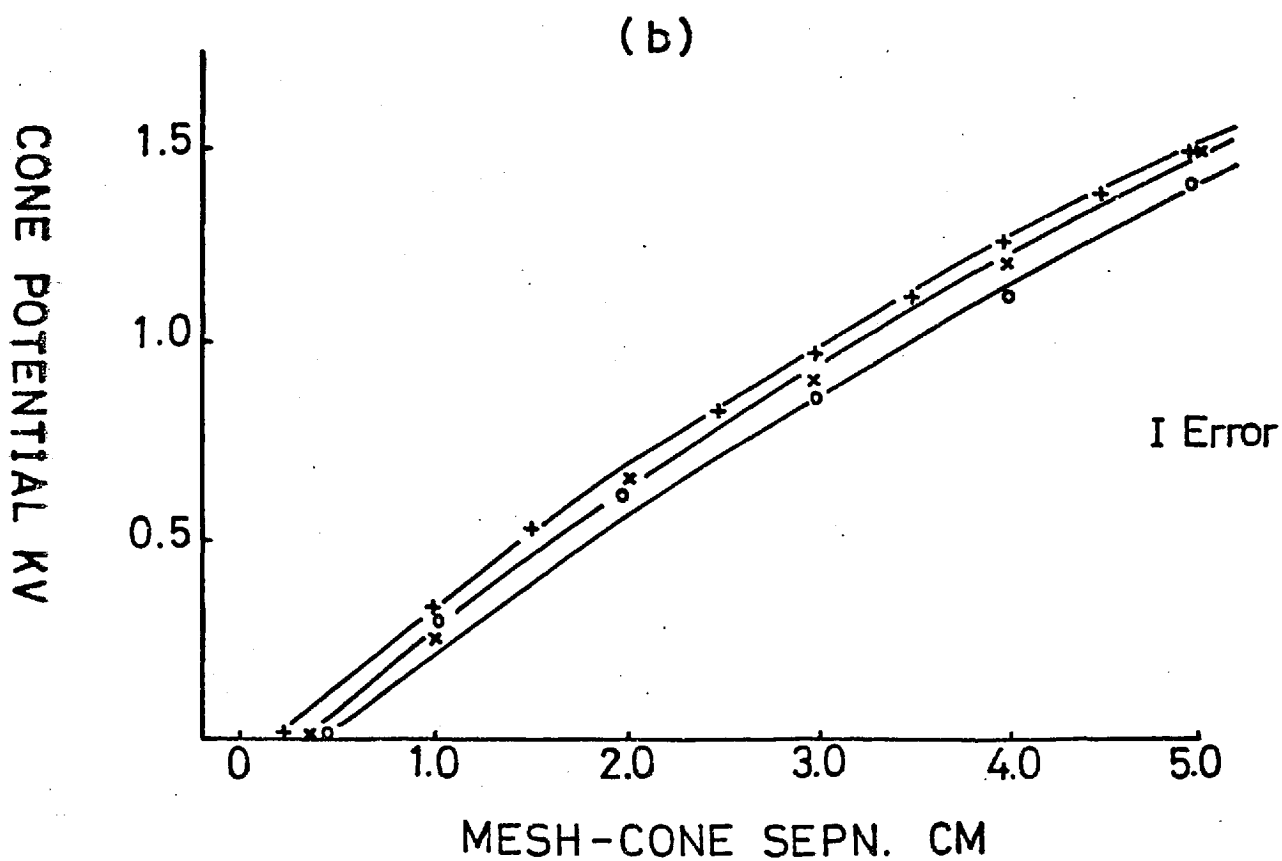
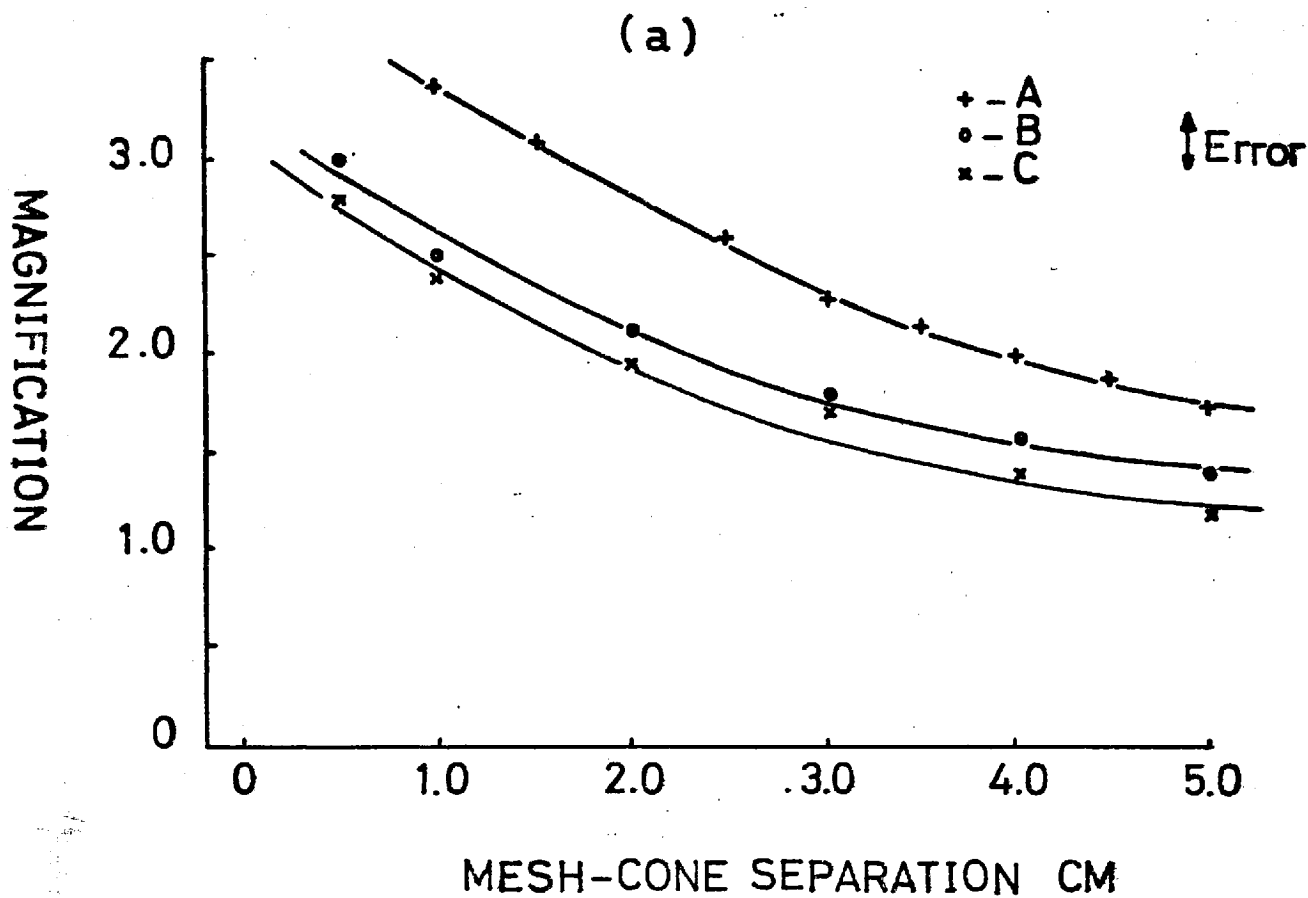


FIG. 17

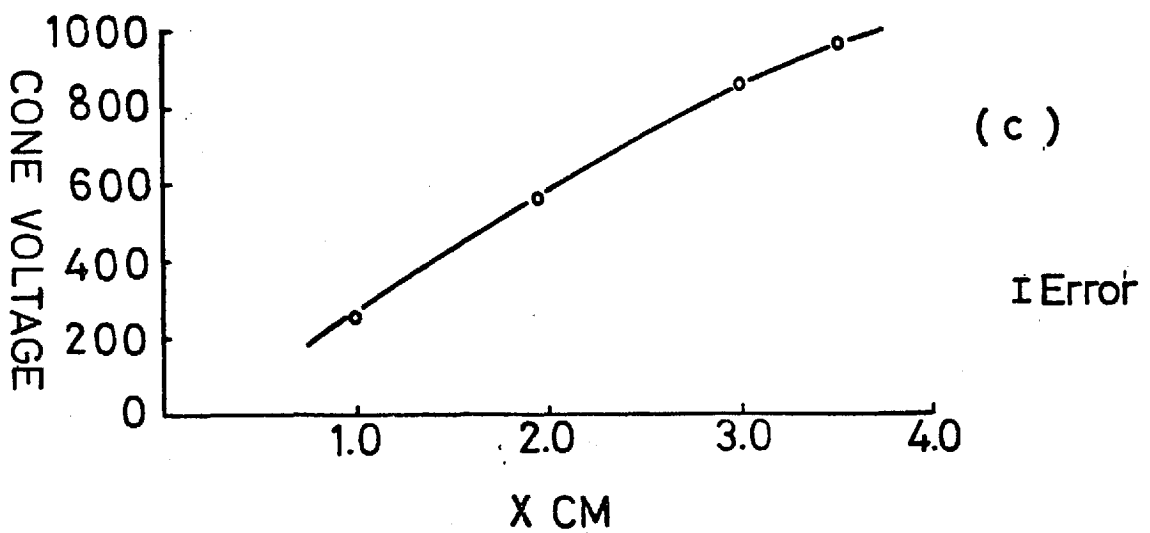
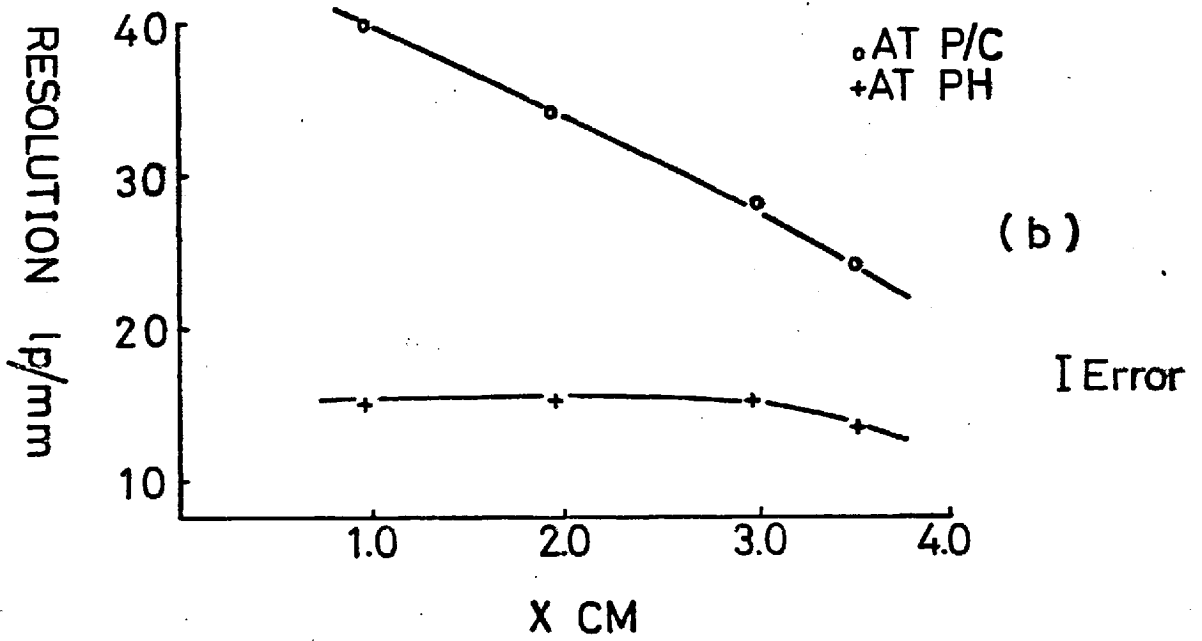
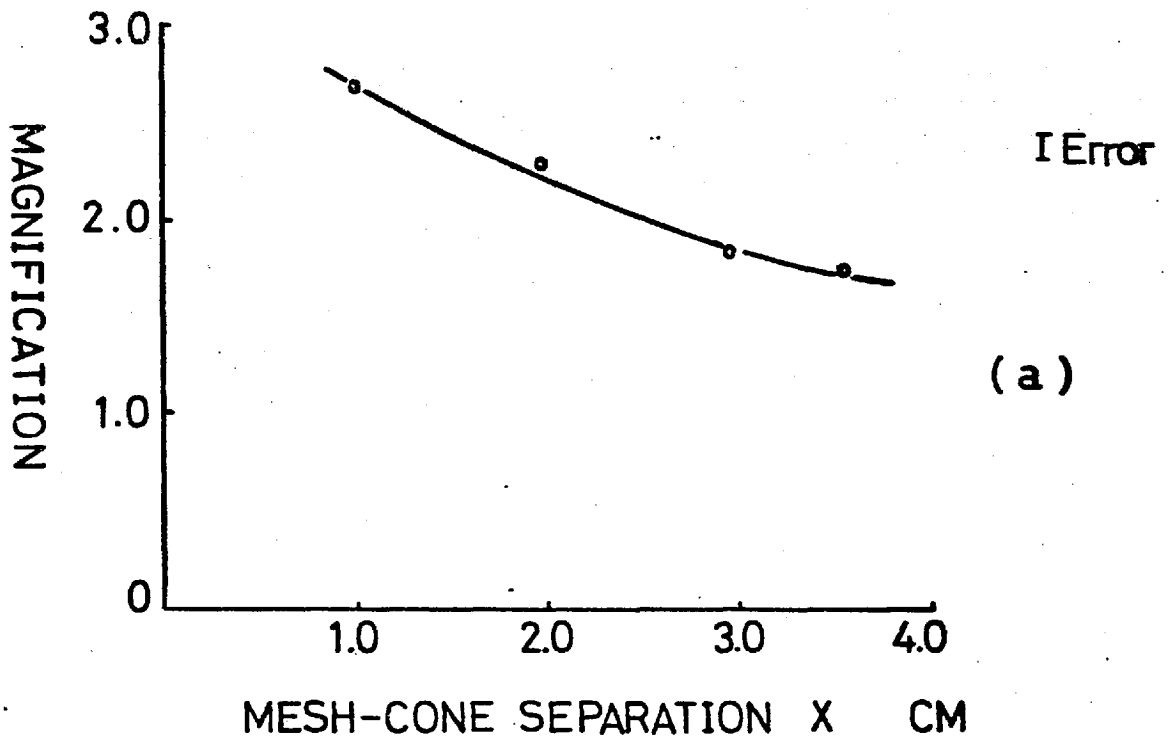
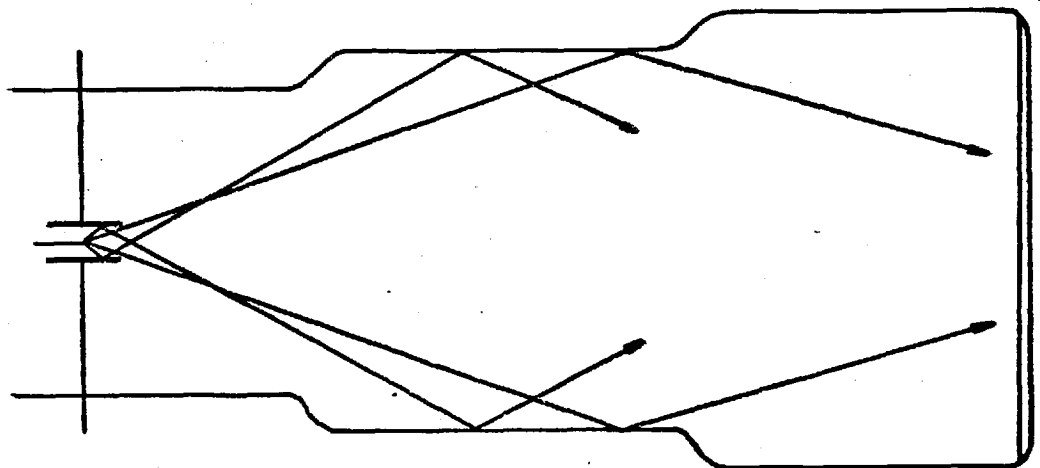
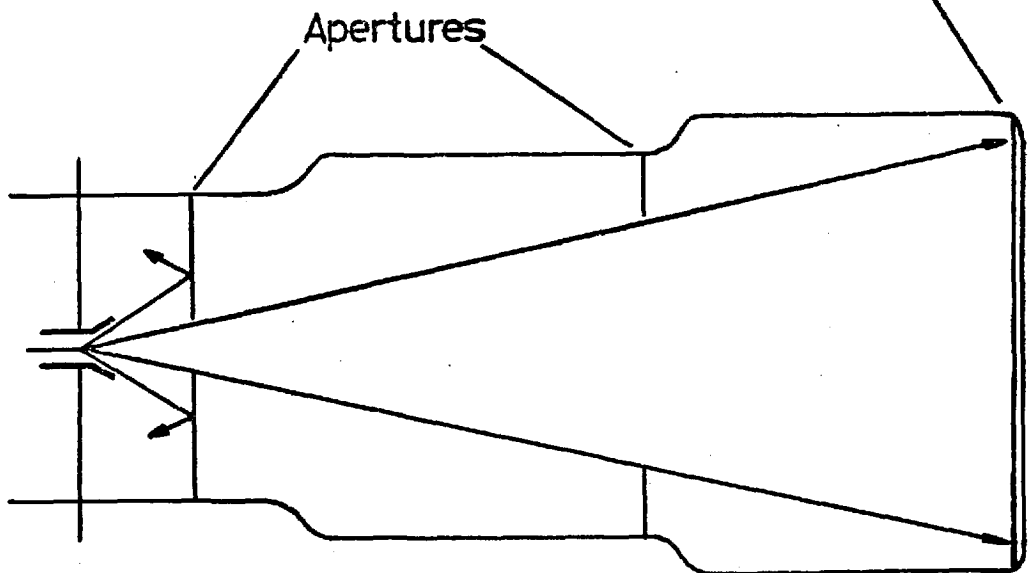


FIG.18



(a)

Phosphor



(b)

FIG. 19



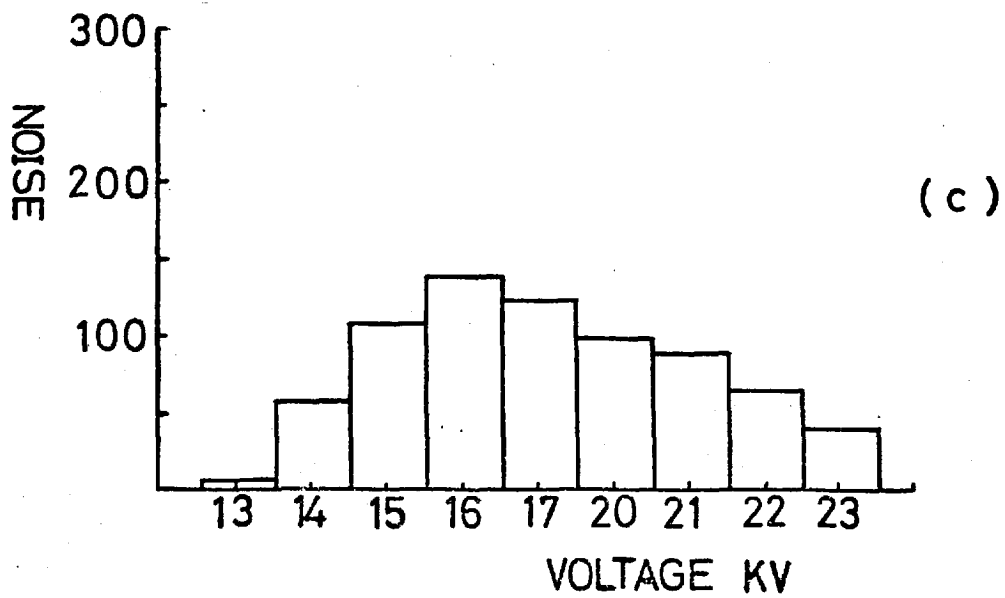
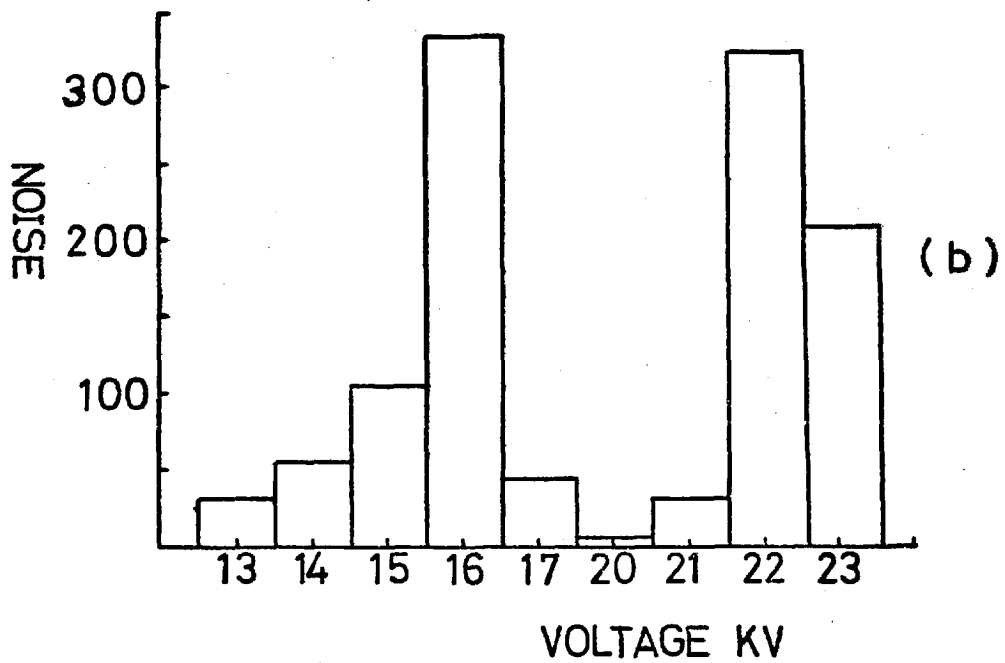
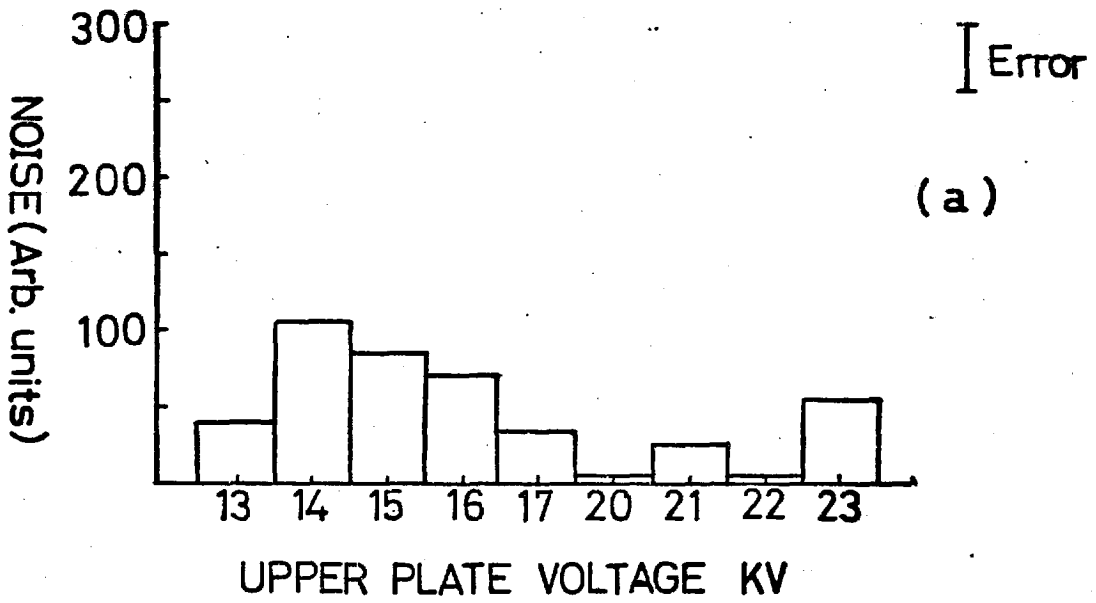


FIG. 21

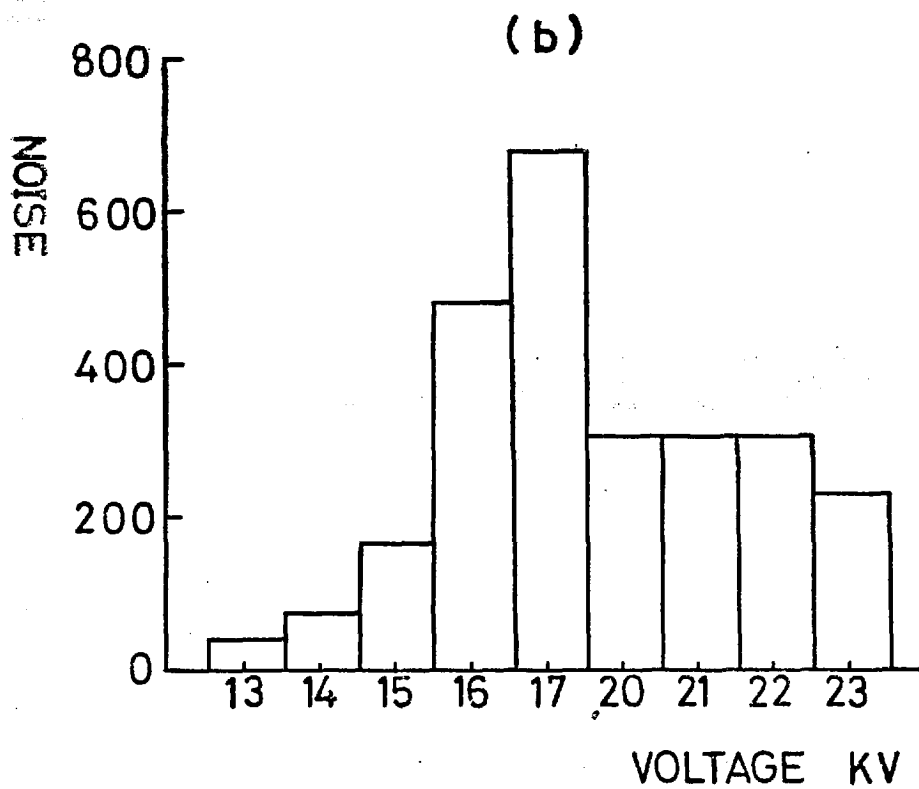
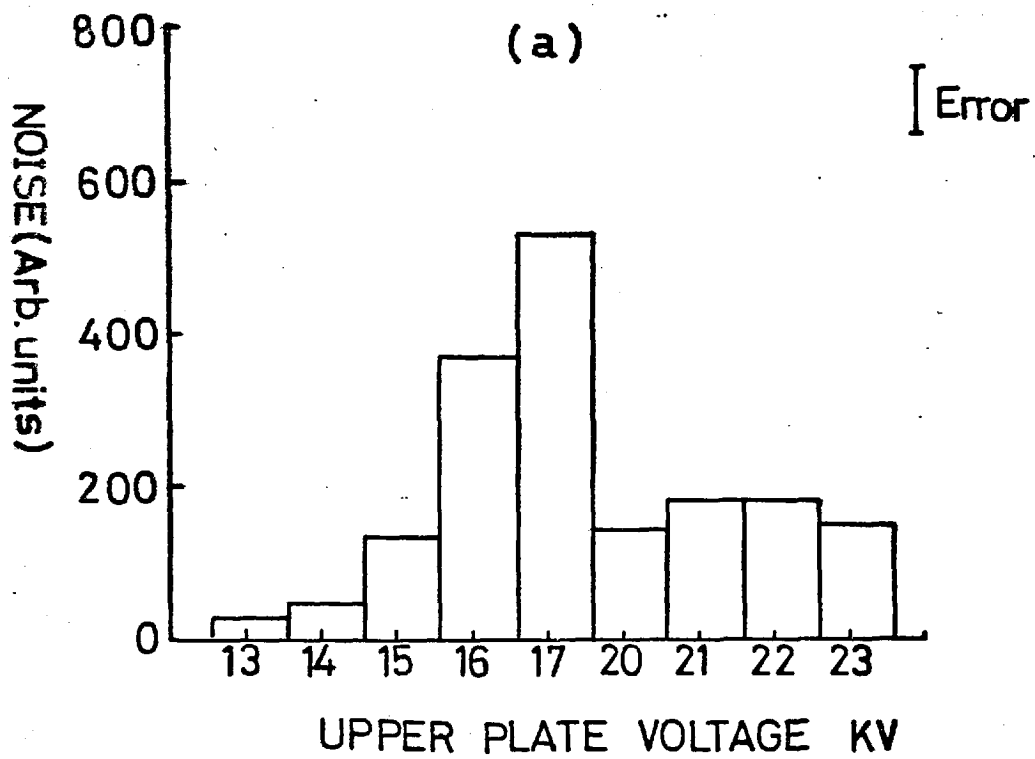


FIG. 22

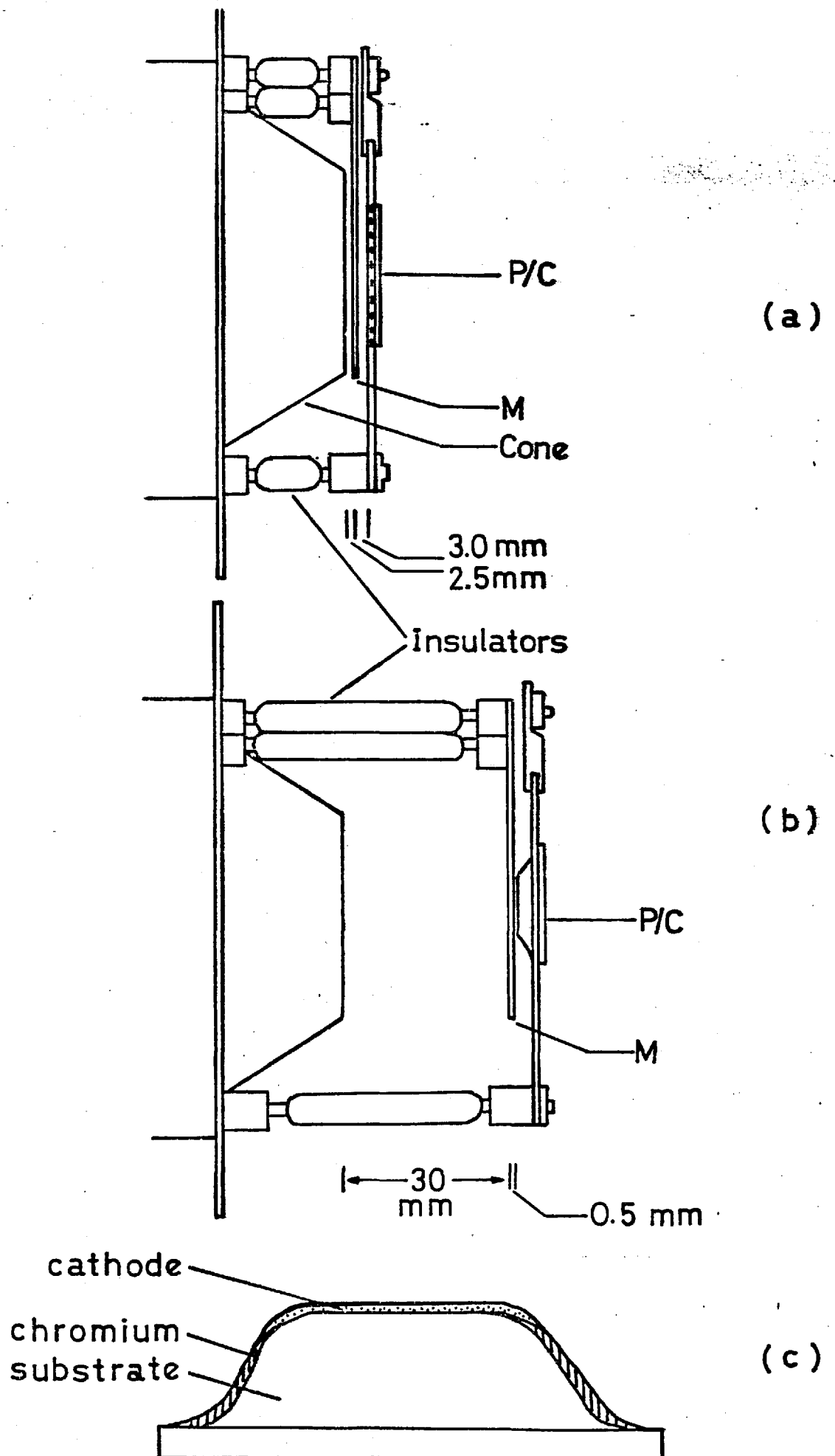


FIG. 23

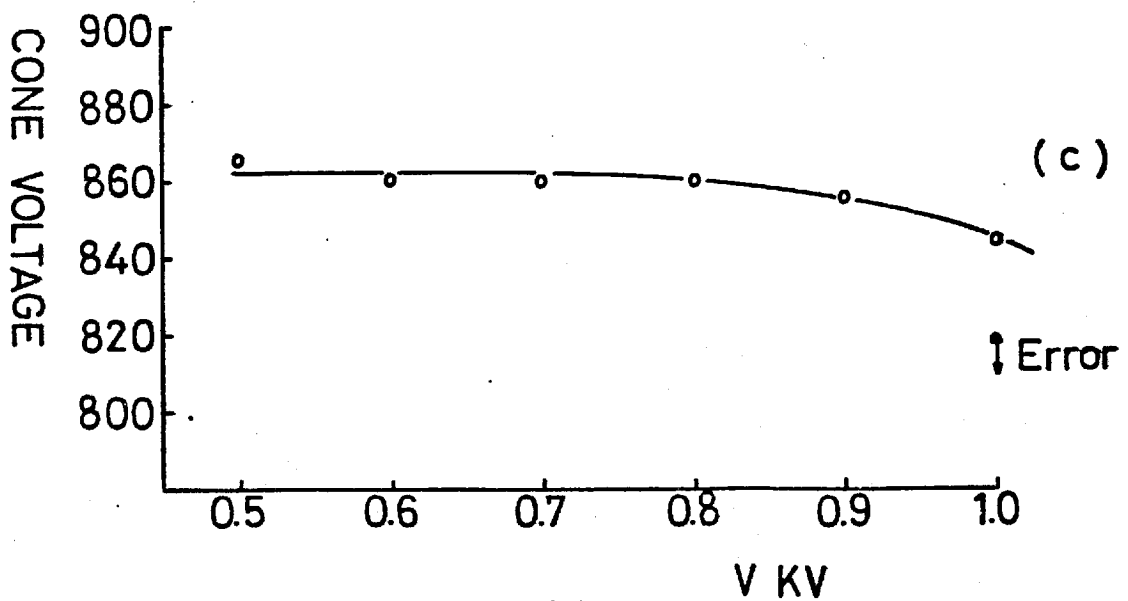
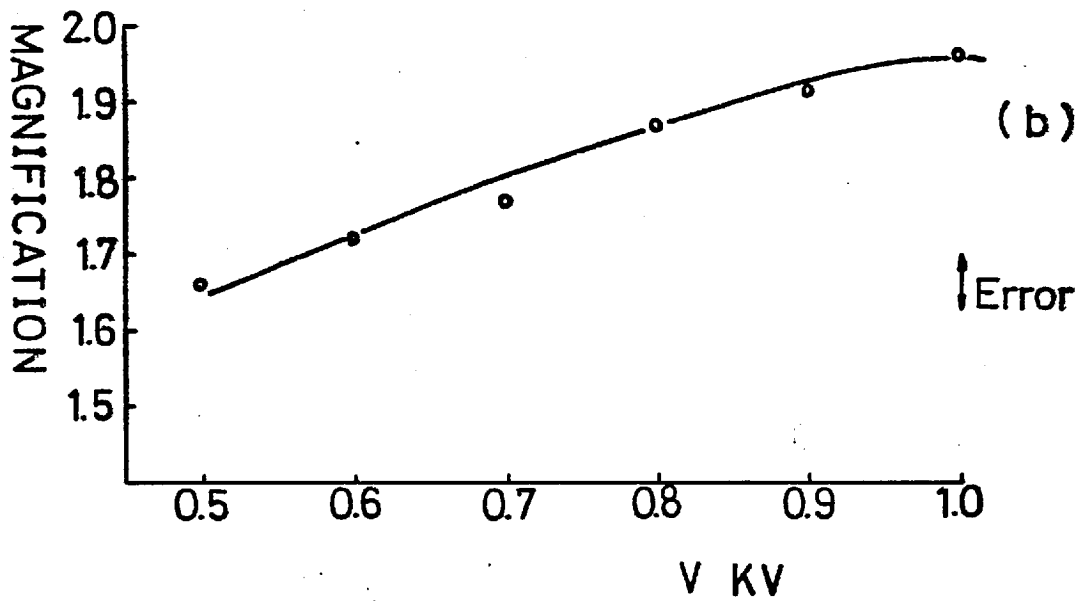
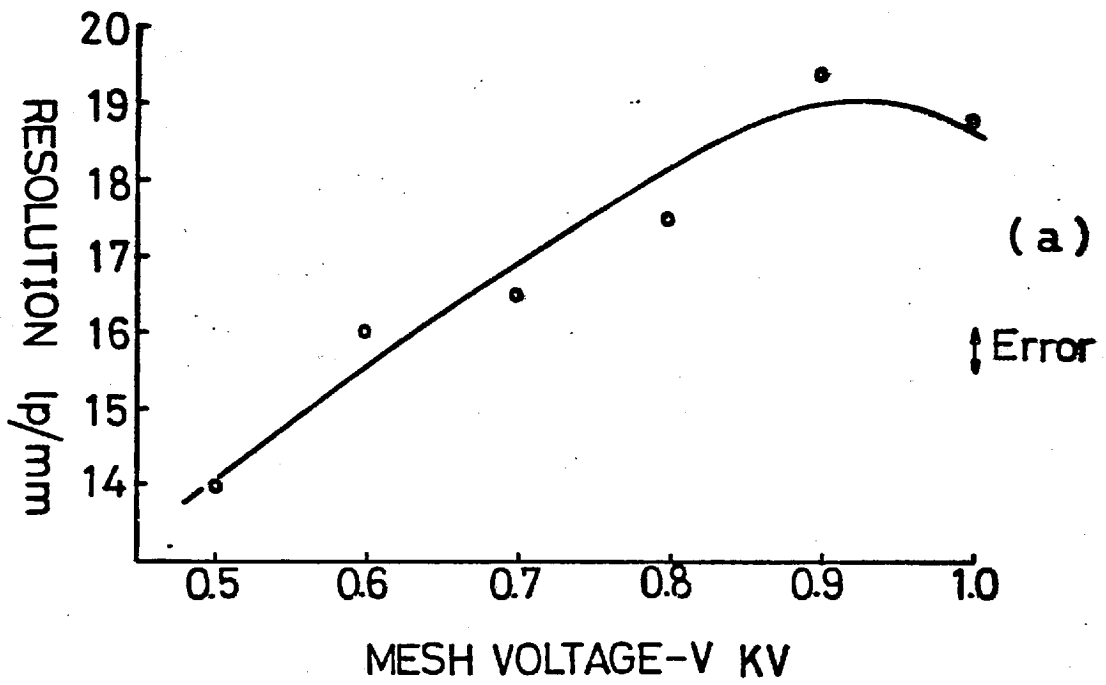


FIG. 24

FIG. 25

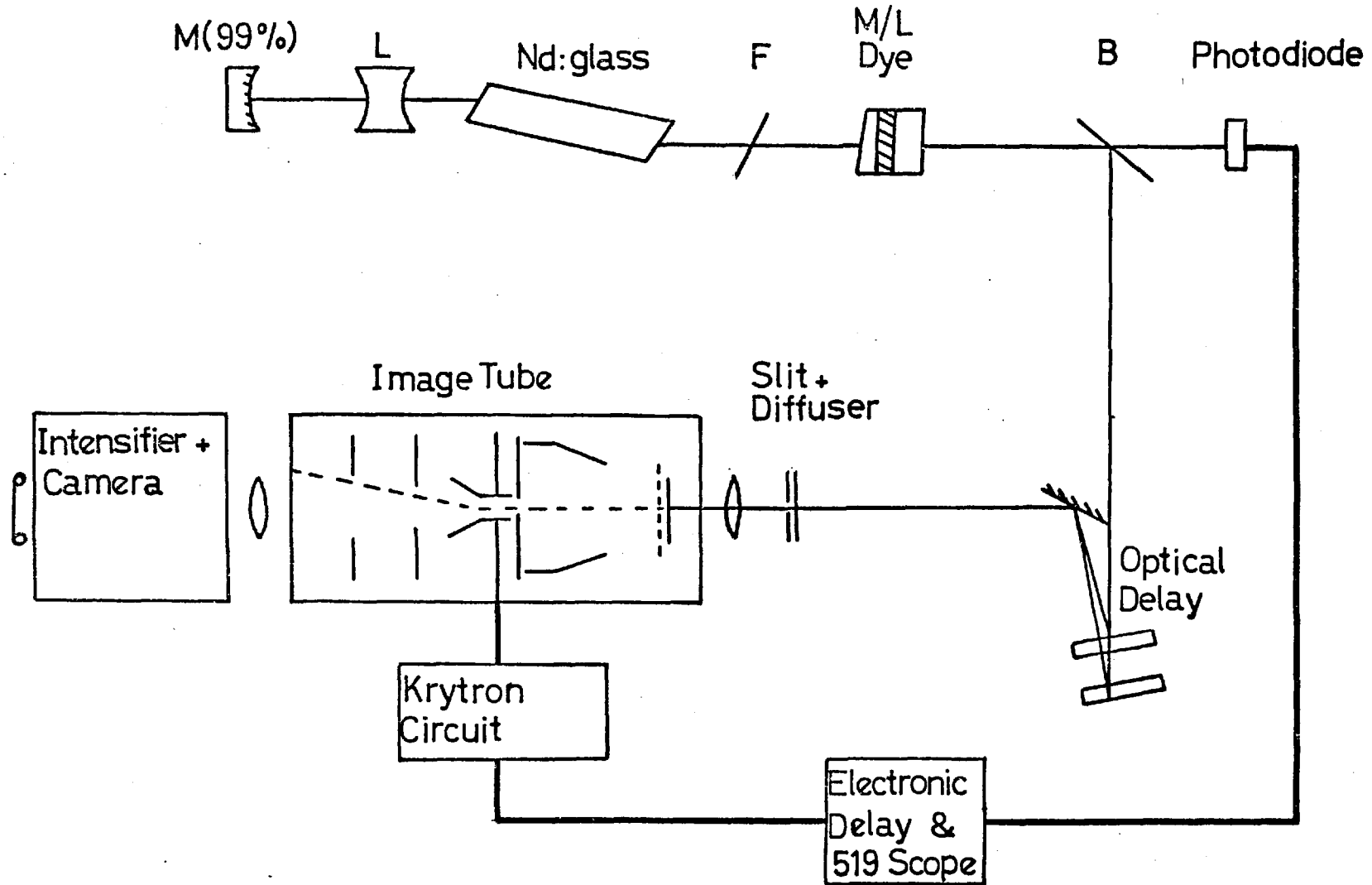
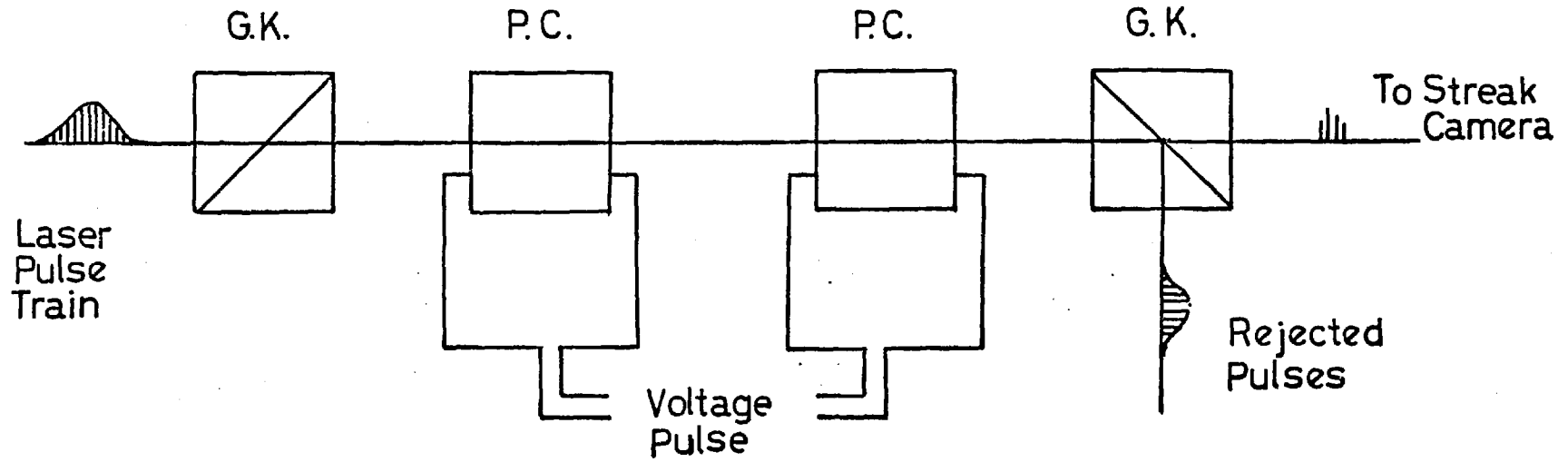
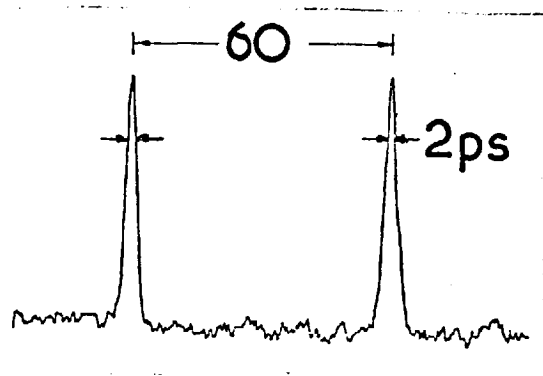


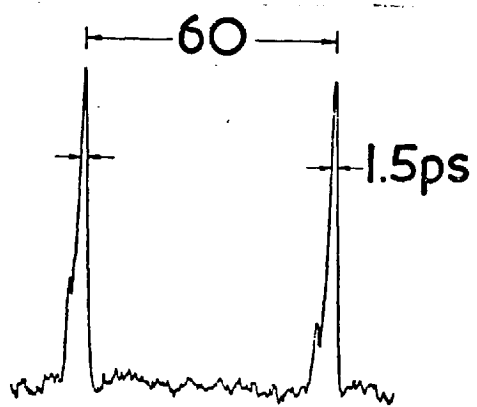
FIG. 26



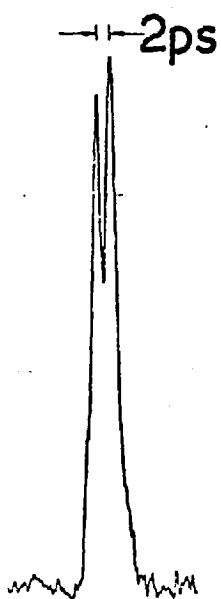
POCKELS CELL PULSE SELECTOR



(a)



(b)



(c)

FIG. 27

PLATE 3

Vacuum chamber containing a demountable image tube with mesh and photocathode electrodes at the front end of the tube.

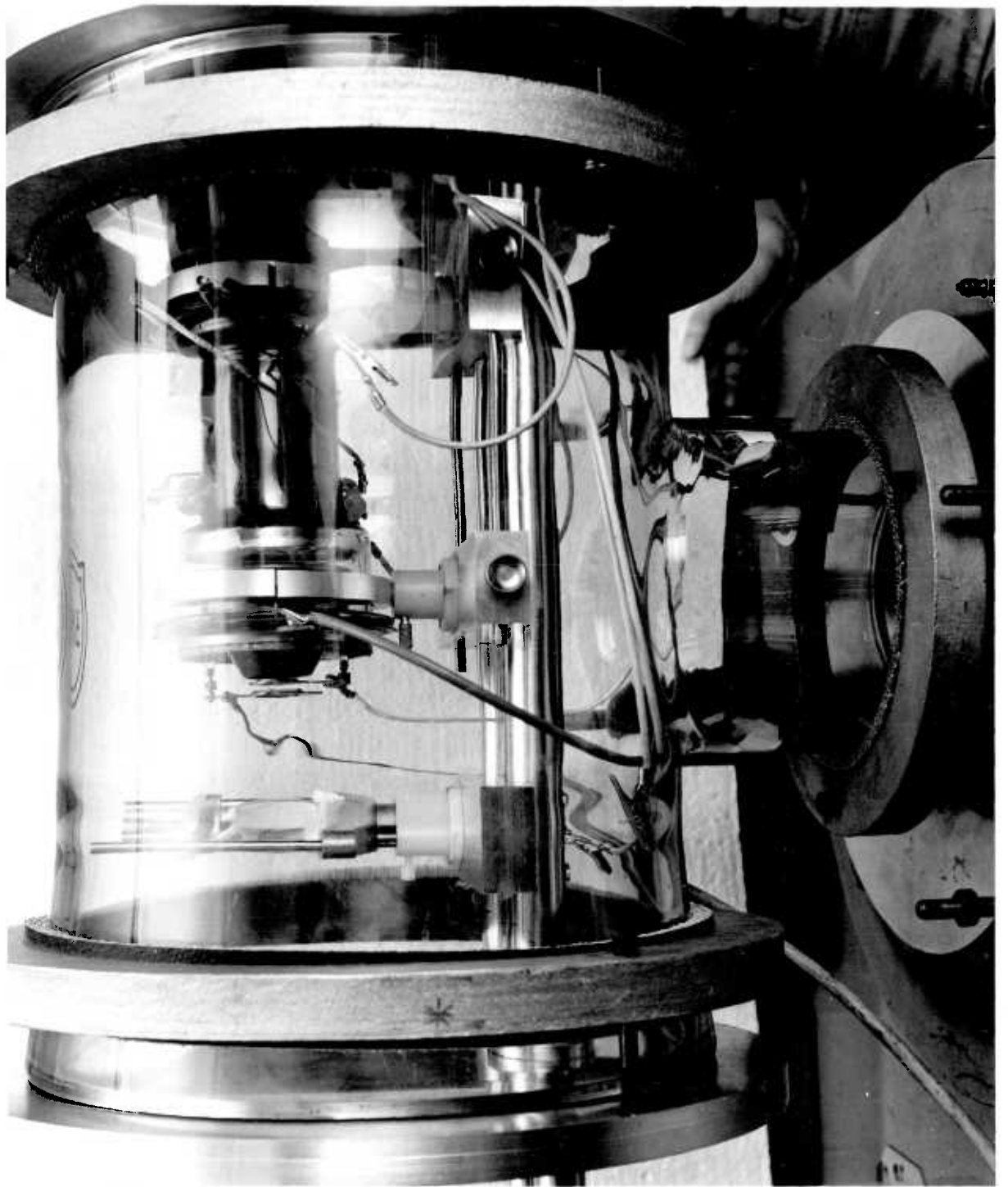


PLATE 4

- (a) Resolution chart photographed at a mesh to cone separation of 1.0 cm, showing a magnification of 2.7.
  
- (b) Resolution chart photographed at a mesh to cone separation of 2.0 cm. Electron-optical magnification of 2.3.
  
- (c) Resolution chart photographed at a mesh to cone separation of 3.0 cm. Electron-optical magnification of 1.8.



PLATE 5

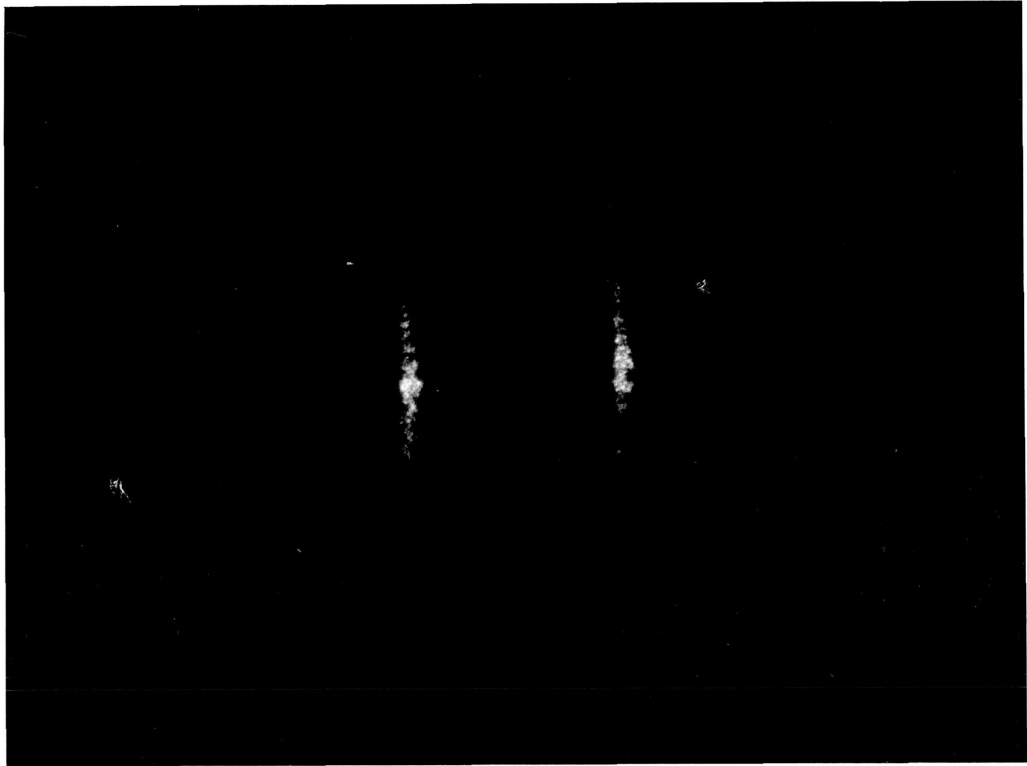
Neodymium: glass laser pulses separated  
by 20 psecs and 60 psecs.



PLATE 6

Streak photograph of dye laser  
pulses separated by 60 psecs

(R6G/DODCI)



## SUMMARY

The advantages of the electron-optical streak camera as a diagnostic tool for the measurement of ultra-short light pulses have been demonstrated. The streak camera provides a direct and unambiguous linear method for laser pulse duration measurements, with a temporal resolution comparable to that of the non-linear methods of TPF, SHG etc.

It has been shown how the temporal resolution of such cameras has improved from the region 20 psecs to 50 psecs to around 2-3 psecs by the inclusion of a mesh electrode near the photocathode of the Photochron I design image tube. Furthermore it has been shown how the camera instrumental function half width may be reduced to the subpicosecond region by simple redesign of the electron-optics of the image tube. This image tube the Photochron II has a higher spatial resolution, a greater electric field strength near the photocathode and is more sensitive to lower intensity radiation. The Photochron II has been used to directly measure pulses of duration  $\sim 3$  psecs in the output of a mode-locked Nd: glass laser and to record pulse durations of  $\sim 1.5$  psecs in the output of the mode-locked R6G dye laser. In the course of these investigations the camera instrumental function has been estimated to be of the order of 1.0 psecs for the infra-red streak camera and to be less than 1.0 psec for the camera operating at dye laser wavelengths. Thus direct linear measurement of laser pulse durations with a subpicosecond temporal resolution has been achieved.

It is likely that with an increased streak velocity and lower transit time spread that this design of streak camera may be capable of a temporal resolution of  $\sim 0.35$  psecs. This approaches the limit of resolution of the most popular non-linear method, TPF, ( $\sim 0.2$  psecs). Further improvements to the streak camera system could be effected by the use of fibre optic coupling instead of lenses, to reduce the photon loss in the transfer optics. The use of a channel plate image intensifier fibre - optically coupled to the image tube phosphor would have several advantages. The transfer efficiency between the image tube phosphor and the intensifier photocathode would be increased.

The channel plate device is also electrostatically focussed and requires no current supply, solenoid or cooling apparatus. The channel plate intensifier is also physically much smaller than the magnetically focussed type and would make a streak camera system more compact and with less peripheral equipment. Even more desirable is the use of an electron sensitive film at the output end of the image tube which would eliminate lossy electron-photon conversions, or the direct readout of the streak information into a computer where processing of that information can take place and the required results may then be output in different modes e.g. visual display unit, or numerically.

Because of its ability to measure pulses of picosecond duration and thus aid in the design of generators of such pulses, the streak camera becomes an increasingly important diagnostic instrument as the number of applications of picosecond pulses grows. Picosecond pulses are finding an increasing popularity in photochemistry where the study of molecular excited states may now be carried out using pulses whose durations are of the order of the vibrational relaxation times of the excited states. In photobiology, picosecond pulses are finding applications in the study of the mechanism of vision within cells, which is believed to occur on a picosecond time scale, and in the study of excited state molecular reactions which may lead to an increase in the efficiency of photosynthesis. Picosecond pulses are also finding applications in optical radar for the measurement of continental drift and the trains of pulses produced by the CW mode-locked laser form the basis for a PCM multiplexed communications system.

The possibility that lasers may be used to drive compression waves causing compressions of up to 10,000 times in a solid has aroused great interest in laser fusion, and picosecond pulses (10<sup>5</sup>). The high powers required for fusion may be provided by high energy picosecond pulses and at this time the Nd: glass laser appears the most popular source. The ability of the streak camera to measure

pulses of these durations make it an invaluable tool for the pulse shaping experiments required for preliminary fusion experiments.

The streak cameras described so far have operated in the visible and near infra-red regions of the spectrum. Streak cameras sensitive to vacuum ultra violet radiation would find use in the study of the Xenon laser (106) and in the study of laser harmonic generation in metal vapours and gases (102, 107). Laser generated plasmas are efficient vacuum ultra violet and X ray sources, and an X ray sensitive streak camera with a temporal resolution of  $\sim 150$  psecs has been designed (108) and used to study the X ray emission from a plasma generated by powerful laser pulses (Nd: glass, 2 GW) incident upon a copper target. Work is in progress to improve the temporal resolution of this camera to around 40 psecs.

The range of streak camera operation now extends from the near infra-red to the X ray region and it is possible that the knowledge gained working at these X ray wavelengths may make available the X ray laser and with it the possibility of femtosecond pulses.

## References

1. A.J. DeMaria, W.H.Glenn, M.J. Brienza, M.E.Mack, Proceedings of IEEE, 57 1, 1969.
2. R.C. Smith, C.O. Alley, Optics Communications, 1, 6, 1970.
3. M.D. Crisp, Optics Comms, 2, 2, 1971
4. H.J. Ruiz, J.J.Turner, T.A.Rabson, Optics Comms, 6, 4, 1972
5. H.P. Weber, J.Appl. Physics, 38, 5, 1967
6. J.A.Armstrong, Appl. Phys. Letts., 10, 1, 1967
7. H.P. Weber, J.Appl. Phys, 39, 13, 1968
8. E.P. Ippen, C.V.Shank, A.Dienes, Appl. Phys Letts 21, 8, 1972.
9. E.P.Ippen, C.V.Shank, Appl. Phys.Letts., 24, 8, 1974
10. R.C. Eckardt, C.H.Lee, Appl. Phys.Letts., 15, 12, 1969
11. P.P. Bey, J.F. Guiliani, H.Rabin, Phys.Letts., 28A, 698, 1969.
12. W.H.Glenn, J.Quant, Electr., QE-6, 8, 1970
13. H. Rowe, J.Quant, Electr., QE-6, 1, 1970
14. H.P. Weber, Phys.Letts., 27A, 5, 1968
15. H.P.Weber, H.G.Danielmeyer, Phys. Rev. 2, 5, 1970
16. J.A. Giordmaine, P.M. Rentzepis, S.L. Shapiro, K.W.Wecht, Appl. Phys. Letts., 11, 7, 1967
17. P.M. Rentzepis, M.A.Duguay, Appl. Phys., 11, 7, 1967
18. S.L.Shapiro, M.A.Duguay, Phys. Lett. 28A, 10, 1969
19. D.J. Bradley, T.Morrow, M.S.Petty, Optics Comms., 2, 1, 1970
20. H.P. Weber, E.Mathieu, K.P.Meyer, J.Appl. Phys., 37, 3584, 1966.
21. P.M.Rentzepis, C.J.Mitschele, A.C.Saxman, Appl. Phys. Letts., 17, 3, 1970.
22. D.J.Bradley, G.H.C.New, S.J.Caughey, B. Sutherland, Phys.Letts. 28A, 7, 1969.
23. D.J. Bradley, G.H.C.New, S.J.Caughey, Phys. Letts., 30A, 2, 1969.
24. J. R. Klauder, M.A.Duguay, J.A.Giordmaine, S.L.Shapiro, Appl. Phys.Letts., 13, 174, 1968

25. K.H.Drexhage, Appl.Phys.Letts., 14, 318, 1969
26. D.J.Bradley, A.F.Durrant, F.O'Neill, B.Sutherland, Phys. Letts., 30A, 535, 1969.
27. M.M.Malley, P.M.Rentzepis, Chem.Phys.Letts., 3, 7, 1969.
28. M.A.Duguay, J.W.Hansen, Appl.Phys.Letts., Optics Comms., 1, 5, 1969.
29. M.A. Duguay, J.W.Hansen, Appl. Phys.Letts., 15, 6, 1969
30. R. Fischer, R. Rossmanith, Optics Comms., 5, 1, 1972
31. N.G.Basov, O.N.Krokin, G.V.Slizkov, S.I. Fedotov, A.S.Shikanov, Sov. Phys. JETP, 35, 109, 1972
32. G. Mayer, F.Gires, Compt. Rend., 258, 2039, 1964.
33. D.J.Bradley, G.H.C.New, Proc. IEEE, 62, 3, 1974
34. S.L.Shapiro, H.P. Broida, Phys. Rev., 154, 129, 1967
35. A.G.Roddie, Ph.D Thesis, Queens Univ. Belfast, 1972.
36. M.A. Duguay, J.W.Hansen, IEEE, J.Quant, Electr., QE-7, 37, 1971
37. L. Dahlström, B.Källberg, Optics Comms, 4, 6, 1972
38. G. Mourou, B. Drouin, M.M.Denariez-Roberge, Appl. Phys.Letts., 20, 453, 1972.
39. E.K.Zavoiskii, S.D.Fanchenko, Appl. Optics, 4, 9, 1965
40. J.P.Mazan, J. Haisma, G.Marie, J.Nussli, IEEE J. Quant, Electr., QE-6, 1744, 1970.
41. T.Ohmi, S.Hasuo, S.Mori, J.Appl.Phys., 43, 3773, 1972
42. F. O'Neill, Optics Comms, 6, 360, 1972.
43. A. Dienes, E.P.Ippen, C.V.Shank, Appl. Phys. Letts. 19, 258, 1971
44. M.A. Duguay, A.Savage, Optics Comms., 9, 2, 1973
45. E.K. Zavoiskii, S.D.Fanchenko, Sov. Phys., Doklady, 1, 285, 1956.
46. A.E. Huston, Appl. Optics, 3, 11, 1964
47. A.E. Huston, R.B.Harris, Advances in Elect. and Electr.Phys., 33B, 1109, 1972.
48. M. Ya. Schelev, M.C.Richardson, A.J. Alcock, Rev. Sci. Instr., 43, 12, 1972
49. D.J.Bradley, B.Liddy, W.Sibbett, W.E.Sleat, Appl.Phys.Letts., 20, 6, 1972
50. D.J.Bradley, B.Liddy, W.Sibbett, W.E.Sleat, A.G.Roddie, Adv.in Elect. and Electr. Phys., 33B, 1145, 1972.

51. V.V. Korobkin, A.A. Maljutin, M.Ya. Schelev. J. Photogr. Sci., 17, 179, 1969.
52. V.V. Korobkin, A.A. Maljutin, M.Ya. Schelev, Sov. Phys. - Tech. Phys., 16, 165, 1971
53. A.J. Alcock, M.C. Richardson, M.Ya. Schelev, Proc. 9th Int. Congr. H.S. Photogr. pp 191-7, 1970.
54. D.J. Bradley, M.H. Key, J.F. Higgins, J. Opto-Electronics, 1, 62, 1969.
55. A.E. Huston, Adv. in Elect. and Electr. Phys., 28B, 957, 1966.
56. N. Ahmed, B.C. Gale, M.H. Key, Adv. in Elect. and Electr. Phys., 28B, 999, 1969.
57. E.G. Arthurs, D.J. Bradley, B. Liddy, F. O'Neill, A.G. Roddie, W. Sibbett, W.E. Sleat, Proc. 10th Int. Conf. H.S. Photogr., pp 117-122, 1972.
58. T.J. Glynn, Ph.D. Thesis, Queens University, Belfast, 1973
59. D.J. Bradley, W. Sibbett, Optics Comms., 2, 1, 1973
60. F. O'Neill, Optics Comms. 6, 360, 1970
61. W. Sibbett, Ph.D. Thesis, Queens University, Belfast, 1973.
62. N.G. Basov et al, Lebedev Physical Institute Reprint, No.82, pp 1-25, Moscow 1972.
63. S.D. Fanchenko, B.A. Frolov, J.E.T.P. Letts. 16, 101, 1972.
64. D.J. Bradley, B. Liddy, A.G. Roddie, W. Sibbett, W.E. Sleat, Optics Comms., 2, 6, 1971.
65. J.P. Hazan, G. Marie, J. Haisma, J. Nussli, IEEE. J. Quant. Electr., QE-6, 1744, 1970.
66. Technical Data on Photodiodes, Spectra Physics, California U.S.A.
67. M.M. Butslov, V.V. Korobkin, A.M. Prokhorov, B.M. Stepanov, M.Ya. Schelev, Proc. 10th Int. Conf. H.S. Photogr., pp 122-126, 1972.
68. T.H. Maiman, Nature, 187, 493, 1960.
69. F.J. McClung, R.W. Hellwarth, J. Appl. Phys., 33, 828, 1962.
70. M. Di Domenico, Jour. Appl. Physics. 35, 2870, 1964.
71. E.G. Arthurs, D.J. Bradley, A.G. Roddie. Appl. Phys. Letts. 19, 480, 1971.
72. E.G. Arthurs, D.J. Bradley, A.G. Roddie, Appl. Phys. Letts. 20, 125, 1972.
73. D.J. Bradley, B. Liddy, W.E. Sleat, Optics Comms., 2, 8, 1971
74. B.M. Driard, L.F. Guvot, U.S. Patent No. 3,439,222.

75. W.E. Sleat, Ph.D. Thesis, Queen's University, Belfast, 1974.
76. E.G.&G. Technical Data on krytrons.
77. High Speed Switching Transistor Handbook,  
Chapter 9, Motorola Inc, Semiconductor products div., 1963.
78. T.H. O'Dell, Electronics Letters, 5, 5, 1969.
79. M. Blanchet, Proc. 9th Int. Congr. H.S.  
Photography, pl13, 1971.
80. Data on Aluminized Phosphor screens, ITT  
Industrial Labs, Indiana, U.S.A.
81. T.H. Bulpitt, Proc. 8th Int. Congr H.S.  
Photography., p30, 1968.
82. V.V.Korobkin, A.A.Maljutin, M.Ya. Schelev, Proc. 9th Int.Congr.  
H.S.Photogr., p232, 1970.
83. B. Liddy, Ph.D Thesis, Queen's University, Belfast, 1971.
84. R.P.Randall, R.E.Trevor, EMI Report. R/S009.
85. B.R.C. Garfield, P.C.Bailey, R.Marshall, Advances in Electronics  
and Electron Physics, 33B, 1137, 1972.
86. E.G. Arthurs, D.J.Bradley, A.G.Roddie, Appl. Phys. Letts.,  
19, 480, 1971.
87. O. Klemperer, Electron Physics, Butterworth Press, 1959.
88. A.H.Sommer, Photoemissive Materials, pl32, J.Wiley and Sons, 1968.
89. D.J.Bradley, W.G.I. Caughey, J.I.Vukusic, Optics Comms.,  
4, 150, 1971.
90. D.J.Bradley, G.H.C.New, S.J.Caughey, Optics Comms, 2, 41, 1970
91. N.A.Soboleva, A.G.Berkovsky, N.O. Chechik, R.E.Eliseev,  
Photoelectronic devices, (Science Moscow), 124, 1965.
92. G.D.Baldwin, E.P.Riedel, J.Appl.Phys., 38, 2726, 1967.
93. S.J.Caughey, Ph.D.Thesis, Queen's University, Belfast, 1970.
94. M.C.Richardson, IEEE J.Quant. Electr., QE-9, 7, 1973.
95. Instrument Technology Ltd. Hastings.
96. D.J.Bradley, Opto-Electronics, 6, 25-42, 1974.
97. A.H.Sommer, RCA Review, Vol. 34, March 1973.
98. A.A.Ionin, V.I. Malyshev, A.V. Masalov, J.E.TP.Letts.,  
16, 284, 1972.
99. P.G. Kryukov, Yu. A. Maveets, S.V.Chekalin, O.B.Shatverashvili,  
J.E.T.P. Letts, 16, 81, 1972.
100. M.J.Colles, Appl. Phys. Letts., 19, 23, 1971
101. D.J.Bradley, W.G.I. Caughey, J.I. Vukusic, 4, 150, 1971.
102. R.S.Adrain, E.G.Arthurs, D.J.Bradley, A.G.  
Roddie, J.R.Taylor, to be published, Optics Comms.

103. V.V.Korobkin, A.A.Maljutin, A.M.Prokhorov, R.V.Serov,  
M.Ya. Schelev, Proc. 10th Int. Congr. H.S. Photogr., p84-91, 1972.
104. J.R.Taylor, Ph.D.Thesis, Queen's University, Belfast, 1974.
105. J. Nuckolls, L. Wood, A.Thiessen, G.Zimmerman, Nature, 239,  
139-42, 1972.
106. D.J.Bradley, D.R.Hull, M.H.R. Hutchinson, M.W. McGeoch, Optics  
Comms, 11, 335-338, 1974.
107. R.T.Hodgson, P.P.Sorokin, J.J.Wynne, Phys. Rev. Letts.,  
32, 343, 1972.
108. P.R.Bird, D.J.Bradley, A.G.Roddie, W.Sibbett, M.H.Key, M.J.Lamb,  
C.L.S.Lewis, Proc. 11th Congr. on H.S. Photography.

### Acknowledgements

Thanks are due to Professor D.J. Bradley for the provision of the facilities with which this work was carried out, and for his guidance throughout its duration.

I would also like to thank Dr. Wilson Sibbett in conjunction with whom the majority of this work was carried out.

I would also like to express my gratitude to those members of the Applied Optics section of Imperial College who gave advice and practical assistance during the course of this work. In particular, Mr. R.S. Adrain, Dr. E.G. Arthurs, Dr. A.G. Roddie, Mr. I.S. Ruddock and Mr. J.R. Taylor.

On the technical side I would like to acknowledge the assistance of Mr. B. Weekly, Mr. G. Busby, Mr. J. Osborne, and Mr. G. Mathews.

Financial support during the course of this work was provided by a grant from the Isle of Man Education Authority and a Research Assistantship from Imperial College.

PUBLICATIONS

## THE PHOTOCHRON II STREAK CAMERA

P. R. Bird, D. J. Bradley and W. Sibbett

Optics Section  
Physics Department  
Imperial College  
London SW7  
England

### ABSTRACT

A new streak image-tube, the Photochron II, has been designed to provide sub-picosecond time resolution. The tube design has been tested both in a demountable vacuum optical-bench arrangement and in a streak camera system. With improved spatial resolution, increased photocathode field strength and reduced electron-optical magnification, sub-picosecond camera resolution has been demonstrated with tubes with S1 and S20 photocathodes, employing mode-locked neodymium:glass and dye lasers as test sources.

### INTRODUCTION

At the 10th International Congress on High Speed Photography we reported the achievement of a time-resolution limit of  $\sim 2$  psec, with ultra-short light pulses from passively mode-locked dye lasers (1-3) to test the performance of the Photochron image-tube streak camera system (4,5). This image-tube employs a mesh extraction electrode (6) to overcome the effects of photo-electron time-dispersion. For some applications of ultra-short laser light pulses, particularly in photo-chemistry and X-ray laser studies, sub-picosecond time-resolution is to be maintained throughout the spectrum of sensitivity of the streak tube photocathode, then the extraction mesh electric-field strength must be sufficiently greater than that necessary to produce the required time-resolution with radiation of wavelength close to the photo-cathode cut-off. This need arises from the considerable variation in the distribution of photo-electron velocities at different wavelengths (4). To permit a substantial increase in the photocathode extraction electric field we have redesigned the electron-optics of the Photochron tube, at the same time improving the spatial resolution and, by reduced magnification increasing the recording speed (7). Extra baffle electrodes have also been added to reduce the signal induced background. With this new Photochron II tube, direct photoelectric sub-picosecond time measurement has been obtained for the first time.

## STREAK CAMERA PERFORMANCE

Figure 1 shows the tube electrode arrangement which is similar to that employed in the original Photochron tube (4). The mesh-photocathode separation is now 0.5mm and with an applied mesh-voltage of 1kV the electric field  $E$  at the photocathode is increased to  $20\text{kVcm}^{-1}$ . Variation of the mesh-voltage changes the magnification of the image at the output phosphor screen in the manner shown in Figure 2. At the working mesh voltage of 1kV, a magnification of X2 is obtained. This results in an increase of light gain by X3 over the previous design of Photochron tube. The spatial resolution of the phosphor, which is also a function of mesh voltage (Figure 3), has been increased to a static value of  $>18$  lp/mm. Design of the tube was optimized employing the demountable vacuum electron-optical test rig shown in Figure 4.

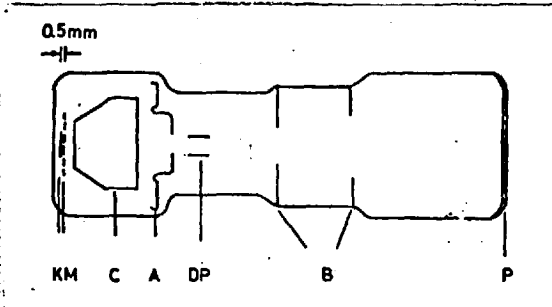


Figure 1. Schematic diagram of electrode configuration of Photochron II streak tube. Cathode K; Mesh M; Cone C; Anode A; Deflection Plates DP; Baffle electrodes B; Phosphor P.

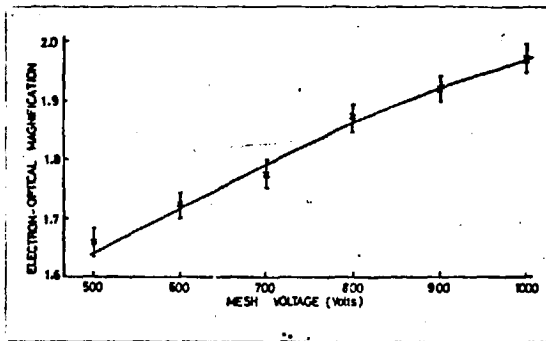


Figure 2. Variation of electron-optical magnification at phosphor as a function of extraction mesh voltage.

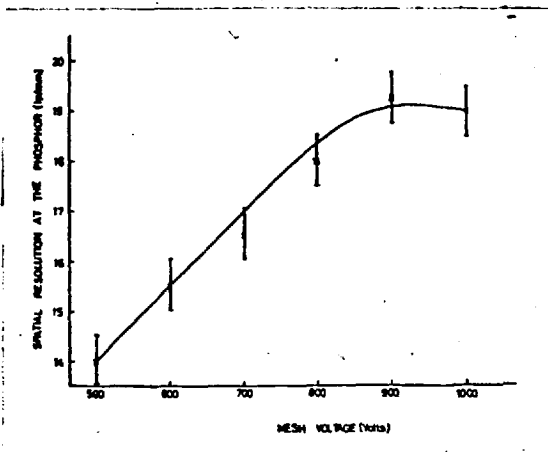


Figure 3. Phosphor spatial resolution dependence upon extraction mesh voltage. Anode voltage was maintained constant while cone voltage was adjusted for maximum spatial resolution.

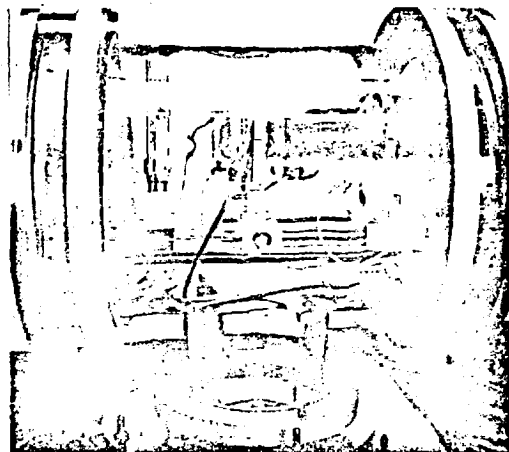


Figure 4. Demountable electron-optical bench arrangements showing prototype Photochron II tube.

For the preliminary investigations an evaporated gold test-pattern cathode was employed with UV illumination and quartz optics. When the optimum tube design was achieved two sealed-off tubes were manufactured (8) with S1 and S20 photocathodes, respectively. When tested statically both tubes met the design performance summarized in Table I. Time-resolution and general characteristics in streak operation were investigated with picosecond pulses from mode-locked neodymium:glass and dye lasers.

TABLE I

<u>Performance Characteristics</u>	<u>Photochron I</u>	<u>Photochron II</u>
Spatial resolution at phosphor	8lp/mm	18lp/mm
Spatial resolution at photocathode	30lp/mm	36lp/mm
Electron-optical magnification	x 3.6	x 2
Photocathode extraction field	6.6kVcm <sup>-1</sup>	20kVcm <sup>-1</sup>

#### TIME-RESOLUTION MEASUREMENTS

The shortest duration pulses are produced by mode-locked dye lasers (2,4) which have the added advantage of being more reproducible in operation than mode-locked solid state lasers. However, because neodymium:glass laser amplifier arrays are capable of producing high energy picosecond pulses which are of great interest for laser compression and fusion experiments (9), the first Photochron II tube was manufactured with an S1 photocathode. Recent investigations (10) with a camera employing the original design of Photochron tube have shown that it is possible to generate  $\sim 1$  mJ pulses of transform limited durations ( $\Delta t \sim 3$  psec,  $\Delta t \Delta \nu \sim 0.5$ ) in a specially designed oscillator, employing optical correction for thermal lensing. With this laser we have obtained recorded pulse widths of 3 psec with the Photochron II tube showing that, as expected, the camera instrumental width is negligible compared with the laser pulse duration. An S20 photocathode tube was manufactured with the intention of employing transient Raman scattering (11), of dye laser pulses to produce sub-picosecond pulses for direct camera testing. While this picosecond Raman oscillator was under construction we have tested the performance of the S20 tube with a pulsed, twin-lamp, mode-locked Rhodamine 6G oscillator. Pulses of 2 psec duration are reliably produced by this laser (2,12). The experimental arrangement has been described earlier (1,2). With a writing speed of  $2 \times 10^{10}$  cm sec<sup>-1</sup> at the streak tube phosphor, a total recorded pulse width of 2 psec was obtained, as shown in Figure 5. When the Rhodamine 6G dye laser was mode-locked using an ethanolic solution of 1,3'diethyl 4,2'-quinolyoxacarbocyanine iodide (DQOCI) (13) and tuned to 605 nm, pulsewidths as short as 1.5 psec were recorded. A microdensitometer trace of a pair of streak images of such pulses is shown in Figure 6. The streak records were

photographed with Ilford HP4 film for quantitative microdensitometry. The pulses, separated by 60 psec, were produced by an optical delay line. This arrangement (2,4) splits a single pulse from the laser train, into any required number of pulses, separated by pre-determined time intervals for camera calibration.

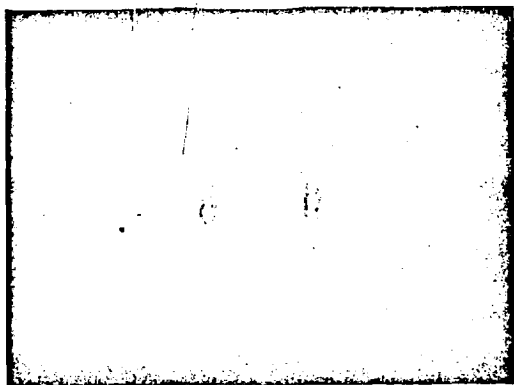


Figure 5(a). Photograph of two streak images, separated by 60 psec, of mode-locked dye laser pulse ( $\lambda$  605nm).

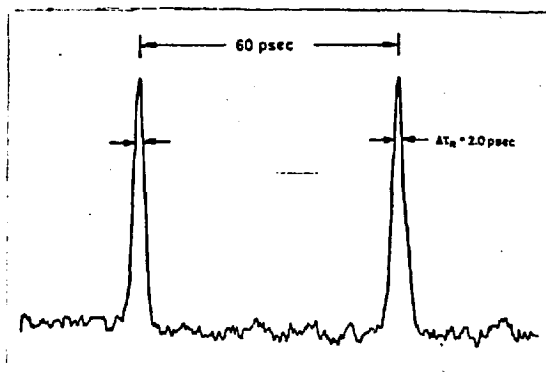


Figure 5(b). Microdensitometer trace of (a) showing recorded pulse width of 2 psec.

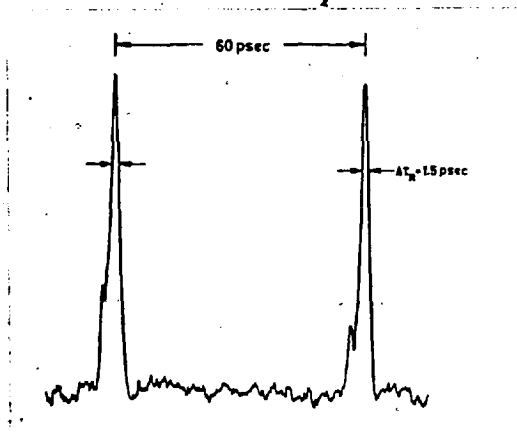


Figure 6. Microdensitometer trace of a pair of streak images of a pulse generated by a Rhodamine 6G dye laser mode-locked using QOC1 showing recorded pulse duration of 1.5 psec.

In an effort to demonstrate directly the sub-picosecond time resolution capability of the camera we recorded many such streaks with the dye laser. Because of the manner in which the mode-locked dye laser builds up from the initial intensity fluctuation pattern (2), there is a finite probability for the production in a pulse of two nearly equal intensity, sub-picosecond components. A streak record

of such an event (R6G/DODCI) is shown in Figure 7. The two components, separated by 2 picoseconds, are clearly resolved and from the microdensitometer trace an instrumental function of  $< 1$  psec is obtained. The dynamic spatial resolution limit and the time dispersion limit are then comparable in magnitude ( $\sim 0.5$  psec). Further experiments are in progress to accurately determine the camera resolution limit employing both transient Raman pulses and beat signals from a dual frequency dye laser (14).

## DISCUSSION

Direct linear measurement of ultra-short light pulses with sub-picosecond time resolution has been obtained for the first time. This new Photochron II tube should permit the study of luminous phenomena throughout the spectrum from the vacuum ultraviolet to the near infrared with a time resolution  $\leq 2$  psec, and with sub-picosecond resolution down to 0.1 psec at particular spectral regions, depending upon the type of photocathode employed. With its higher light gain, the range of usefulness is extended to weaker light sources while the improved spatial resolution increases the information capacity available. As a result, the art of time measurement of light pulses is again ahead of the techniques of ultra-short pulse generation.

## ACKNOWLEDGEMENTS

We wish to thank E. G. Arthurs and A. G. Roddie for useful discussions and experimental help with ultra-short pulse generation, and Instrument Technology Ltd for their collaboration in manufacture of the two streak tubes.

## REFERENCES

- (1) E. G. Arthurs, D. J. Bradley, B. Liddy, F. O'Neill, A. G. Roddie, W. Sibbett and W. E. Sleat. Proc. of the 10th Int. Congress on High Speed Photography, Nice, September 1972, pp. 117-122.
- (2) D. J. Bradley, *Opto-Electronics* (1974), 6, 25-42.
- (3) E. G. Arthurs, D. J. Bradley and A. G. Roddie, *Appl. Phys. Letts.* (1972), 20, 125-127.

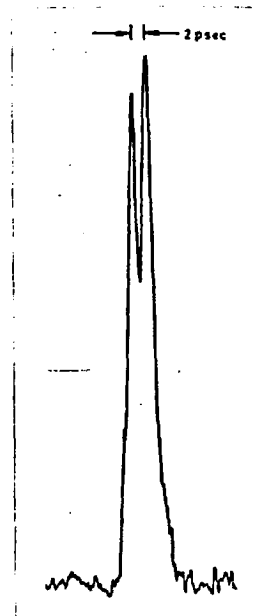


Figure 7. Microdensitometer trace of dye laser sub-pulses with 2 picosecond separation, showing a camera resolution limit of  $< 1$  psec.

- (4) D. J. Bradley and G. H. C. New, Proc. IEEE (1974), 62, 313-345.
- (5) D. J. Bradley, B. Liddy and W. E. Sleat, Optics. Commun. (1971) 2, 391-395.
- (6) D. J. Bradley, UK Patent 1329977 (1973), US Patent 3761614 (1973)
- (7) D. J. Bradley and W. Sibbett, UK Provisional Patent Specification 25357/74, (1974).
- (8) Manufactured by Instrument Technology Ltd.
- (9) J. Nuckolls, L. Wood, A. Thiessen and G. Zimmerman, Nature (1972) 239, 139-142.
- (10) D. J. Bradley and W. Sibbett, Optics. Commun. (1973), 9, 17-20.
- (11) K. Darée and W. Kaiser, Optics. Commun. (1974), 10, 63-67.
- (12) W. Sibbett, PhD Thesis (1973). The Queen's University of Belfast.
- (13) R. S. Adrain, E. G. Arthurs, D. J. Bradley, A. G. Roddie and J. R. Taylor, to be published in Optics Communications.
- (14) D. J. Bradley, W. G. I. Caughey and J. I. Vukusic, Optics Commun. (1971), 4, 150.